TESIS DE LA UNIVERSIDAD DE ZARAGOZA

2019 74

Ismael González Valverde

Modeling and simulation of multi-cellular systems using hybrid FEM/Agent-based approaches

Departamento
Instituto de Investigación en Ingeniería [I3A]

Director/es
GARCÍA AZNAR, JOSÉ MANUEL

ISSN 2254-7606

Prensas de la Universidad
Universidad Zaragoza

ISSN 2254-7606

Universidad Zaragoza
1542

Tesis Doctoral

MODELING AND SIMULATION OF MULTI-CELLULAR SYSTEMS USING HYBRID FEM/AGENT-BASED APPROACHES

Autor

Ismael González Valverde

Director/es

GARCÍA AZNAR, JOSÉ MANUEL

UNIVERSIDAD DE ZARAGOZA

Instituto de Investigación en Ingeniería [I3A]

2018

Modeling and simulation of multi-cellular systems using hybrid FEM/Agent-based approaches

Universidad Zaragoza

Ismael D. González Valverde

Aragón Institute of Engineering Research (I3A)

University of Zaragoza

A thesis submitted for the degree of

Doctor of Philosophy in Biomedical Engineering

March 2018

A mis padres

Caminante, son tus huellas
el camino y nada más;
Caminante, no hay camino,
se hace camino al andar.
Al andar se hace el camino,
y al volver la vista atrás
se ve la senda que nunca
se ha de volver a pisar.
Caminante no hay camino
sino estelas en la mar.

Antonio Machado
Proverbios y Cantares XXIX
Campos de Castilla (1912)

Agradecimientos/Acknowledgements

En primer lugar quiero darle las gracias a Laura, por su apoyo, su comprensión y su cariño durante todo el doctorado. Sinceramente, creo que no podría haber terminado esta tesis sin tu ayuda. Gracias por estos años que hemos compartido, y por todo lo que nos queda por vivir juntos.

A mis padres, porque sin ellos no podría haber llegado a ser lo que soy a día de hoy. Gracias por los esfuerzos que habéis hecho por mi y por haberme apoyado en todos mis proyectos. Espero volver a estar más cerca de vosotros a partir de ahora. A los que ya nos están, seguro que les hubiera encantado ver como terminaba este trabajo el *Doctor Pelaito*.

A mi amigo y director de tesis Manu, se que va a echar de menos nuestras largas discusiones. Gracias por haber sido tan atento y haberme ofrecido tu ayuda siempre que me ha hecho falta. No me puedo olvidar de mis compañeros Jorge, Andrea y Mar, por *"los momentos tan bonitos"* que hemos vivido estos últimos meses. A todos los compañeros que han pasado por la sala de becarios, en especial a Diego, Sergio, Raquel, Javi y Carlos. A Tirso, Mª Ángeles, Mª José y al resto de miembros del grupo de investigación. Por último, a todos mis amigos que siguen donde siempre, aunque ya no vivan cerca de casa.

I also want to thank Paul, Dirk and his team for always supporting me and appreciating all my efforts. They made me feel very comfortable during my stay in Paris.

Finally, this research was supported by the *European Research Council* (ERC) through project (ERC-2012-StG 306571) and the *Spanish Ministry of Economy and Competitiveness* (DPI2015-64221-C2-1-R). This document was also backed by the *L.E.S.* (LKTS-17-18-0.70). I would like to acknowledge open-source projects that were used in this research: *deal.II* library [1] for FE analysis, *CGAL* library [2] for geometrical representation, *seaborn* [3] for data analysis and *Paraview* [4] for data representation.

Abstract

Many biomechanical properties of multi-cellular organisms directly emerge from cell interactions. Cells in organs and tissues interact between them and with their environment in different ways. Due to this fact, it is fundamental to analyze how these interactions are translated to tissue level properties. For instance, cell-cell adhesions will determine the apparent stiffness of an epithelial layer. Further, cell-matrix interactions may determine the formation of many biological structures and their morphology. These multi-cellular systems cannot be regarded as static structures since they are suffering constant changes such as cell proliferation, reorganization or migration. Therefore, it is necessary to study cell dynamics and individual interactions to fully understand how higher level phenomena work, from tissue development to tumor growth.

Recently, the use of agent-based approaches has become very popular to model multi-cellular systems. Agent-based models represent cells as individual entities. These models are especially adequate to study biophysical phenomena that occur at the cell level. Here cell-cell interactions can be directly modeled in a mechanistic way. Also, these models capture really well the inhomogeneities present in the biological structures. Otherwise, continuum models are commonly used in larger scale problems. In contrast to agent-based models, they do not represent cells as individual entities. They define constitutive laws to model biological, physical and chemical processes. Hence, cell properties are averaged using macroscopic parameters and these models often work with the cell density instead of separate cell entities. However, these models present a good scalability and an excellent representation of particular physical phenomena such as mass transport and force transmissions in continuum media.

In this thesis, we aim to explore the possibilities that hybrid approaches can offer to develop novel models of multi-cellular systems. We present two different hybrid models that combine an agent-based and a continuum model. Both approaches have in common that the continuum model is solved using the Finite Element method. Also, we show how to overcome the many intrinsic limitations of each model type following this design pattern.

First, we present a hybrid model to simulate epithelial monolayer mechanics. In this model, we focus on cell-cell and cell-substrate mechanical interactions, but also on tissue topology and cell morphology. We reproduce proliferating epithelial tissues, collective cell motion and migration processes using this approach. Our second model has been designed to simulate cell aggregates in three-dimensional environments. We study cell mechanical interactions but, especially, how cells are affected by oxygen transport in a 3D cell clustering process.

Finally, we compare both model results with experimental data from other authors and discuss the benefits of combining different types of models. We demonstrate that the hybrid approaches we propose in this work are able to simulate a wide variety of multi-cellular systems. In fact, they are particularly useful to study how some phenomena emerge from individual cell interactions to larger biological scales.

Contents

List of Figures

1 Introduction

Contents

1.1 Biological background

In this section, we offer a brief biological background of different multi-cellular systems studied in this thesis. First, we show an introduction to epithelial tissues and, in particular, cell monolayers. Monolayers can be regarded as two-dimensional (2D) structures since one of their dimensions is notably smaller than the others. We highlight their fundamental mechanical properties and their topological characteristics. Otherwise, we describe the formation of cell aggregates in three-dimensional (3D) environments. These structures differ from 2D ones in many aspects, for instance, oxygen and nutrients availability or cell-substrate interactions are notably different. We summarize important aspects that should be considered to model these systems, and we note unique phenomena that only occurs in 3D cultures.

1.1.1 Epithelial tissue mechanics

Epithelial cells can form structures of one cell thick called monolayers. This is one of the simplest tissues found in multicellular organisms, yet it has a fundamental role in embryo development, as a support structure for organs and to separate different physiological environments both mechanically and chemically. The mechanical properties of this tissue arise from both cell properties and junctions between cells in the monolayer. Remarkably, these cell adhesions are dynamic and, in consequence, cells can rearrange in the layer, change their morphology and even display a fluid behavior [5–7].

The adhesive junctions between cells are mainly formed by E-cadherin molecules, and they are stabilized by actin filaments and catenin molecules as shown in Figure 1.1A [8–10]. Moreover, there is a mechanical balance between the adhesives forces and the contraction forces generated by actomyosin activity. Hence, the contact adhesions are continuously under tension and they transmit forces from one cell to another. This interplay between both phenomena regulates the mechanics and dynamics of cell junctions. In fact, they define the cell ability to deform and remodel the contacts with its neighbors, but also cell morphology itself.

In epithelial monolayers, cells are tightly connected by these adhesion contacts and they form a junctional network (Figure 1.1B). This network is able to integrate cell cytoskeletons into a continuum mechanical structure that propagates forces through the layer [10, 11]. Therefore, it is not possible to directly extrapolate the mechanical parameters from single cell measurements to determine the tissue rheological properties.

The characteristic polygonal topology of epithelial cells is given by these tight adhesions [12–14] (Figure 1.1C). Cell geometry resembles a polygon where the

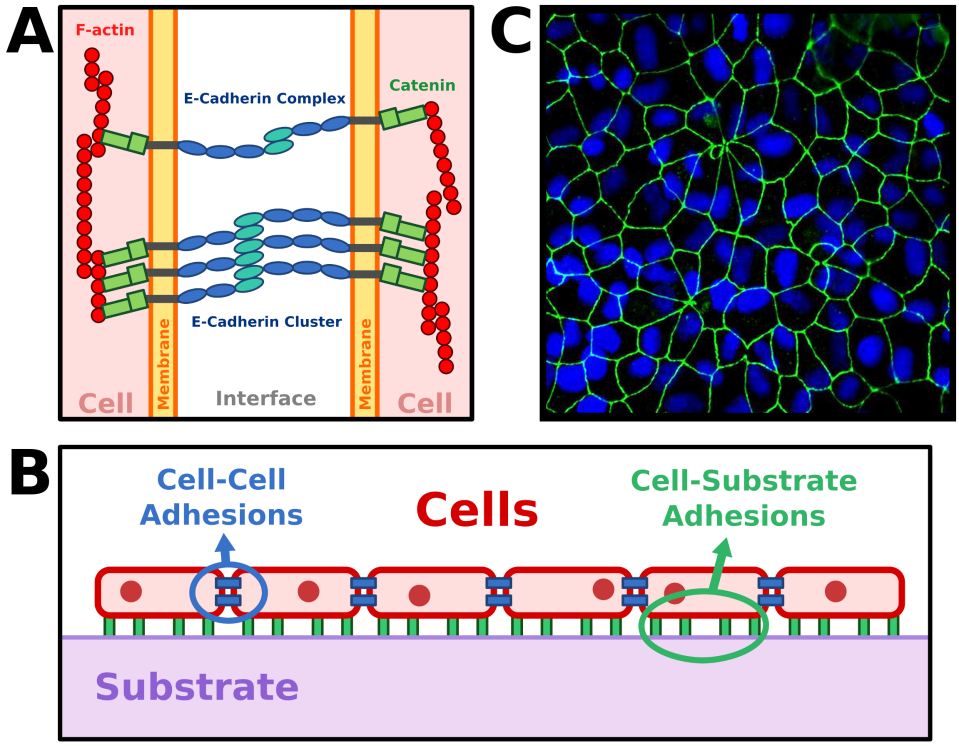

Figure 1.1: Epithelial monolayer mechanics. (A) Cell-cell adhesions are mainly formed by e-cadherin complexes. E-cadherin forms extracellular junctions that are stabilized by catenin and actin inside the cell. (B) Diagram of an epithelial monolayer structure. Cells adhere between them to form a junctional network that is highly dynamic. Moreover, the cell-substrate adhesions will determine cell migration phenomenon. (C) Fluorescence microscopy image of an epithelial monolayer. Image adapted from Thermofisher gallery.

junctions between cells are the polygon edges, and the contact points between three or more cells are the vertices. Indeed, the cell organization in epithelial monolayers can be described and characterized by the distribution of the number of polygon edges.

It has been observed that epithelial tissue responds as an elastic material when a short duration external force is applied to the system [11]. Cells keep the number of shared edges and their organization in the tissue under these circumstances. However, when the force is applied on a longer time scale, the tissue shows a visco-plastic behavior that can even resemble a fluid. In this case, cells rearrange in the layer and alter their junctions. Further, they also restructure their cytoskeletons to adapt to the new conditions. Therefore, these mechanisms allow cells to dissipate stresses in the epithelial tissue [11, 15, 16].

Similarly, cell proliferation and division also play a major role in the topology and mechanical behavior of epithelial monolayers [12–14]. Cell division alters the cell organization in the tissue, driving the biological system to clearly defined topological patterns. For instance, cells that are elongated tend to divide in a cleavage plane perpendicular to the largest direction [13, 17]. This phenomenon forces the epithelial cells to keep a preferential hexagonal shape, and also helps to dissipate accumulated stresses in the layer.

Finally, the importance of epithelial mechanics is not limited to cell layer structural organization and its inherent mechanical properties, but it is also related to other biophysical phenomena such as collective cell migration. Epithelial collective migration is involved in many physiological and pathological processes [18]. For instance, collective migration is fundamental in morphogenetic events during the embryogenesis [9, 19]. Further, gap closure and, in particular, wound healing are entirely regulated by this process [20, 21]. Therefore, the understanding of epithelial tissue mechanics goes beyond the mere observation of cell layer mechanical properties. In fact, the active role of the cells in the tissue will determine the mechanical and dynamical behavior of the tissue, and also the ability to keep and restore its integrity.

1.1.2 Cell aggregates in 3D environments

The formation of multi-cellular aggregates from individual cells is known as cell clustering [22]. In this process, the generation of adherent junctions is also a fundamental aspect that determines aggregate mechanical properties as in epithelial monolayers (Figure 1.1A). It has been observed that cell-cell contacts regulate not only the mechanical behavior of cells but also its metabolism, life cycle and protein expression [23–26]. In addition, cell migration also determines the cell clusters generation and morphology. In fact, migration is highly regulated by chemical and mechanical stimuli from other cells and its environment [26–29].

However, there are many differences between monolayers and 3D clusters. Cell distribution and morphology are completely different in 2D and 3D environments. In Figure 1.2A, we show an image of a cell spheroid, that is a common 3D spherical structure generated by different cell types [30–32].

In 2D cultures, oxygen and nutrients are highly available and homogeneously distributed since all cells are in contact with culture medium. Otherwise, cells in the center of a 3D cluster may find low levels of oxygen or nutrients depending on the cluster size [33–35]. In fact, cluster core can even become necrotic in these cell structures. Moreover, 3D *in vitro* cultures are usually embedded in gels of extracellular matrix, that reduce even more nutrient and oxygen levels in the cell

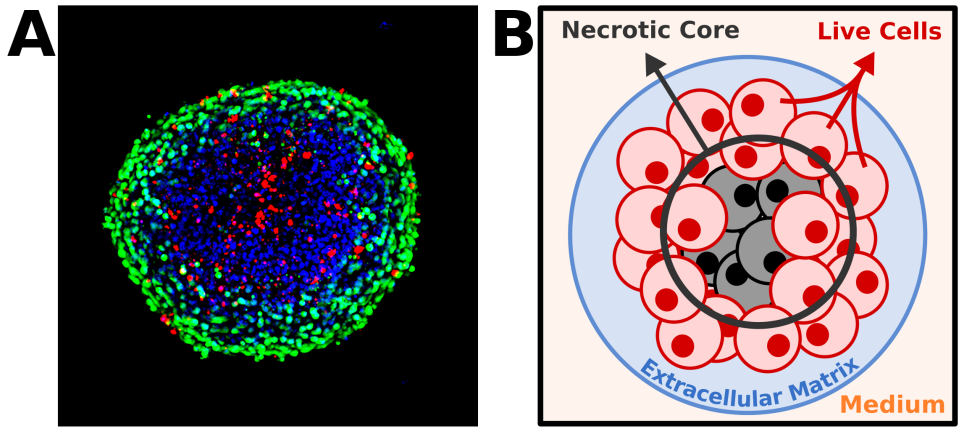

Figure 1.2: Cell aggregates in 3D. (A) Reconstruction of a 3D cell spheroid using confocal microscopy. Adapted from Molecular Devices gallery. (B) Representation of a cell spheroid in a 3D culture. Cells in the cluster center are necrotic due to the lack of oxygen and nutrients.

aggregates (Figure 1.2B). Hence, mass transport and cell consumption must be considered to determine the viability of these multi-cellular systems.

Cell cluster formation is necessary for many biological processes. For instance, they are present in tissue formation during different stages of embryonic development. Also, they are essential to regulate hormonal activity in pancreatic cells [36] or protein expression in bone marrow cells [25]. On the other hand, cell clustering is found in several diseases too. Cancerous tumor formation and spreading is intimately related to 3D aggregates. Moreover, drug penetration in tumors is affected in the same way that nutrient and oxygen transport [37, 38]. Thus, the effectiveness of drug-based treatments may be limited depending on the size of cell aggregates. Finally, cell clustering has been also used in 3D tissue printing, relying on spheroid fusion and aggregation [39].

1.2 Computational modeling of multi-cellular systems

Here we show a brief state of the art in the mechanical modeling of multi-cellular systems. This section is based on several excellent reviews of this topic [40, 41]. In summary, we exhaustively describe a category of discrete modeling approaches that are known as agent-based models. In addition, we also mention some remarkable examples of continuum models. Finally, we analyze some recent hybrid models and how the combination of several modeling approaches is useful to overcome their individual limitations.

1.2.1 Agent-based models

A agent-based models is by definition a discrete modeling approach. The main characteristic of these models is that cells are represented as separate units in the system. In contrast, continuum models do not consider cells as independent entities and the mechanics of the biological system is based on macroscopic properties. This fact implies that it is easier to represent the spatial inhomogeneities and variability inherent to biological systems in agent-based models, or at least in a more direct and intuitive manner. In addition, the recent improvements in experimental imaging techniques also facilitate the observation of histological scale phenomena. Hence, agent-based models can be fed with more information about the lower scale mechanics and cell behavior.

The modeling community is adopting agent-based models to simulate a wide variety of complex multi-cellular systems. They are becoming more popular every day since they naturally provide a direct description of the cells and their interfaces. In addition, they provide a clear strategy to study the emergent behavior of many multi-cellular systems. Historically, these models were computationally expensive, and some of them were complex to implement. In fact, it is needed a reasonable number of cells in the simulation to represent the mechanics at the tissue level. Moreover, agent-based models need to spend computing power not only on representing cells, but also to compute interactions between them. However, the continuous decrease of computational power costs has made possible to run these models even on personal computers. Further, there is an increasing number of open source applications and libraries that use this modeling approach nowadays. For instance Morpheus [42], CompuCell3D [43], Chaste [44], CellSys [45] or SEM++ [46] are popular tools that relies on agent-based models.

We borrow the categorization of the different types of agent-based models from the work of Van Liedekerke and Drasdo [41]. Basically, agent-based models can be organized in two families defined by cell spatial representation: lattice and off-lattice models. In the first family, cells positions and representation are spatially linked to fixed lattices. On the contrary, cells in off-lattice models are not constrained to a predetermined spatial discretization.

Lattice models

Lattice models can be divided into three major types: a lattice site is occupied by many cells (type A), a lattice site is occupied by exactly one cell (type B) and a cell occupies several lattices sites (type C or Cellular Potts model). These models only consider cell position except for a special type of model: the lattice gas cell

automata (LGCA). LGCA models also consider cell velocity, and, actually, we can put them in a different category from the rest (type D). Nevertheless, LGCA models usually represent several cells in the lattice site like the type A models.

In type A models, each lattice site is larger than the cell size as shown in Figure 1.3A. Hence, processes such as cell migration and division may occur in the same lattice site or between neighboring sites. For instance, when a cell divides and the lattice site is still not filled, the cell count in that site is increased. Otherwise, the closest non-filled site increases its number of cells. Moreover, cell exact position is not resolved in this type of lattice models. However, they clearly define the compartment or lattice site where the cell is located. One of the main advantages of these models is the low computational cost for a high number of cells. Type A models can even represent efficiently systems on the scale of centimeters. In fact, these models have been used as a coarse-grained model of type B models since they are intimately related [47]. On the other hand, cell size, exact position and shape are not considered. Furthermore, all dynamic phenomena are represented as jump-type stochastic processes.

Type B models can be described as a particular case of the type A models that only simulates one cell per lattice site (Figure 1.3B). These models are extensively used in cancer modeling to study tumor growth and morphology [48, 49]. Cell volume is related to the volume of lattice site and, in contrast to type A models, cell position is precisely defined. Despite regular lattices are commonly used, there are also type B models that rely on lattices generated using Delaunay triangulation and Voronoi diagram [50, 51]. In addition, cell growth and division can exert forces on neighboring cells and displace them. For example, when a cell is dividing surrounded by other cells, a neighboring cell is moved to its closest free site. Then, the daughter cell occupies the free position that neighboring cell left. This shifting method can be used to simulate growth kinetics of monolayer and 3D cell clusters. However, only rigid body movements are simulated in this modeling approach, and cells cannot be deformed or compressed. Type B models are also a good choice for large-scale simulations since they are computationally cheap. They are more expensive than type A, but, in general, better than other agent-based models in this aspect. Here the dynamic cell processes are stochastic too, like in Type A models. Although cell shape is represented here, it depends on the lattice geometry and it is not a cell property.

Cellular Potts models (or type C) are based on the minimization of a function that defines the energy in the system [52–55]. Cells are represented in more than one lattice site and, therefore, cell size and shape are considered in this approach as shown in Figure 1.3C. Cell migration and morphology changes are computed

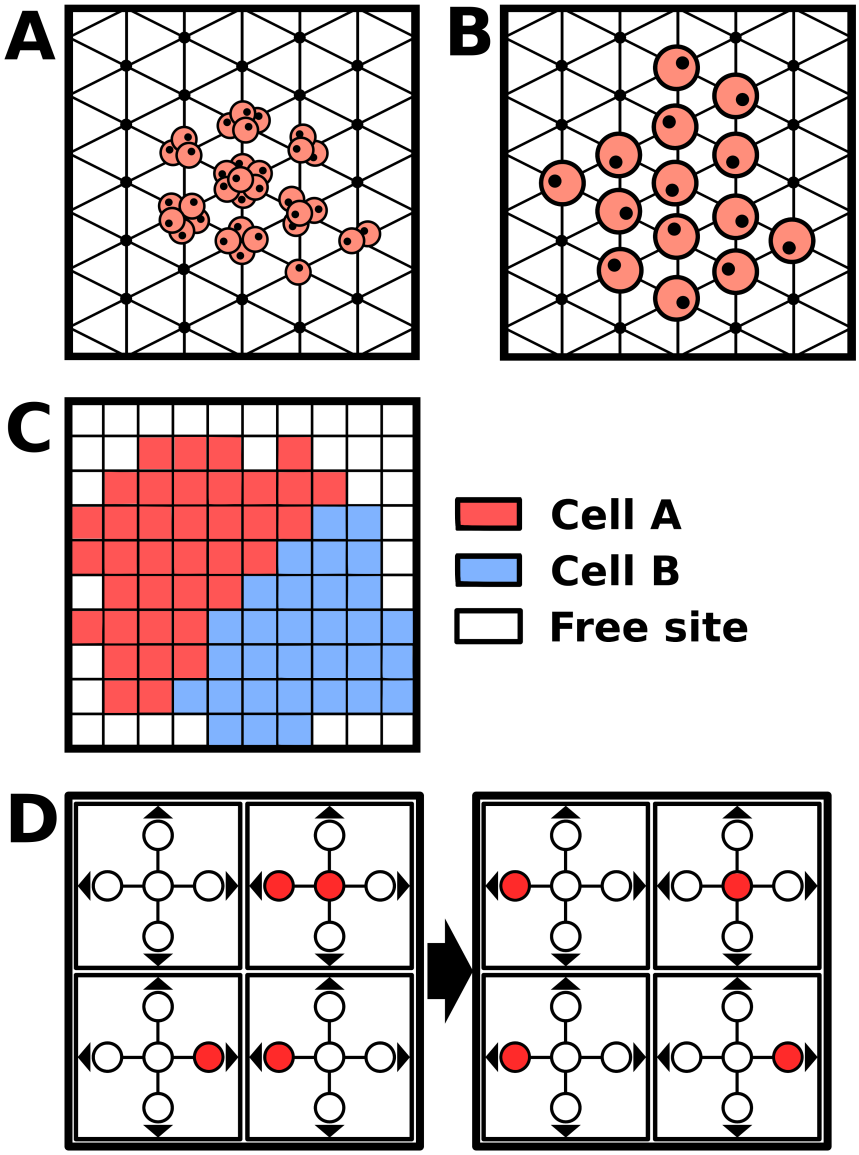

Figure 1.3: Types of lattice models. (A) In lattice model type A, each lattice site can be occupied by more than one cell. (B) Only one cell can be located in each lattice site in type B models. (C) In Cellular Potts models, one cell is represented in more than one site. (D) In LGCA models, Each lattice site is composed by cell position and several velocity channels. Usually, lattice site is also occupied by more than one cell as in type A models.

using a stochastic method (Markov chain Monte Carlo). In Potts models, the state of a randomly chosen lattice site is defined by an energy function. In particular, these models use the Metropolis algorithm with the effective energy variation to determine if the lattice site changes its state. These models can also simulate cell-cell adhesion and cell-substrate interaction. In addition, Potts models are able to represent some cell mechanical properties but, however, cell behavior and volume are usually coupled to cell motility. Although some authors consider Cellular Potts models to be excessively phenomenological, they have been successfully applied to describe and simulate the mechanical behavior of cells and tissues in many occasions. These models are popular in 2D and quasi-3D simulations since their computational cost is not very high. Also, they are able to naturally reproduce biological systems with high cell density.

Finally, LGCA models (or type D) are usually designed as a special case of type A models. Nevertheless, these models include cell velocity and not just its position [56, 57]. The main characteristic of LGCA is that particles dynamics emerges from probabilistic interactions but deterministic transport step (Figure 1.3D). Each LGCA lattice site has a number of velocity channels equals to the number of neighboring sites. In contrast to type A and B, cells can move in one time step more than one lattice site. These models have been extensively applied to fluid dynamics simulations due to they consider mass and momentum conservation.

Off-lattice models

Off-lattice models can be divided into two categories: center-based models (CBM) and deformable cell models (DCM). The first type represents cells as a non-deformable particle located at the cell center. Usually, the cell interactions are based on forces or potentials between the centers. On the contrary, deformable cell models represent cell shape accurately and cell morphology changes are computed in detail.

Center-based models (CBM) represent cells as simple geometrical objects such as circles, spheres or ellipsoids as shown in Figure 1.4A [58–60]. Basically, each cell is ruled by motion laws in analogy to physical particles. Usually, these equations are a sum of different forces. For instance, it is common to find in this approach frictional forces, cell-cell interaction forces or migration forces. In particular, friction is related to passive mechanics of cell cytoskeleton but also to dissipative forces of interacting cell membranes. In addition, migration forces have been modeled as stochastic random forces, depending on chemical cues or even related to extracellular matrix mechanical properties [61, 62]. Cell-cell interaction forces usually present a repulsive and an adhesive term. There is a wide range of approaches used to

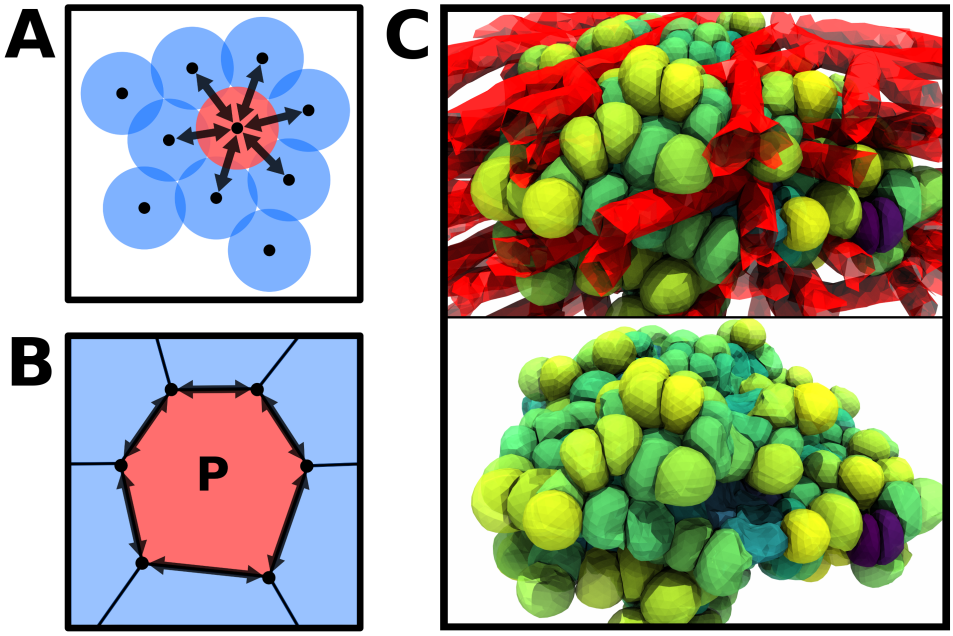

Figure 1.4: Types of off-lattice models. (A) Cell interaction forces are applied to cell centers in CBM. (B) In VBM, cortical tension and adhesion forces are computed in the cell vertices. Also, VBM usually considers a hydrostatic pressure that depends on cell area/volume. (C) Example of a DCM in 3D. Cells interact with a vessel network mesh while they grow and divide.

model these forces; from simple linear springs to Lennard-Jones potential or Herz contact models. This mechanical problem is commonly computed using sparse symmetric matrix solvers after all the former forces are determined. Interestingly, the computing time can be notably reduced using friction with the medium and avoiding the explicit matrix resolution in some cases [46, 63].

In CBM, cell volume can be manipulated to simulate cell growth during the cell life cycle. Moreover, cell division is trivially reproduced by locating daughter cell near the parent cell. These cells will push each other away until they reach a new mechanical equilibrium. However, the division distance between cells must be handled carefully since it may produce unrealistic force peaks when cells are too close. In addition, CBM may be inaccurate when cells are too densely packed. The accuracy of the solution in these cases will depend on the interaction model chosen since the contact area of several cells may be overlapped at the same time. In any case, it is possible to add other forces related to cell volume conservation to overcome some of these issues. Some authors have included a Voronoi tesselation related to the cell centers that it is adequate to approximate cell surface and volume in densely aggregated tissues [64, 65]. Nevertheless, the Voronoi diagram is not

bounded by definition and it fails to represent isolated cells or tissue boundaries. Some solutions have been proposed to solve this problem using a circle associated to the cell particle [66, 67]. In general, CBM are more expensive computationally compared to lattice models. This limitation can be overcome using parallelization techniques, but they are not trivial to implement.

Deformable cell models (DCM) represent the cell body as a deformable object, that is a discretized approximation of the cell geometry [68–71]. In other words, each cell is composed of several nodes connected by segments in 2D or a triangulation of its surface in 3D. In the case of 2D DCM, there is a particular type called Vertex-based Model (VBM) that is used in densely packed systems [13, 14]. These models only consider the vertices of the cell, while the space between cells is ignored (Figure 1.4B). VBM compute cell adhesion, cortical tension, and contraction forces on these vertices. The edges of the cells are commonly modeled as springs with an added dissipative term. In addition, the area/volume is related to an internal pressure. Further, the optimal configuration is usually analyzed using energy-based methods. Moreover, there is a type of DCM known as subcellular element method (SEM) that includes subcellular details. We find a few works that include the cell cytoskeleton and even the cell nucleus in 3D [72, 73]. There is also examples of SEM in 2D that consider the internal components of the cell [74].

To conclude, DCM have been used to reproduce many mechanical phenomena successfully. However, the computational costs of these models are notably higher than the rest of the agent-based models presented before, especially when the DCM is used to simulate 3D systems. On the other hand, they offer an excellent level of detail of the cell shape and the mechanical interactions compared to other models (Figure 1.4C).

1.2.2 Other modeling approaches

Continuum models

Continuum models have been used to model tissue mechanics for a long time [75–81]. In contrast to agent-based models, these models do not represent directly individual cells in the tissue. Instead, tissue mechanics is defined by constitutive laws that are related to cell life cycle, transport of chemical substances or cell migration. These models are a good choice to reproduce the mechanics of large-scale biological systems such as organs or large tissue volumes. On the other hand, constitutive laws can be difficult to define when several biological processes are occurring simultaneously, and this will dramatically determine the model reliability.

In fact, these models tend to grow in complexity very fast in heterogeneous systems due to coupled biophysical phenomena.

Basically, the mechanical problem resolution is based on solving partial differential equations of mass and momentum balance. The Finite Element Method (FEM) is one of the most applied technique [76–79, 81]. Moreover, other authors use derived methods such as Immerse Boundaries Method [69] or Smoothed-particle Hydrodynamics (SPH) [82]. Continuum models have been applied to different biological processes such as bone mechanics and remodeling [76, 77, 79] or wound healing and tissue regeneration [78, 81].

Hybrid models

We define a hybrid model as the combination of two or more models that were described above. Hybrid models are usually developed to overcome the intrinsic limitations of its own individual models. Nevertheless, one of the main drawbacks is that their implementation may be more complex since models must share information mutually. In fact, the interfaces between models must be carefully designed to avoid a performance loss and unexpected behavior in the simulations.

There are multiple examples of hybrid models in the current literature. Although the possible combinations to build a hybrid model are countless, we will try to illustrate some interesting modeling approaches that have been developed in the recent years:

- A continuum model combined with an agent-based model to simulate angiogenesis developed by Milde *et al.* [83].
- A center-based model combined with a vertex-based one to simulate wound healing developed by Mosaffa and Muñoz [84].
- A center-based combined with a deformable cell model to simulate cell interaction in 3D developed by Odenthal *et al.* [68].
- Multi-scale combination of a Potts model and a continuum model developed by Alber *et al.* [85].

Hybrid models are especially adequate to represent multi-scale and multi-level systems. A low resolution but computationally cheap model may be used as a coarse-grained approach of a more detailed and costly model. In particular, the combination of models in different levels can simulate large scale problems (p.e. organs) retaining lower scale details and heterogeneity.

1.3 Motivation and Objectives

This thesis is focused on exploring and developing novel hybrid approaches to model multi-cellular systems. In particular, we combine the Finite Element Method (FEM) with agent-based models in two different ways to study 2D and 3D cell structures. We aim to design frameworks that are based on the combination of simple individual models. In addition, these hybrid models must be flexible enough to simulate a variety of biophysical phenomena, but also easy to be implemented.

First, we propose a combination of an agent-based model and a continuum material model to study epithelial tissue mechanics. In particular, we use a center-based model to describe the individual cells in our hybrid approach. However, cell shape representation is extended using a Voronoi diagram of the cell centroids. Moreover, we combine the former discrete approach with a continuum material model. We map the cell geometry and the forces generated in the agent-based model to a mesh that represents the continuum tissue material. This mechanical problem is solved using the Finite Element Method. Finally, the results of the material deformation are fed back to the agent-based model as cell displacements. Therefore, we demonstrate how this approach takes advantage of the global mechanical properties that emerge from cell interactions in the agent-based model. Further, we compare and validate our hybrid approach with previous experimental and computational studies on epithelial tissue mechanics. Our analysis includes both topological and mechanical description of biological processes related to monolayers: tissue proliferation, collective motion and cell jamming, and cell migration.

Second, we propose a combination of an agent-based model and a continuum reaction-diffusion model to study 3D cell aggregate formation. We describe cells using a simple center-based model, that is extended with an independent life cycle and health model for each cell. Otherwise, we determine the distribution of the oxygen concentration in the system with a reaction-diffusion model, that is directly affected by the agent-based model. In fact, cell density alters the oxygen diffusion constant and adds oxygen consumption. We solve this problem using the Finite Element Method. Similarly, oxygen concentration affects cell life cycle and health model of the discrete approach. In fact, cells may stop proliferating or even die if the oxygen concentration is too low in their location. Finally, we compare and validate our results with different studies of 3D cell clustering.

1.4 Outline

This thesis is divided into six chapters. The first and the last chapter describe the background of the multi-cellular systems and provide a global overview of this work.

The rest of chapters can be separated into two blocks. The first block is formed by Chapters 2, 3 and 4. In this block, we describe a hybrid approach to simulate epithelial monolayer mechanics. The second block is formed by the Chapter 5, that describes a different hybrid model to simulate 3D cell cluster formation. We show a more detailed description of the chapters below:

- In this chapter (Chapter 1), we describe the background of the biological problems. We summarize different relevant aspects of epithelial monolayer mechanics and 3D aggregates that have determined the development of this work. In addition, we review the state of the art of the different models used to represent multi-cellular systems. Finally, we clarify the motivation of this thesis and the objectives of these hybrid modeling approaches.

- In Chapter 2, we show a hybrid modeling approach applied to a topological analysis of a proliferating epithelial monolayer. In particular, we study how monolayer topology is affected by cleavage plane during cell division, cell-cell interaction forces and boundary conditions.

- In Chapter 3, we extend the framework shown in Chapter 2 to explore cell jamming and collective motion. We study how cell motility and cell jamming process are affected by cell-cell interactions and passive mechanical properties.

- In Chapter 4, we apply the previous modeling approach to collective cell migration phenomena. Here, we extend our framework to consider cell contraction forces and cell-substrate interaction forces (cell crawling and purse-string). We simulate two relevant collective migration processes: collective durotaxis during monolayer expansion and gap closure.

- In Chapter 5, we show a hybrid modeling approach to simulate 3D cell clustering. We analyze how cluster formation and growth is affected by cell-cell interaction forces, oxygen concentration, initial cell distribution and cell size. In addition, we study how oxygen spatial distribution changes depending on cluster size, cell oxygen consumption, and other biophysical parameters.

- In Chapter 6, we show the general conclusions of this work. Further, we discuss some possible future lines to expand our modeling approaches and other biological problems that can be simulated in these frameworks.

This document and its supplementary material are accessible from:
`https://m2be-storage.unizar.es/pydio_public/ismael-thesis`

2

Epithelial Monolayer Topology

Contents

This chapter is published as:

Ismael González-Valverde and José Manuel García-Aznar. *A hybrid computational model to explore the topological characteristics of epithelial tissues.* International Journal for Numerical Methods in Biomedical Engineering, Vol. 33, Issue 11, e2877. February (2017).

2.1 Introduction

Cells in the epithelial tissue layers commonly present a characteristic geometry that can be represented as polygons, which share their sides with their neighboring cells. Usually, the prevailing polygon type in the apical cell surfaces is the hexagon. The hexagonal cell patterning maximizes the space that fills each cell in the tissue [9]. Nevertheless, in specific conditions such as proliferating tissue, the distribution of the cell geometries is not completely regular, although it is not random either. For instance, cells of proliferating epithelial layers in metazoans form irregular lattices, where the distribution of polygon types remains constant [12]. The topology of the epithelial monolayers and, therefore, the polygon type distribution is strongly dependent on cell proliferation [9]. During the mitotic state, cells increase its size pushing neighboring cells and modifying the packing structure. Additionally, cell rearrangements occur in the monolayer when the mitotic cell divides.

The structural integrity of the tissue directly depends on the cell organization, but also on the mechanical properties of the cells. The cytoskeleton of the cells is connected by cell-cell junctions forming a junction network in the tissue, which transmits the adhesion and contractility forces that each cell exerts to its neighbors. Therefore, junctions dramatically determine the tissue mechanical properties [11, 16]. Furthermore, passive mechanical behavior of the individual cells is determined by the properties of the cell body, mainly due to the cytoskeleton and the cytosol [86].

In the literature, we can find many computational studies that numerically simulate different aspects of the epithelial tissue topology. For instance, *Gibson et al.*[12] mathematically modeled the effect of the cell division on the topology of the metazoan epithelia using a probabilistic Markov model, but without taking any mechanical consideration or representing the spatial distribution of the tissue in the space. To consider the epithelial tissue mechanics, we could distinguish between two main types of computational approaches that represent epithelial tissues. First, those focused on a discrete approach, where epithelial cells are simulated by individual discrete components. Second, those models that consider the cell monolayer as a continuum medium, where cells are not simulated as individual objects. Actually, modeling individual cells in the epithelial tissue facilitates the simulation of proliferation and cell-cell interaction [41]. Within this kind of models, it is remarkable the number of models that use a vertex-based approach [13, 14, 87–91]. One of the reasons of its extended use is that the vertex-based models are suitable for representing deformable cells. For example, *Farhadifar et al.*[13] developed a 2D network model using a vertex-based approach to simulate the effect of the cell mechanics on the topology. Using the minimization of a potential

function, they considered the forces generated on the junctional network to simulate the effect of cell adhesion and contractility on the epithelial tissue. Additionally, *Aegerter-Wilmsen et al.* extended these works by studying the polygon distribution of the mitotic cells on the tissue and also included cell growth in their model [14]. However, there are other studies that use a center-based approach [92–95]. For instance, *Mosaffa et al.* [94] focused their work on modeling curved monolayers using a center-based approach, interestingly, they connected cells using a Delaunay triangulation to model the mechanical behavior of the tissue. *Ramis-Conde et al.*[93] also modeled curved epithelial monolayers using the center-based approach but they focused on the intravasation of cancerous cells, which is regulated by mechanical and chemical interactions with the tissue. In addition, other studies also implemented subcellular components of the cell but this approach heavily increases the computational cost [96].

Moreover, continuum models are less used in epithelial tissue modeling, but there are some examples of this approach. To calculate stresses and deformations in the tissue, *Brodland et al.*[97] modeled embryonic epithelia using a constitutive model considering that the monolayer is a continuum cellular fabric. Furthermore, *Gibson et al.*[98] focused on the effect of the cleavage plane of mitotic cells on the epithelial topology. In this study, they used two separated models to simulate the topology, a Monte-Carlo model and a finite element (FE) based model using rod-like elements to simulate cells. Although a 2D simplification of the tissue appears to be enough to describe the topology and the mechanics, some recent models are considering 3D conditions on a continuum-based approach [99]. There are other models in 3D that use individual cell approach to study the mechanics in cell cultures and colonies [100, 101]. These studies include detailed cell contact forces and motion laws to describe collective cell behavior.

The main aim of this work is to computationally simulate the effect of cell dynamics on the epithelial tissue topology. We consider that cell proliferation and the mechanical cell-cell interaction regulate the individual cell movement generating rearrangements at the tissue level. These rearrangements determine the stable configuration of the cells in the tissue and consequently the topological equilibrium. Therefore, we show a novel phenomenological framework that simulates the dynamics of the epithelial tissue using a hybrid approach, which integrates both approaches: an off-lattice agent-based model and a continuum mechanics model. The agent-based model represents cells as individuals and it considers cell-cell interactions and the cell cycle. With this approach, we achieve a tight control of the individual information of each cell in the tissue. In contrast, continuum model represents the epithelial tissue as a continuum material and it defines how the monolayer behaves at the mechanical level.

Hence, with this hybrid approach, we investigate how the proliferation and mechanical parameters affect the simulation outcome. In particular, we mainly focus on the effect of proliferation rate, mitotic behavior, stiffness and interaction forces. Besides the polygon distribution, we also analyze the influence of these parameters on the average cell area. Furthermore, we analyze the simulation results of the framework under different boundary conditions, which include unconstrained, partially constrained and fully constrained conditions.

To evaluate the potential of our numerical approach, we compare our numerical results with the experimental results from *Gibson et al.*[12], *Farhadifar et al.*[13], *Aegerter-Wilmsen et al.*[14] and *Gibson et al.*[98]. In these experiments, they analyzed polygon distribution of Drosophila epithelial tissue during its development. They studied the polygon distribution of the entire cell population and the mitotic cell population. Actually, we show that the results of our approach are compatible with the topological characteristics of these experimental data. Finally, we discuss the impact of our results on improving the knowledge of growing epithelial tissue topology.

2.2 Methods

We simulate the epithelial tissue as a continuum medium built up from individual cells, but whose cytoskeletons are connected in a junctional network. These junctions between cells bring continuity to the tissue, determining its mechanical properties. Hence, we assume that cells generate interaction forces through the junctional network that drive cell movements and regulate cell shape.

Therefore, we use a hybrid approach that combines an off-lattice agent-based model and a continuum elastic cell material model. In the agent-based model, each cell is simulated by a discrete point and its associated polygon, which is obtained from the Voronoi diagram. In this model, we evaluate the interaction forces that exist between cells that define the epithelial tissues. Furthermore, the cell proliferation is also included in the agent-based model. The cycle of each cell is considered on this approach and we model aspects such as the duration of the cycle phases, the mitotic cell dilation and the cleavage-plane of the cell division. Otherwise, we model the passive mechanics of cells considering them as a uniform cell material. We solve the mechanical problem using a finite element approximation, where forces are determined in the discrete agent-based model. As a simplification, we consider that this cell material simulates the mechanical properties of the whole cell, including cell nucleus, cytoskeleton and cytosol. Thus, cell displacements are

the result of the cell material deformation, which is due to the forces that the cell-cell interaction generates on the tissue.

Next, we present the main mathematical and computational implementation aspects of this work. First, we define the agent-based model to simulate cell dynamics in the tissue, describing cell-cell interactions and cell proliferation phenomena. Moreover, we simulate the cell cycle of each cell individually to model their proliferation in the tissue. Second, we present the mathematical model proposed to simulate the passive behavior of the cell material, which is approximated using the finite element method to solve the mechanical problem. Finally, the framework workflow and the integration of both models are described in detail among other additional computational considerations.

2.2.1 Modeling active mechanical behavior of epithelial cells: an agent-based approach

The basis of the agent-based approach is that each cell is simulated as a discrete and separated unit. To define the epithelial layer morphology in our framework, cells are represented as discrete points, in particular, as the centroid of each cell. Likewise, cell morphology is defined by the generation of the Voronoi Diagram from these points as seen in Figure 2.1A. Consequently, each cell has an associated polygon that determines its geometrical representation. Due to this geometrical approach, epithelial layer morphology directly depends on the position of the cell centroids. A detailed description of the Voronoi Diagram can be found in Text S2.12.

The result is a tessellated representation of the tissue that maintains its mechanical continuity. The hybrid nature of our framework lies on its representation, we keep a continuum medium that simulates the cell layer as a material but we also consider each individual cell. Despite being contained in the continuum material, cell remains as a discrete entity represented as a polygon and it keeps its own information separated from the other cells.

However, Voronoi diagram presents some limitations when is used to represent the geometry of cells in the epithelial tissues. First, the most external cells are represented as an unbounded infinite polygon due to the nature of the diagram. Second, two cells that are separated by a distance much larger than their radii may generate an unreliable Voronoi polygon. To avoid these geometrical artefacts, we use the alpha shape technique to bound the representation into a finite plane. The alpha shapes are a family of simple curves that reconstruct a shape from an associated set of points [102]. In our case, we generate a discretized circumference around each cell using the cell radius. Later, we use these points from the circumferences to generate the alpha shapes and, then, we intersect the alpha shape with our Voronoi diagram.

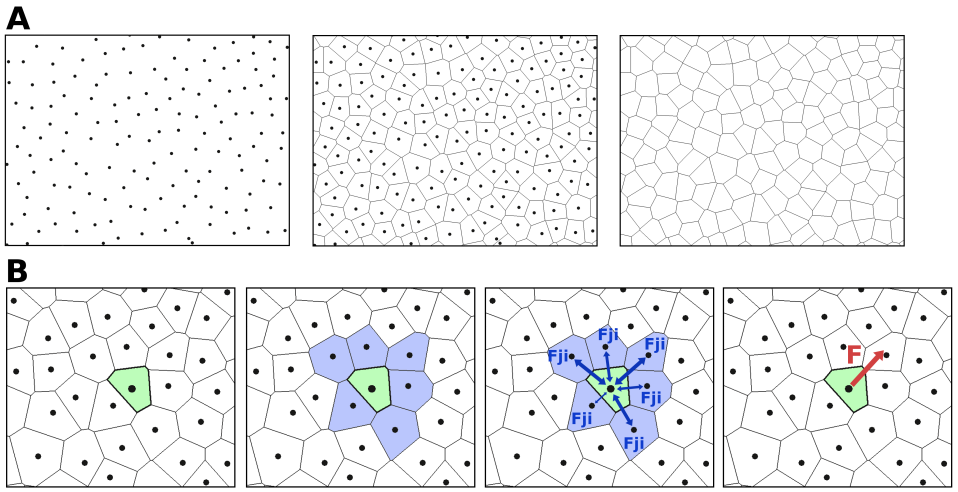

Figure 2.1: Cell geometrical representation and forces calculation. (A) Voronoi diagram is generated from cell centroid position. Each cell is represented in the monolayer by its associated Voronoi polygon. (B) Interaction forces are calculated considering the neighboring cells for each individual cell. First, we determine neighboring cells using Voronoi diagram, cell shares one side of its polygon with each of its neighbors. Second, each neighbor cell applies a force on the cell, which is given by the cell-cell interaction model. This model uses the distance between the cell centroids to calculate the interaction forces. Finally, total forces applied on the cell is obtained by the sum of these interaction forces.

Cell-cell interaction

In the epithelial tissue, cells actively interact with all the adjacent cells generating forces among them. Actually, we assume that this is a consequence of the interaction of their cytoskeletons and junctions. Hence, we model the mechanical cell-cell interaction using the Lennard-Jones potential (V_{ji}) in equation 2.1:

$$V_{ji} = 4\varepsilon \left[\left(\frac{\sigma}{r}\right)^{12} - \left(\frac{\sigma}{r}\right)^{6} \right] \tag{2.1}$$

Where (r) is the distance between two cells, σ is the distance at which potential V_{ji} is zero and the parameter ε is the potential well intensity. This potential has a repulsive and an attractive term. The attractive term models the contractility and adhesion of the anchoring junctions between cells, which tend to keep cells together. In contrast, the repulsive term models the passive cytoskeleton interaction that occurs if cells are too close. This repulsive term also defines the forces generated after the cleavage on cell division [103]. The cell-cell interaction force (F_{ji}) is obtained after we derive equation 2.1, as it is shown in equation 2.2:

$$F_{ji}(r) = -\frac{dV_{ji}}{dr} = 24\varepsilon \left[\left(\frac{2\sigma^{12}}{r^{13}} \right) - \left(\frac{\sigma^6}{r^7} \right) \right] \tag{2.2}$$

We obtain the distance where the potential is minimum (r_m) solving equation 2.2 when force is zero:

$$F_{ji}(r_m) = 0 \quad \Rightarrow \quad r_m = 2^{1/6}\sigma \tag{2.3}$$

Later, we substitute σ by r_m using the equation 2.3 in the equation 2.2:

$$F_{ji}(r) = 12\varepsilon \left[\left(\frac{r_m^{12}}{r^{13}} \right) - \left(\frac{r_m^6}{r^7} \right) \right] \tag{2.4}$$

The forces generated in each cell by all the neighboring cells are defined by the equation 2.4.

The cell-cell interaction forces are exclusively determined in the agent-based model as it is shown in Figure 2.1B. We calculate the interaction of each cell with its neighboring cells. Likewise, we consider that cells are neighbors if they share any side in the Voronoi diagram representation. To solve the Lennard-Jones equation (equation 2.4), we use the distance between the centroids of the cells as r and the sum of their radii as r_m. In addition, the potential well intensity parameter (ε) is determined by a parametric analysis of the model. Therefore, we apply the sums of all the forces generated by the adjacent cells on the cell centroid.

Additionally, in order to understand how the system is affected by different interaction models, we modify the order of the potential and analyze the results in the Figure S2.1.

Cell proliferation

In the cell layer, the cell proliferation follows several phases until the cell duplicates as it is shown in Figure 2.2A (left). Before cell division occurs, the cell notably increases its size due to the formation and the splitting of chromosomes. During the mitotic state, the cell prepares itself for the division. Cell keeps growing until it reaches a certain size, then the cell divides. After cell division, cells are rearranged in the tissue until a new equilibrium is achieved, and, as consequence, a new topology emerges.

We must note that in other biological processes cells mainly grow during the interphase and not during the mitotic phase. However, in the case of proliferating epithelial tissue of the wing disk in Drosophila, cell apical area mostly changes in the mitotic phase [12–14]. Cells in this tissue alter their morphology during the mitotic phase and this causes an important increment of the apical area, which is much

greater than the cell growth during the interphase. For modeling cell proliferation, we assume that cells only increase their size during the mitotic phase and, also, that cells divide at a uniform rate [104]. In our proliferation model, we individually simulate the proliferation cycle of each cell considering two different phases as it is shown in Figure 2.2A (right): interphase ($G1$, S, $G2$) and mitotic phase. In the interphase, the cell is preparing itself for the next division, but it has no apparent changes in its morphology. Therefore, we assume in our model that the cell does not suffer any topological changes during the interphase. Furthermore, we consider that the interphase is much longer than the mitotic phase. After completing this phase, the cell starts the mitotic phase and increases its size and, in consequence, it pushes its neighboring cells altering the current topology. When the mitotic phase finishes, the cell divides into two daughter cells, which both return to the interphase (Figure 2.2B). In addition, we also consider in our model the direction of the cleavage in the division. The cleavage-plane is assumed to be orthogonal to the longest geometric axis of the cell [98].

We assume that the cell can not leave the cell cycle to enter in a resting phase ($G0$). This assumption is valid considering that our model is centered on the early development of the epithelial tissue, where the cells continuously proliferate.

In our framework, the equations that regulate cell proliferation are:

Interphase:

$$\tau^n_{phase} < \theta_{interphase} \Rightarrow \begin{cases} \tau^{n+1}_{phase} = \tau^n_{phase} + \lambda_{phase} \cdot \Delta t \\ \\ R^{n+1} = R_{initial} \end{cases} \tag{2.5}$$

Mitotic phase:

$$\theta_{interphase} < \tau^n_{phase} < \theta_{mitotic} \Rightarrow \begin{cases} \tau^{n+1}_{phase} = \tau^n_{phase} + \lambda_{phase} \cdot \Delta t \\ \\ R^{n+1} = R^n + \lambda_{radius} \cdot \Delta t \quad \text{if } R^n < R_{max} \end{cases} \tag{2.6}$$

Cell Division:

$$\tau^n_{phase} \geq \theta_{mitotic} \Rightarrow \begin{cases} \tau^{n+1}_{phase} = N(mean = 0.2 \cdot \theta_{interphase}, \\ \qquad\qquad dev = 0.1 \cdot \theta_{interphase}) \\ \\ R^{n+1} = R_{initial} \end{cases} \tag{2.7}$$

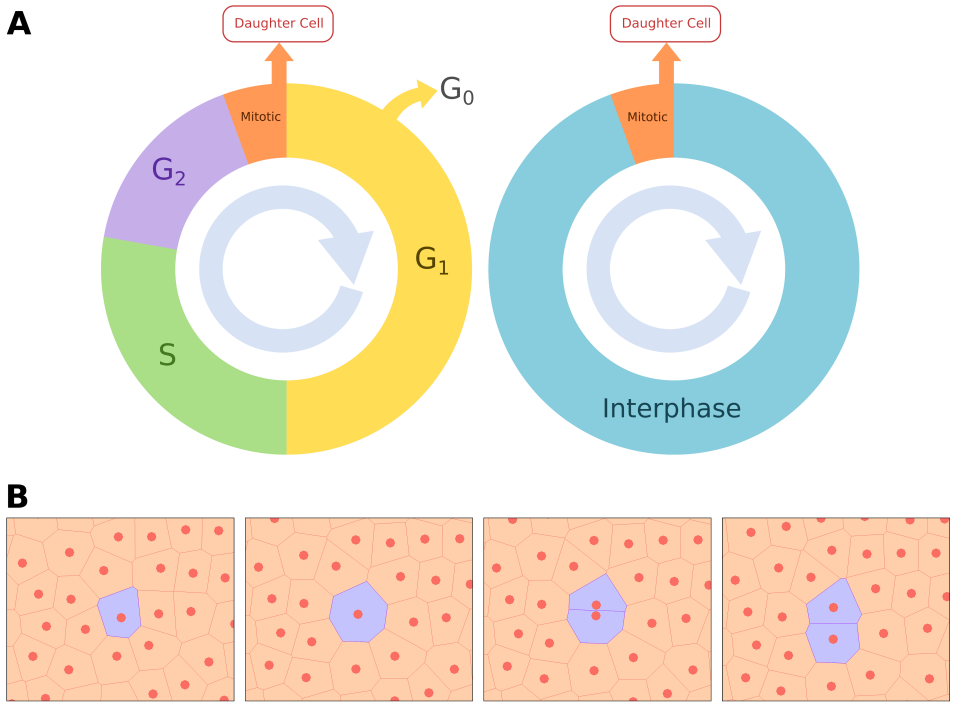

Figure 2.2: Cell cycle and proliferation. (A) Biological cell cycle is shown on the left and simplified cycle used on the simulation is shown on the right. Phases G1, S and G2 are unified as the Interphase and G0 (resting phase) is neglected. (B) Cell increases its size in the mitotic phase pushing other cells in the monolayer. Later, mitotic cell divides and both parent and daughter cells are accommodated in the monolayer.

Therefore, the time that each cell is in the interphase is determined by a counter (τ_{phase}), which is associated to time steps as shown in equation 2.5. Moreover, we use two additional parameters to model cell cycle: a transition rate (λ_{phase}), which determines the increase rate of the counter, and a threshold ($\theta_{interphase}$), which defines when this phase ends. For each cell, this counter (τ_{phase}) is increased in every time step (Δt) using the transition rate (λ_{phase}). In the interphase, we do not consider any changes in the cell geometry. This phase ends when the cell reaches the phase threshold ($\theta_{interphase}$), then the mitotic phase starts.

To represent the cell dilation in the mitotic phase, we increase the cell radius (R) in our model as it is defined in equation 2.6. This radius increment is driven by a cell dilation rate (λ_{radius}) and a maximum value of the cell radius (R_{max}). In consequence, this radius increment directly alters the equilibrium distance with its neighbors in the cell-cell interaction model. As a reaction, cells generate forces to achieve a new mechanical equilibrium. The cell divides when this phase reaches the mitotic threshold ($\theta_{mitotic}$), which lasts a specified fraction of the interphase

duration as shown in equation 2.7. In addition, every time a cell divides, this counter (τ_{phase}) is initialized for both resulting cells (parent cell and daughter cell) using a normal random distribution (N), whose mean is equal to 20% of the interphase threshold ($\theta_{interphase}$) and a standard deviation equals to 10% of the interphase threshold ($\theta_{interphase}$). After cell division, cell radius is reset to its initial value ($R_{initial}$). This computational implementation avoids unnatural synchronization of the phases of the cell cycle.

We assume that cell cleavage-plane is orthogonal to the largest axis of the cell. To determine the cleavage-plane, we directly consider the longest segment inscribed in the polygonal representation of the cell. We analyze the effect of cleavage-plane on the polygon type distribution by comparing it with cell division with a completely random cleavage-plane. After cell division, both cells are placed in this axis separated by a distance equals to the 30% of the cell radius. Figure S2.2 presents a detailed explanation about this method. We also study the effect on the topology of the distance that separates cells after cleavage in the Figure S2.4 and we conclude that it does not affect the polygon distribution.

2.2.2 Modeling passive mechanical behavior of epithelial cells: a FE-based approach

We simulate the passive mechanical behavior of the cells in the epithelial layer, assuming that the layer is a continuum medium approximated as a structural material. This cell material describes the apparent mechanical properties of the cell, which includes cell nucleus, cytoskeleton and cytosol. Therefore, to solve the mechanical problem, we use the Finite Element Method (FEM). In this analysis, we assume that the cell monolayer is under plane stress conditions. Actually, the mesh used in the FEM analysis is generated by a dynamic algorithm that is coupled with the agent-based model. It is necessary to update the mesh since there are notable morphological changes in the layer due to cell proliferation and strong cell rearrangements. In consequence, the mechanical problem can not be solved using a static mesh and the material model. The mesh used in our framework is not static, we generate a new mesh in each step of the simulation using the cell information provided by the agent-based model. This dynamic mesh is generated using a Delaunay triangulation of the geometrical representation of the cells. In particular, we use the cell centroids and all the vertices of their polygons to calculate the triangulation as it is shown on Figure 2.3A. By using this technique, we overcome the problem derived from the model simplicity and the framework is capable to adapt to a diverse range of conditions, where the morphology of the epithelial layer suffers large geometrical changes.

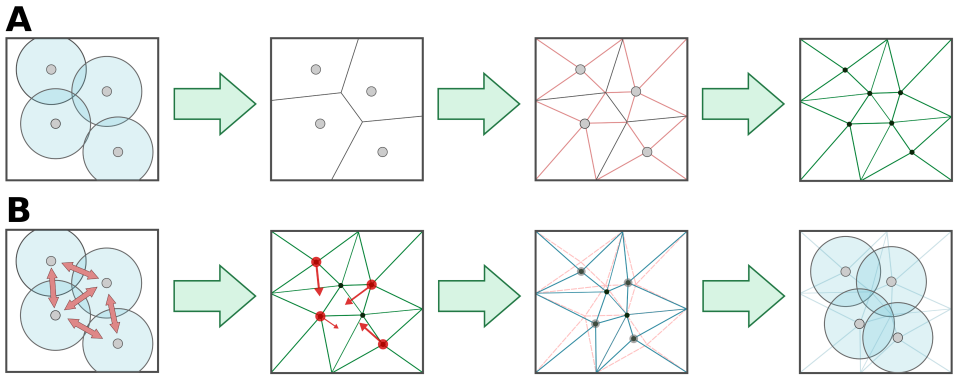

Figure 2.3: Mesh generation and forces application. (A) Mesh is generated from the Delaunay triangulation of the Voronoi diagram vertices and cell centroids. (B) Interaction forces are applied to the mesh nodes corresponding to cell centroids. Mesh deformation defines how cells move in the agent-based model.

To be precise, forces generated by cell-cell interactions cause a deformation in the material. The cell-cell interaction forces are calculated in the agent-based model. The sum of all interaction forces for each cell is applied at the mesh node corresponding to the position of the cell centroid. After FEM resolution, cell displacements are obtained by the deformation of the cell material as it is shown on Figure 2.3B. Thus, the position of the cell centroid is updated, modifying the organization of the cell layer and changing the mesh (see Video S2.6).

Boundary conditions

In this work, we also study the packing geometry of the cells under several boundary conditions. Basically, we assume three different boundary conditions: constrained, partially constrained and unconstrained. In the first case, we assume that displacements are null in the boundary of the tissue layer (Figure 2.4A). In the second case, we impose no displacements in all the sides of the boundary except one, which remains unconstrained (Figure 2.4B). In the last case, we assume free displacements in all the boundaries (Figure 2.4C).

In the scenario where the displacements in the boundary are not constrained, we assume that the cell layer is surrounded by a material with the same mechanical properties as the cell material. However, the surrounding material does not present the active mechanical behavior of the cells that the agent-based model provides. To implement this configuration, we add a regular grid to the existing mesh where cells are not present, as it is shown in Figure 2.4.

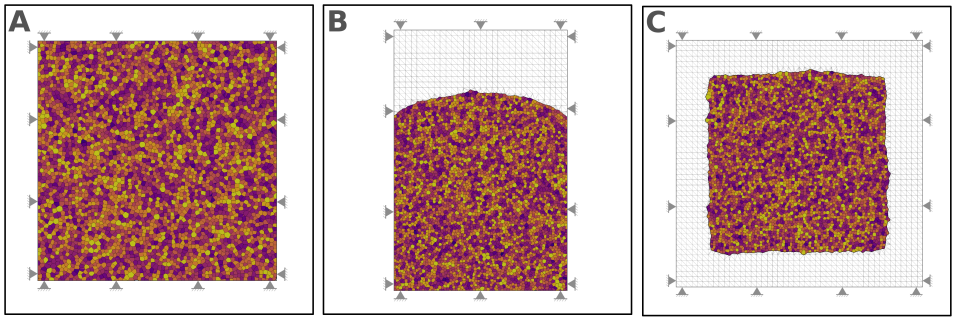

Figure 2.4: Boundary conditions. (A) Completely constrained boundary condition. (B) Free top boundary condition. (C) Unconstrained boundary condition.

2.2.3 Simulation workflow

Our framework is based on two clearly separated numerical approaches that are combined to simulate different phenomena. First, an off-lattice agent-based model that manages individual cell information and biological processes such as cell proliferation, positioning and geometry generation. Second, the finite element (FE) approach to solve the mechanical problem of the epithelial monolayer.

Figure 2.5 shows a schematic representation of our simulation workflow. Basically, we initialize the framework and, then, it enters the main loop of the calculation. We can divide this loop into several processes: cell proliferation, geometrical representation, cell-cell interaction forces calculation, mechanical problem resolution by FEM and cell rearrangement.

First, we initialize all the variables in our framework. To obtain a randomized initial position of the cells, we place them in a uniform lattice with a distance between cells of two cell radii and, then, we alter this uniform lattice applying random displacements on the cells. We assume that these random displacements are lower than the cell radius. Actually, the initial distribution of the cells has not significant impact on the cell topology on the steady state as it is shown in S5 Figure. Additionally, we use a random value from a uniform distribution from zero to the interphase threshold value ($\theta_{interphase}$) in the phase counter (τ_{phase}), which will determine when a cell enters the mitotic state. We initialize the framework parameters with the values shown in Table 2.1, unless otherwise indicated. After the variable initialization, the framework enters the main loop of the simulation.

In the proliferation process, we check the proliferation status of each cell in the agent-based model. If the cell is in the interphase, we just increase the phase counter (τ_{phase}). However, the cell enters the mitotic phase when this counter (τ_{phase}) exceeds the interphase threshold ($\theta_{interphase}$). Otherwise, if the cell is in

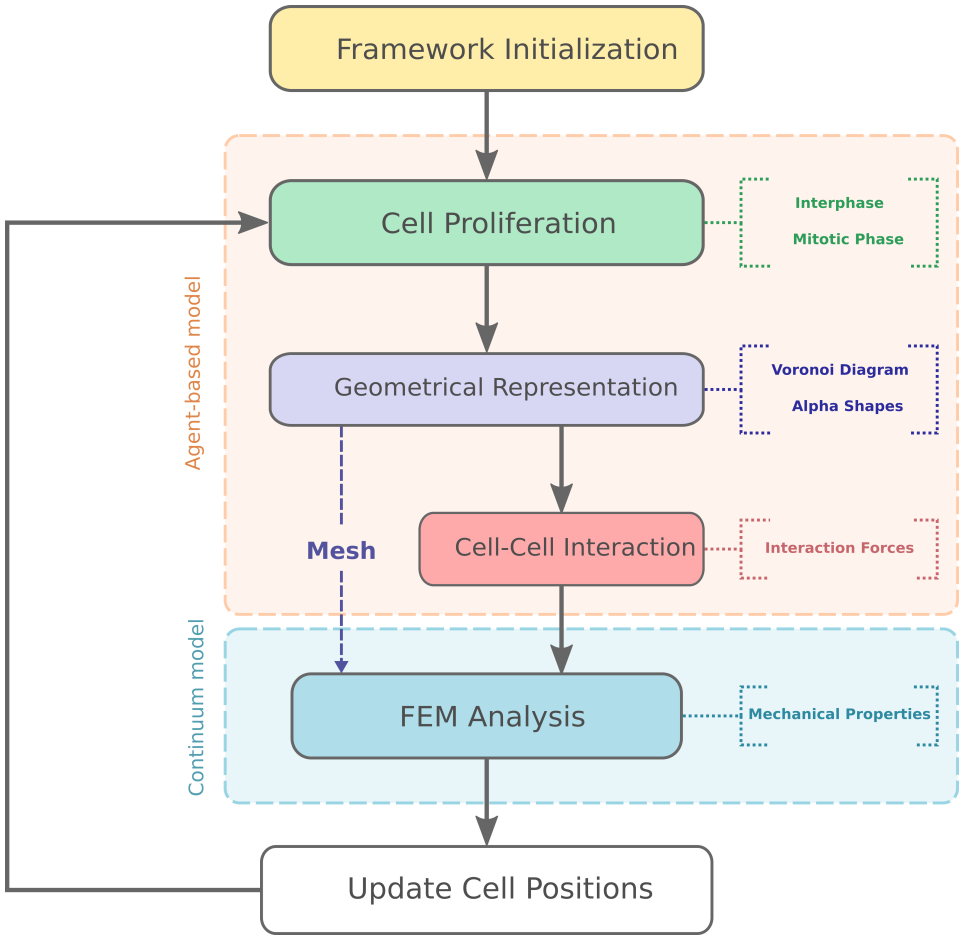

Figure 2.5: Simulation workflow. First, variables are initialized in the Framework Initialization step and, then, simulation enters in the main loop. On the agent-based approach, we analyze the status of the cell cycle and cells proliferate if the proper conditions are fulfilled. We generate the geometrical representation from the current cell positions using the Voronoi diagram. At this point, we also generate the mesh used in the FE Analysis. Knowing the neighboring cells from the Voronoi diagram, we calculate the cell-cell interaction forces for each cell. On the continuum approach, we solve the mechanical problem by FE using previous interaction forces and mechanical properties of the material. Finally, we update the cell positions from these results and we start the loop again.

General Parameters	
Initial number of cells	400
Cell radius - $R_{initial}$ (μm)	12
Total time steps	8000
Proliferation Parameters	
Cleavage plane	Oriented
Phase transition rate - λ_{phase}	0.05
Interphase threshold - $\theta_{interphase}$	100
Mitotic threshold - $\theta_{mitotic}$	105
Dilation rate - λ_{radius}	0.1
Maximum radius - R_{max} (μm)	12
Mechanical Parameters	
Young's modulus - E ($\mu N/\mu m^2$)	0.02 [11]
Poisson's ratio - ν	0.49*[11]
Potential well intensity - ε (μN)	1e−4

* Approximately incompressible

Table 2.1: Simulation parameters

the mitotic phase, its radius is increased. We check if the mitotic cell has reached its maximum size (R_{max}) and, in that case, the cell stop growing. Cell divides if the counter (τ_{phase}) passes the mitotic threshold value ($\theta_{mitotic}$). On cell division, both cells return to the interphase and we reset their phase counters (τ_{phase}). We slightly randomize their phase counter initialization to avoid the creation of artificial clusters of cells that always divide at the same time.

To generate the geometrical representation, we use the current position of the cells in the agent-based model to calculate the Voronoi diagram. Next, we generate the alpha shapes using several points located on the circumference drawn around each cell. This circumference has cell radius value as its own radius. Then, we calculate the union between the selected alpha shape and the Voronoi diagram. To generate the mesh, we obtain a Delaunay triangulation from the cell centroids and all vertices in that representation. Additionally, if the analyzed case has any unconstrained boundary condition, we create a regular grid outside the cell domain and we add it to the current mesh.

To calculate the cell-cell interaction forces, we consider the forces exerted on the cell by the neighbor cells (F_{ji}) in the current geometry. We compute the sum of all forces generated in each cell and this calculated force is associated to the mesh node corresponding to the cell centroid. Furthermore, we apply the boundary conditions and solve the mechanical problem using FEM. We obtain the cell displacements from the displacements of the mesh node on which the

cell force is applied. Finally, the framework returns to the proliferation process closing the main loop of the simulation.

In the numerical implementation of this framework, we use our own code in C++ and some third party open source libraries. We use InSilico library [105] to solve the mechanical problem by the FEM. This FEM library was previously developed in our research group and was extended in this work to include the discrete cell modeling. Furthermore, we use *CGAL* library [2] to generate and manipulate the geometry.

2.3 Results

2.3.1 Cleavage plane of the cell division influences tissue topology

To elucidate the effect of the cleavage plane of the mitotic cells on the polygon distribution, we analyze the numerical results comparing both conditions in cell division: oriented cleavage and random cleavage. These results are also compared with experimental data taken from [12, 14] to test the polygon distribution of entire cell population and mitotic cell population, as it is shown in Figure 2.6A and Figure 2.6B, respectively. We must remark that the error bars that represent the standard deviation of the polygon frequency are only shown in the Figure 2.6. The standard deviation is similar in the rest of simulations and, given that adding the bars makes the figures confusing, we do not included them in the rest of figures.

Our model reproduces the global topology of the tissue according to the experimental data presented in [12, 14]. In particular, hexagons present the highest frequency in the tissue followed by pentagons and heptagons. Analyzing only mitotic cells, our model successfully simulates the topology of this subset of proliferative cells. In contrast to the global topology, heptagons predominate in the mitotic polygon distribution followed by hexagons and octagons. Nevertheless, oriented cleavage condition in the model reproduces better the topology according to the experimental measurements in both cases. In particular, random cleavage condition shows greater differences with the experimental polygon distribution of mitotic cells. Interestingly, these results are in accordance with the experimental data shown in [98].

2.3.2 Cell proliferation regulates polygon distribution of the epithelial monolayer

We study how cell proliferation determines the tissue topology analyzing three parameters of our model related to this biological process. First, we study the effect of the transition rate parameter (λ_{phase}), which determines the duration of the

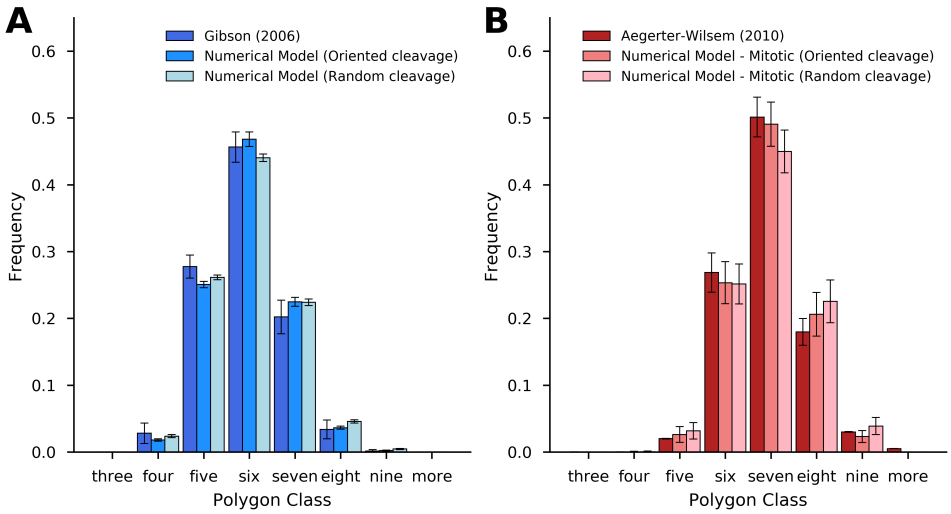

Figure 2.6: Cleavage plane of the cell division influences tissue topology. Numerical model is compared with experimental data considering shortest-axis cleavage and random axis cleavage in the cell division. (A) Global cell topology is compatible with experimental data from Gibson (2006), hexagons are prevalent in the monolayer followed by pentagons and heptagons. (B) Polygon distribution of mitotic cells is compatible with experimental data from Aegerter-Wilmsen (2010), heptagons are prevalent followed by hexagons and octagons. Shortest-axis cleavage shows a better fit than random axis cleavage in both (A) and (B). Error bars represent the standard deviation of the polygon frequency in the experimental data analyzed. In the simulations, error bars are the standard deviation of the polygon frequency when the simulation reaches a steady state.

interphase in a cell cycle (Figure 2.7A,B). Second, we examine how the increment of cell size (R_{max}) in the mitotic phase affects the polygon distribution and the average area of cells (Figure 2.7C,D,E). Third, varying mitotic phase threshold ($\theta_{mitotic}$), we study the effect of the mitotic phase duration on the tissue topology and the average area of cells (Figure 2.7F,G,H). (See Video S2.7).

Considering that the transition rate (τ_{phase}) is directly related to the proliferation rate, we observe that lower proliferation rates produce a global polygon distribution with more hexagons in proportion. In the case without proliferation, the topology of the monolayer tends to a hexagonal lattice. However, cells do not necessarily form a perfect lattice since they can reach a locally stable configuration in the steady state. Additionally, Video S2.8 shows the results of a simulation without proliferation to illustrate the model behavior in that case. Furthermore, we find an optimal transition rate value in the model (transition rate equals to 0.01) that fits better to the experimental results [12, 14]. The effect of proliferation on mitotic cell topology is not clear but it seems to increase the number of polygon sides at low transition rates. This effect could be due to the fact that –at low proliferation rates–

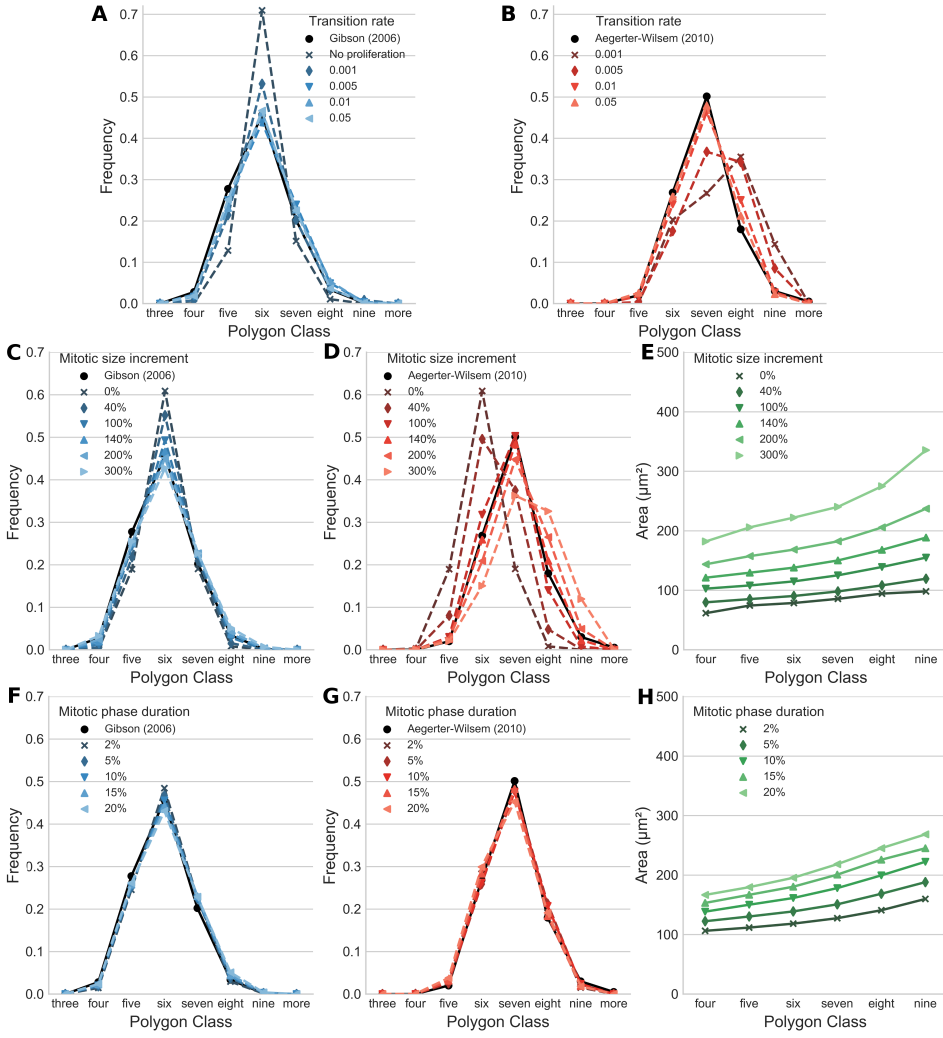

Figure 2.7: Cell proliferation alters polygon distribution. Our numerical model is compared with experimental data considering the influence of several proliferation parameters (A, B) The transition rate parameter defines how long the cell is in the interphase. Variations in the transition rate are predicted to change the polygon distribution of the entire cell population (A) and the mitotic cell population (B). (C, D, E) The magnitude of the cell dilation during the mitotic phase determines the global polygon distribution (C), the mitotic polygon distribution (D) and the average cell area (E). (F, G, H) The duration of the mitotic phase alters the average cell area (H), besides, it does not appear to affect the global polygon distribution (F) nor the polygon distribution of mitotic cells (G).

mitotic cells are sufficiently separated enough in the monolayer to avoid any kind of interaction between them. We believe that mitotic cells create distortions of the local topology that affects the shape of the surrounding cells, including other mitotic cells.

Size increment of mitotic cells is regulated by the maximum cell radius (R_{max}), which directly affects to the equilibrium distance between cells. Lower size increments show a tendency similar to low proliferation rate, actually, the observed effect is that the frequency of hexagons in the monolayer are noticeable higher compared to experimental data. In contrast, we observe that lower size increments drive the topology of mitotic cells to a distribution where polygons present a lower number of sides. In the particular case without size increment, the polygon distribution of mitotic cell population is the same as the entire cell population. Increasing the mitotic cell size causes an increment of the average polygon sides. We observe that a cell size increment of 140% (from $5\mu m$ to $12\mu m$) reproduces the experimental results, however higher values present a mitotic distribution with an excessive number of polygon sides. Additionally, average cell area also increases with the mitotic cell size. These results suggest that the size increment of mitotic cells is fundamental to determine the topology in growing tissues.

Nevertheless, mitotic phase duration has a negligible effect on the polygon distribution. It presents a slight effect on the average area of cells, which increases when mitotic phase is longer.

2.3.3 Mechanical properties of the cells and the cell-cell interaction forces modify the equilibrium topology of the epithelial monolayer

To determine how the topology is affected by the mechanical properties of cells, we analyze the apparent stiffness of cells and the magnitude of interaction forces. We simulate the monolayer with a wide range of cell stiffness values as it is shown in Figure 2.8A,B,C.

The magnitude of the interaction forces is directly related to the epsilon parameter (ε), which represents the intensity of the potential used in the model. In consequence, we use a range of epsilon values to determine the effect of the interaction forces as it is shown in Figure 2.8D,E,F.

Apparent stiffness of cells presents a negligible effect on the global polygon distribution, however it clearly affects the topology of mitotic cells. Low stiffness produces a mitotic polygon distribution with more polygon sides, while higher stiffness values have the opposite effect. Therefore, we believe that this is caused by the capability of cells to rearrange themselves in the monolayer. If the stiffness

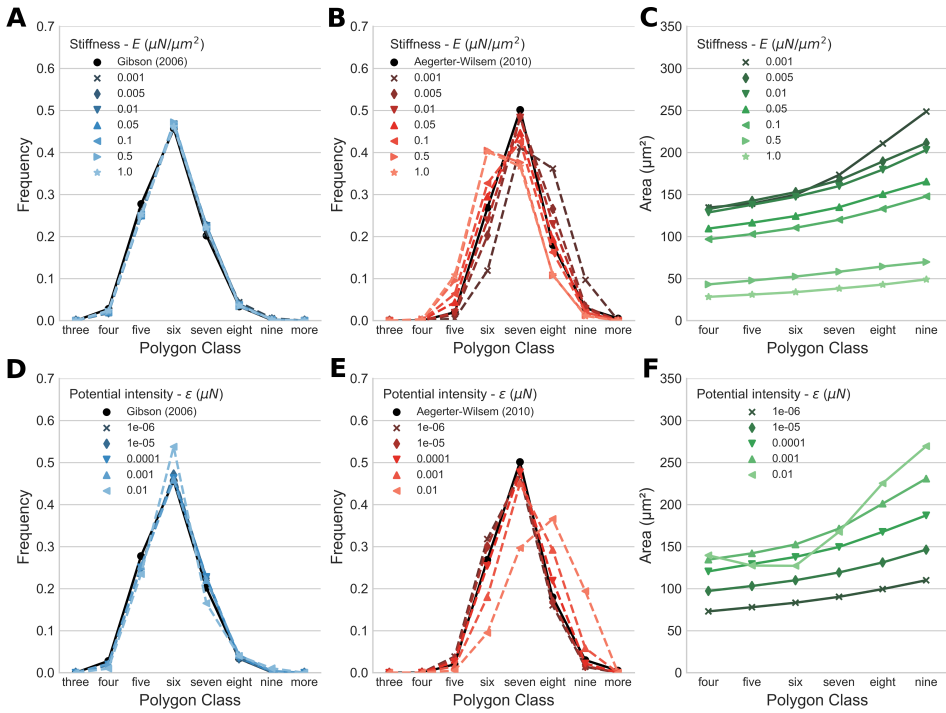

Figure 2.8: Mechanical properties of the cells modify equilibrium topology. Numerical model is compared with experimental data considering the effect of the interaction forces and stiffness. (A, B, C) Changes in the cell stiffness alters the polygon distribution of mitotic cells (B) but it does not affect global polygon distribution (A). Lower cell stiffness produces a monolayer with larger average cell area (C). Cell stiffness is represented in μN/μm². (D, E, F) Epsilon parameter in the potential is directly related to the magnitude of interaction forces. Variations in this parameter slightly affect the topology of the entire cell population (D) and mitotic cell population (E). Higher epsilon value produces a monolayer with larger average cell area (F).

is very high, cells are less capable of producing rearrangement in the tissue and, in contrast, low stiffness eases the cell motility in the tissue. Previous studies have focused on the liquid-solid behavior of biological tissues depending on rigidity and how affects the cell rearrangements and cell migration [89]. In addition, we find that stiffness value that fits better with experimental data ($E = 0.01\mu N/\mu m^2$) is in the order of magnitude of epithelial monolayer stiffness consulted in the recent literature [11], which is approximately $E \approx 0.02\mu N/\mu m^2$. Furthermore, cell area is also affected by stiffness, low values produce that cells present higher average areas and vice versa. In other words, our model results suggest that a rigid monolayer is more compact than a softer one.

On the contrary, the magnitude of interaction forces presents the opposite behavior. Despite its limited effect on global polygon distribution, the magnitude

of forces alters the polygon distribution of mitotic cells. Higher interaction forces produce a mitotic polygon distribution that tends to generate polygons with more number of sides. Additionally, we observe that very high interaction forces (ε = 1e−2) cause some instabilities in the model that exacerbate this effect. Considering the experimental data, we find an optimal value for this parameter about 1e−4. Furthermore, average area of cells is increased with higher interaction forces. We hypothesize that this behavior is also related to the capability of cells to rearrange themselves in the monolayer. In consequence, higher forces facilitate the cell motility in the epithelial tissue.

2.3.4 Boundary conditions determine the topology in the monolayer simulations

We observe that boundary conditions strongly determine the topology of the epithelial monolayer. Figure 2.9 presents the results of the simulation under three different boundary conditions (constrained, one free side and unconstrained) described in the Models section. We analyze the polygon distribution of the monolayer (Figure 2.9A, B) and the average area of cells (Figure 2.9C). Additionally, we study the pattern of displacements under these boundary conditions as it is shown in Figure 2.9D,E,F. Actually, these simulations help to clarify how the topology of the monolayer behaves under certain constrains associated with other surrounding tissues. (See Video S2.9, Video S2.10 and Video S2.11).

Totally unconstrained boundary condition is clearly the condition that better fits the polygon distribution of experimental data. Actually, in the experiments of *Gibson et al.* and *Aegerter-Wilsem et al.* [12, 14], the experimental conditions are similar to the unconstrained boundary conditions of our framework since the tissue is expanding and it is surrounded by other cells. However, constrained conditions –constrained and free top– show a polygon distribution of the entire cell population and the mitotic population completely different and they tend to generate polygons with higher number of sides (Figure 2.9B). These boundary conditions may match in vitro cultures where the growth is limited by the space in the culture or some specific in vivo processes where the surrounding tissue limits the cell movement.

As expected, average area of cells is higher in unconstrained condition compared to the two constrained conditions. Under these boundary conditions, displacements near the boundary are higher than in the edge of the cell mass, which is a well-known behavior on growing cell aggregates [50, 106]. In the free top condition case, cells apparently flow in the normal direction of the boundary that is not constrained. In contrast, completely constrained boundary condition presents a

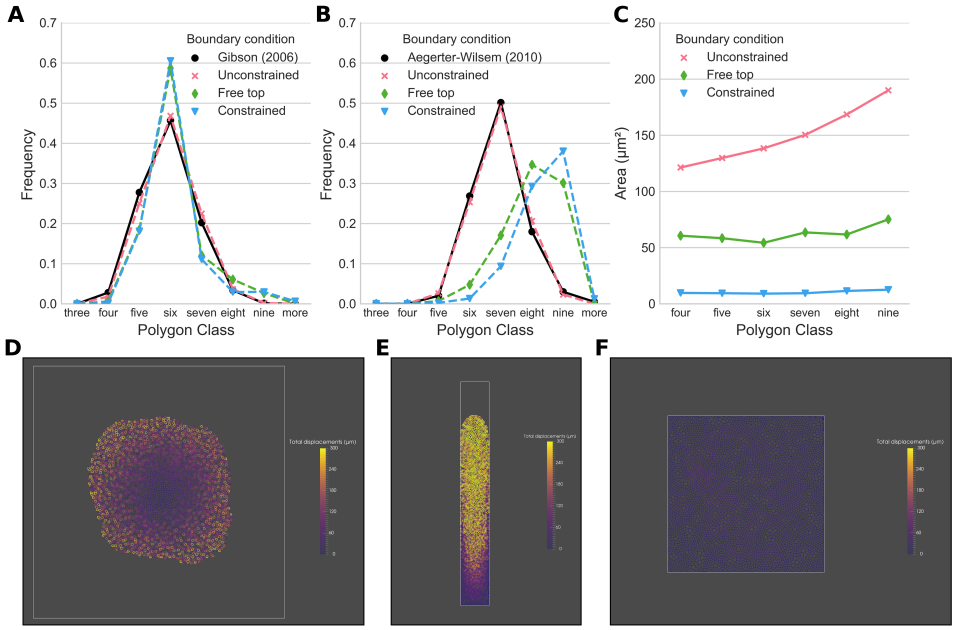

Figure 2.9: Boundary conditions of the simulations. (A, B) Unconstrained boundary condition shows the best fit to the in-vivo polygon distribution of the entire cell population (A) and the mitotic cell population (B). (C) Unconstrained boundary condition presents the largest average cell area, in contrast, completely constrained boundary condition shows the smallest one. (D, E, F) Cell displacements in the monolayer are influenced by the boundary conditions. Unconstrained boundary condition (D) shows a radial pattern of cell displacements, cells near the boundary tend to present higher displacements compared to cells in the center. Free top boundary condition (E) shows a directional pattern of the cell displacements, where these are higher in the direction of the unconstrained side. Constrained boundary condition (F) presents homogeneous cell displacements in the monolayer.

homogeneous displacement field in the entire monolayer. Therefore, cells near an unconstrained boundary are pushed by the rest of cells due to the proliferation and the cell interaction forces.

2.3.5 Monolayer reaches a stationary polygon distribution

To describe the topology of the epithelial monolayer, it is also necessary to consider the temporal evolution of the polygon distribution. Figure 2.10 presents the polygon frequency of entire population (Figure 2.10A) and mitotic population (Figure 2.10B) during the simulation. Our model reaches a stationary polygon distribution, which is consistent with the results shown in [13, 98], where the system also reaches a stable state. To analyze the rest of data in this work, we used a range of time-steps where polygon distribution is stabilized. Polygon distribution of entire population

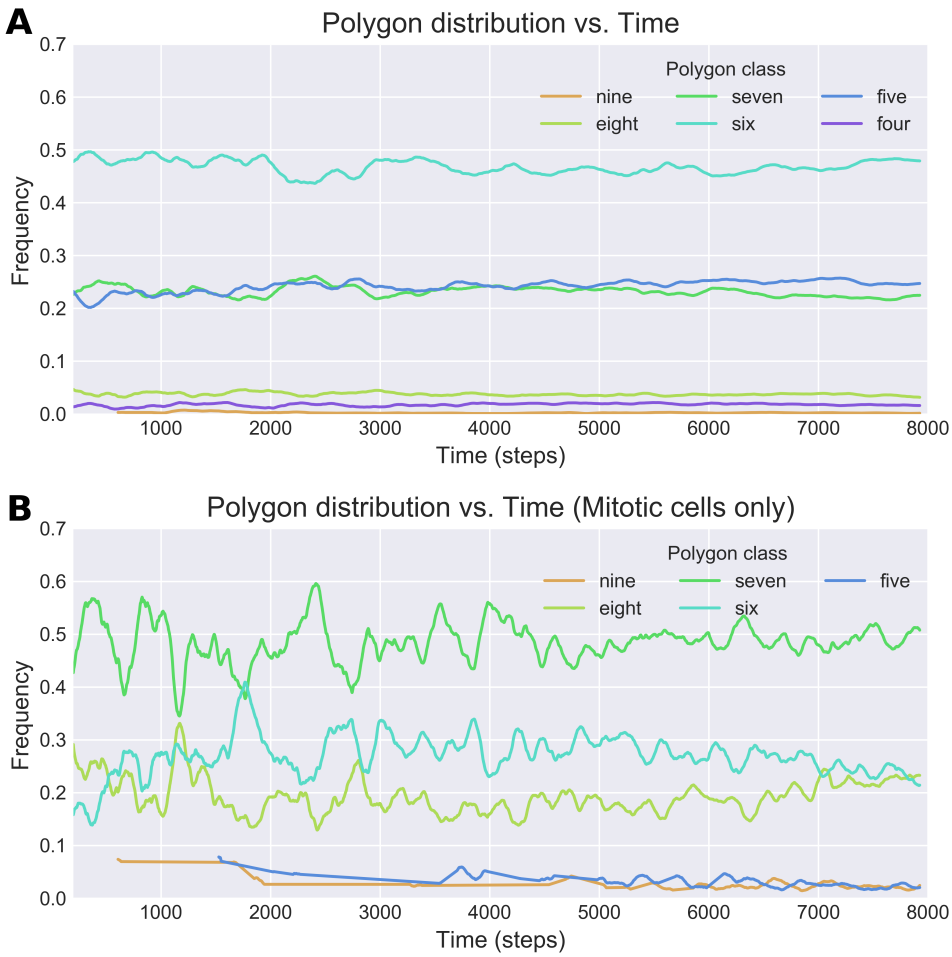

Figure 2.10: Polygon distribution in the simulation time. (A) Global polygon distribution stabilizes in early steps of the simulation. (B) The polygon distribution of mitotic cells shows stabilization in the simulation and a noticeable noise reduction over 5000 time steps.

and mitotic population stabilizes over the time-step 5000. Moreover, the polygon distribution of the entire cell population is less noisy compared to the mitotic population. This fact is due to mitotic population is only a small fraction of the entire cell population (approximately a 3%) and, in consequence, the amount of data available to produce reliable statistics is not enough in the early steps in the simulation. In Figure S2.3, it is shown the evolution of entire cell population and mitotic population during the simulation.

In consequence, we analyze all the data in the other figures when the polygon distribution is the steady state, from the time step 6000 until the end of the

simulation on step 8000. We also must note that the simulation time does not aim to quantitatively describe the actual time in the tissue development process.

2.4 Conclusions

In this chapter, we present a hybrid framework for modeling the emergent topology of a growing epithelial monolayer. The cell and tissue models consist of a collection of particles, which represent the cells, and their associated domains with the corresponding mechanical properties. The cell-cell interactions are defined by Lennard-Jones potential, which is a simple and well-known potential that is widely used in the scientific computations. We must note that this approach to simulate the interaction forces is purely phenomenological and it does not represent any specific biophysical phenomena beyond the global interaction between cytoskeletons and cell junctions. Although other interaction models could be implemented, we have demonstrated that the kind of potential used has a low impact on the model results as it is shown in Figure S2.1, where we compare the simulation outcome using several potentials. In addition, the work of *Drasdo and Hoeme*[92] suggests that the exact form of cell-cell interaction may not be decisive on the simulation of large multi-cellular systems. For these reasons, we used the Lennard-Jones potential, whose implementation is relatively easy and computational efficient. Nonetheless, we are aware that some limitations are derived from this phenomenological approach compared to other models that are more mechanistic [100, 101]. These models clearly describe phenomena as the force-based contact inhibition based on explicit physical equations at the cell level. Though we can implement force-based contact inhibition in our framework, it would be difficult to conclude the biological origin of these forces beyond the global cell-cell interaction.

Therefore, based on this particle approach, we explicitly describe the spatial location of the cells. With this information, we create the corresponding Voronoi diagram to represent the cell topology. Based on this representation, we construct a simple and effective FE model of the epithelial tissue to simulate its mechanical behavior. This approach leads to a simulation model that is easy to implement and with a low computational cost. Nevertheless, our cell representation presents some limitations such as the area of the cells are not necessarily conserved after the cell cleavage. Though we find that the resulting areas are approximately conserved after the cell division because of the nature of the Voronoi diagram. There are models that address this aspect of the representation in a more accurate way [13, 14, 101].

We have shown that this hybrid model can accurately reproduce the topological characteristics of growing epithelial tissues. In particular, we have studied the

polygon distribution of the entire cell population of the tissue, but we have also analyzed the topology of the mitotic cell population. The model parameters that allow a quantitative description of the experimental measurements are easily estimated from the data itself. We have chosen parameter values in our model to capture the major features of epithelial cell dynamics. Moreover, we also considered the standard deviation of our simulation results to compare them with the experimental data. These error bars are only included in Fig 6. In the rest of figures, the standard deviation of the simulation data is similar but we have not included these bars to ease the visualization of the information.

A relevant aspect of our model is the simulation of cell proliferation, including the influence of the cleavage plane on the topology of the epithelial tissue. Our results show that oriented cleavage plane in the cell division matches the experimental data noticeable better than cell division with a random cleavage plane. Additionally, our model suggests that tissue topology is heavily influenced by proliferation rate but also by the dilation of mitotic cells. Considering this increment on the cell size, we achieve to represent experimental data for both entire population and mitotic population. The change of the mitotic cell size produces local perturbations on the tissue topology and, consequently, it modifies the global polygon distribution. However, in other biological processes, cells usually grow during phase G1 and G2 and not in the mitotic phase. This numerical framework can be easily adapted and expanded to simulate these processes, regulating the cell growth in the interphase instead of the mitotic phase.

Remarkably, although we have used a linear elastic behavior in the mechanical model, tissue mechanical behavior is far from being linear in our simulations. Due to a new mesh is generated each step from cell positions, cell rearrangements and displacements in the model cause permanent deformations in the tissue. Moreover, cell-cell interaction forces depend on the cell position relative to its neighbors and it is intimately related to the system dynamics. Therefore, we solve tissue mechanics considering a transient equilibrium on each step and, consequently, this generates a metastable cell conformation that defines the tissue topology. In other words, we model cell material as a linear elastic material but the tissue behaves as a viscoplastic-like material due to the nature of the hybrid approach. The emergent properties of our model confer the possibility to analyze the mixed liquid-solid behavior of growing tissues, which is described in the recent literature [88].

In conclusion, the originality of this work resides on using a hybrid approach to simulate epithelial tissue dynamics and topology that emerge from simple models. With relative simple adjustments of the model parameters, we can reproduce topological characteristics of epithelial cells. Although in this first work we have

mainly focused on mechanical and geometrical aspects, it is possible to easily incorporate chemical stimulus to regulate cell behavior in the agent-based model. Therefore, we consider the computational framework here presented is a promising tool to model a variety of biophysical phenomena associated to the emergent behavior of monolayers.

2.5 Supplementary material

Figure S2.1: Cell-cell interaction potential.

To analyze how the chosen cell-cell interaction potential affect the tissue topology, we change the order of the second term of the Lennard-Jones potential. We normalize the force output taking the standard Lennard-Jones potential as reference (A,B) Polygon distribution seems to be unaltered under these changes (C) Average area tend to slightly increment with the order of the second term. (D, E) Forces of the potential used changing the order of the second term and its normalization.

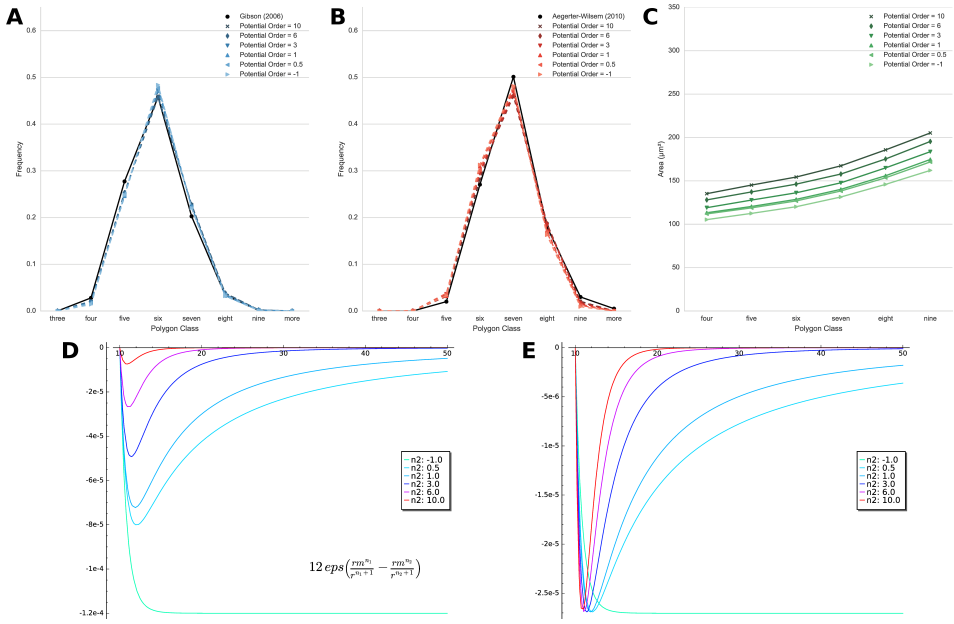

Figure S2.2: Oriented cleavage plane of mitotic cells.

We circumscribe the minimum ellipse on the mitotic cell. Knowing the length of both axes of the ellipse, cell divides by the shortest axis. This method was implemented using the Bounding Volume package of *CGAL* [2].

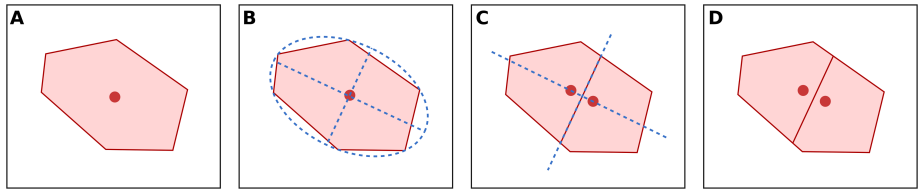

Figure S2.3: Cell population during the simulation.

Cell population grows from 400 cells up to roughly 6500 in the simulation time range. Additionally, mitotic cells stay at approximately 3% of the total population during the whole simulation.

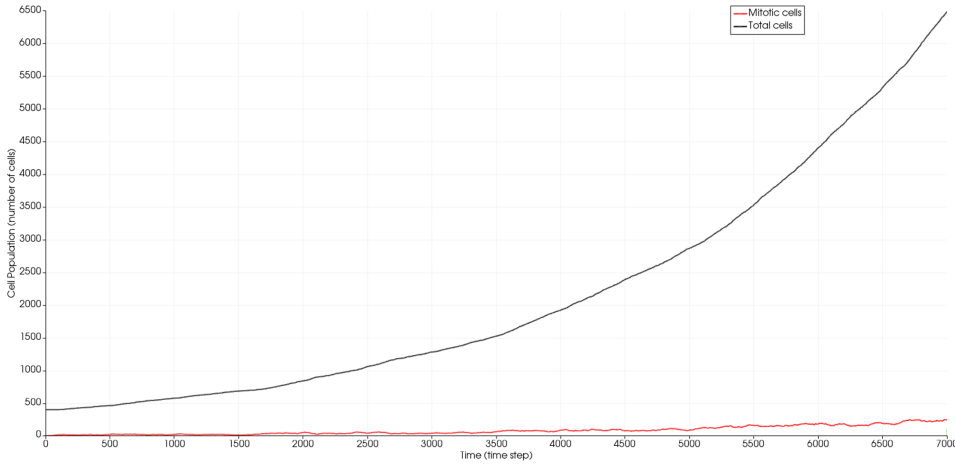

Figure S2.4: Distance between cells in the cleavage.

The distance that the cells are separated after the cleavage in our model is defined as a percentage of the cell radius. We observe that the polygon distribution and the average area s to be unaltered by the cleavage distance in the range analyzed.

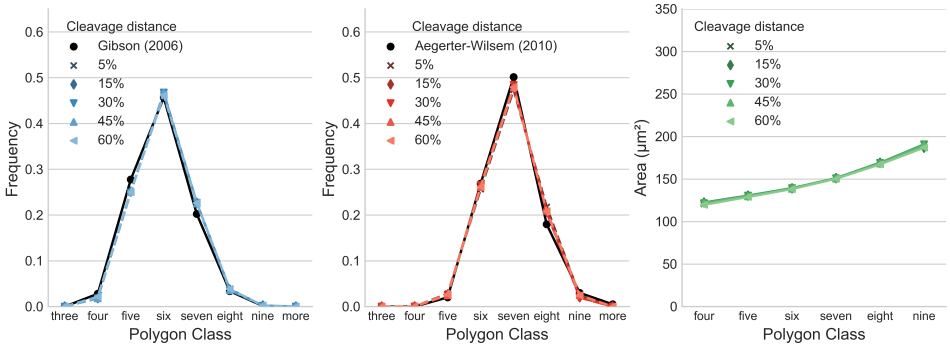

Figure S2.5: Initial distribution.

Several initial distributions of the cells: regular lattice of squares, regular lattice of hexagons and three random configurations. We observe that the polygon distribution and the average area on the steady state seems to be unaffected by the initial distribution of the cells.

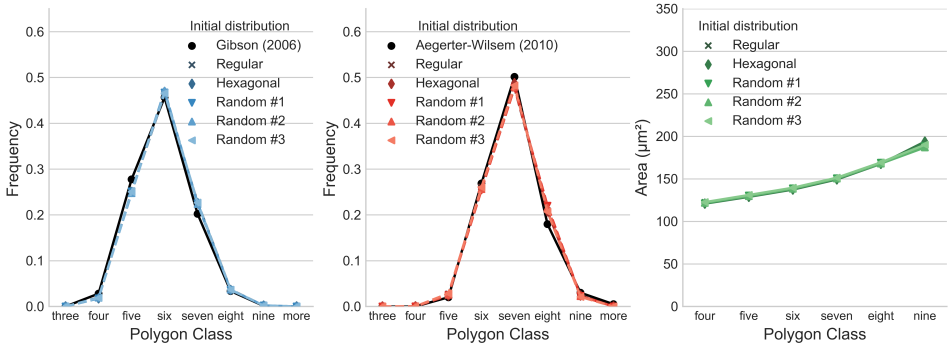

Video S2.6: Dynamic mesh generation.
Video S2.7: Cell proliferation example.
Video S2.8: Layer without proliferation.
Video S2.9: Fully constrained condition.
Video S2.10: Free top condition.
Video S2.11: Unconstrained condition.

Text S2.12: Voronoi Diagram

Voronoi diagram is a partitioning of the plane generated from a specific set of points contained in that plane. The division of the plane in different regions (Voronoi cells) is based on the distance between these points. We use in our framework the simplest case of the Voronoi diagram: a set of points (cell centroids) in an Euclidean plane (cell monolayer). In our case, each segment of a Voronoi cell is formed by all the points that are equidistant to the two nearest cell centroids. Each Voronoi cell is associated to a cell centroid and it represents its cell body in the monolayer. We must note that all the Voronoi cells are convex polygons by definition. Interestingly, the Voronoi diagram of the given points is dual to the Delaunay triangulation, which is also used to generate our mesh in the model.

3

Collective Motion and Cell Jamming in Epithelial Monolayers

Contents

This chapter is based on:

Ismael González-Valverde and José Manuel García-Aznar. *An agent-based and FE approach to simulate cell jamming and collective motion in epithelial layers.* (Submitted)

3.1 Introduction

It has been observed that collective cell motion can resemble a fluid-like flow in confluent epithelial monolayers during tissue development. However, cell motility decreases during tissue aging, and cells start to behave more like a solid than as a fluid. Cells seem to get 'jammed' in this solidification process, entering in a 'frozen' state where motility is almost non-existent. These jamming and unjamming transitions are observed in tissue development, remodeling or wound healing processes [107, 108]. Moreover, it is also associated with several diseases as cancer and asthma [109, 110].

Unlike previously hypothesized, recent studies suggest that cell density is secondary to the cell jamming process when the monolayer is already confluent [111]. In fact, this transition is related to the maturation of cell-cell adhesions and the cell interaction with its neighboring cells [11, 16, 111, 112]. In addition, cell organization and motility are known to be intimately connected. Cell shape is also related to the jammed and unjammed states of the epithelial tissues. The relation between monolayer topology and jamming states have been clearly defined using adimensional parameters associated with cell geometry [66, 88, 109, 110].

There are many studies focused on modeling the relation of cell motility and cell-cell interactions using discrete particle-based models [7, 41, 61, 111, 113, 114]. This approach is similar to other models that simulate jamming processes in inert granular systems [108]. In contrast, other studies simulate collective cell motion using vertex-based models. These models present some advantages for simulating cell organization in epithelial monolayers since cell geometry is explicitly defined [109, 110]. So, vertex-based models have been extensively used to study the topology of epithelial tissues, and they are usually based on energy minimization [13, 14, 41, 87, 88]. Nevertheless, they also show some limitations, for instance, the edge transitions on cell rearrangements and cell division must be explicitly modeled. Likewise, the modeling of cell propulsion forces is not straightforward compared to particle-based models. Recently, a new kind of approach called self-propelled Voronoi model has been applied to jamming transition simulations [66, 89, 115]. This type of model overcomes some vertex-based model disadvantages mentioned before, but it keeps the capacity to simulate cell geometry.

In the present study, we show a novel approach that joins discrete and continuum modeling techniques. First, our hybrid model is based on an agent-based model that describes cells individually in a similar way as the self-propelled Voronoi models. Further, this discrete approach is coupled with a Finite Element-based model that defines the mechanical behavior of the epithelial monolayer as a continuum material. This approach has been extensively described in a previous work focused

on modeling monolayer topology in proliferating epithelial tissue [116](Chapter 2). In this work, we extend this modeling technique to analyze how cell-cell interactions regulate collective cell motion and cell jamming. Furthermore, our approach allows investigating some additional aspects of the collective motion that are not commonly assessed in previous studies, for instance, the effect of passive mechanical properties on cell motility.

3.2 Methods

Here we use a hybrid approach to model cell dynamics in epithelial monolayers. This approach is based on the assumption that epithelial monolayer can be simulated as a continuum material whose properties emerge from individual cell behavior. In fact, we combine a discrete and a continuum model as shown in Figure 3.1. Cells are defined on an agent-based model as particles that keep their own properties and identity. Moreover, each cell is associated to a polygon that describes its body. In reality, cell geometry is defined by the Voronoi diagram. This tessellation is generated from each particle position on the spatial domain. On the other hand, we use a continuum material model that describes the cell passive mechanics. We connect both models by means of the geometry approximation. We use the cell geometrical representation to define the Finite Element mesh in the continuum model. In addition, forces generated on the discrete model are also applied to the continuum material as internal forces. We solve the mechanical problem using the Finite Elements Method (FEM), and tissue deformation is fed back to the discrete model as cell displacement.

This hybrid approach is also used in a previous work to analyze the topological characteristics of proliferating cell layers [116](Chapter 2). However, here we extend this modeling technique to study the collective cell motion in epithelial layers and, in particular, the cell jamming phenomenon.

To analyze cell morphology, we use an adimensional parameter called shape index. This shape index is related to polygon perimeter and area, and it has been used before to relate jamming states and cell morphology [66, 88, 109, 110]. Additionally, we consider the distribution of the cell polygon types in order to enrich the analysis of the simulation results.

3.2.1 Agent-based model

We use an agent-based model to represent cells (S^{cell}) as separated units in the tissue as shown in equation 3.1. In this discrete approach, each cell S_i^{cell} carries

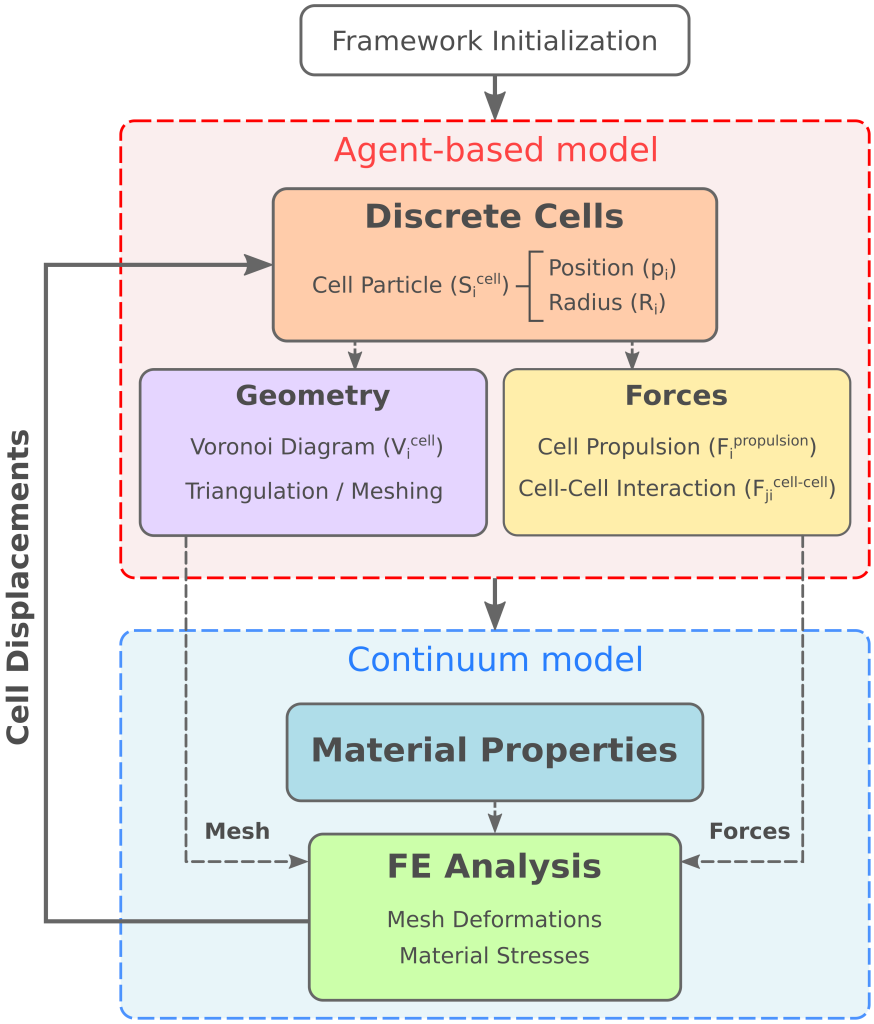

Figure 3.1: Workflow of our hybrid modeling approach. First, we initialize all the framework variables. In the agent-based model, we represent the cells as particles (S^{cell}) with an associated position ($\mathbf{p}_i$) and radius (R_i). Then, we compute the Voronoi diagram (V_i^{cell}) from the cell centroids and the forces generated for each one (F_i^{cell}). We triangulate the polygonal cell representation to generate a mesh for the FE analysis. We solve the FE problem using the material properties and the forces computed before. Cell displacements are obtained from the mesh deformation of the FE results. Finally, we move the cell particles in the agent-based model using these displacements and the simulation proceed to the next step.

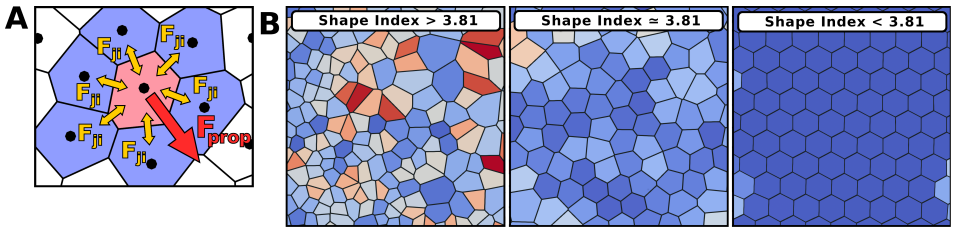

Figure 3.2: Model forces and shape index. (A) Representation of cell forces in the model. Interaction forces between neighboring cells are denoted by Fji and the propulsion force applied to each cell is denoted by Fprop. (B) Average shape index in three tissues with different topology. The left panel shows high average shape index (unjammed state), the middle panel shows an average shape index close to transition point and the right panel shows low average shape index (jammed state). The color of each cell represents the individual shape index, from lower values (blue) to higher values (red).

its own information, and it is defined in the space as a particle with an associated position $\mathbf{p}_i$ and radius R_i:

$$S^{cell} = \{S_1^{cell}, S_2^{cell}, ..., S_n^{cell}\} \quad \text{where} \quad S_i^{cell}(\mathbf{p}_i, R_i) \tag{3.1}$$

In addition, we associate a polygon V_i^{cell} to each cell S_i^{cell} that is generated using the Voronoi diagram:

$$V_i^{cell} = \{\boldsymbol{x} \in \mathbb{R}^2 : d(\boldsymbol{x}, \mathbf{p}_i) < d(\boldsymbol{x}, \mathbf{p}_j) \quad \text{for} \quad i \neq j\} \tag{3.2}$$

where $d(\boldsymbol{x}, \mathbf{p}_i)$ is the function that returns the distance between the point $\boldsymbol{x}$ and the position $\mathbf{p}_i$ of the cell S_i^{cell}. The polygon V_i^{cell} contains all the points that are closer to the cell S_i^{cell} than to any other cell S_j^{cell} .

We calculate cell propulsive forces ($F_i^{propulsion}$) and the forces generated by the interaction with its neighboring cells ($F_{ji}^{cell-cell}$) in the agent-based model (Figure 3.2A). Hence, the total force applied to each cell can be written as:

$$F_i^{cell} = \sum_{j=1}^{N_i} F_{ji}^{cell\text{-}cell} + F_i^{propulsion} \tag{3.3}$$

We denote by F_i^{cell} the total force applied on the cell S_i^{cell} in equation 3.3. This force is the sum of the interaction forces F_{ji}^{cell} between the current cell and all its neighboring cells S_j^{cell} and cell propulsion forces $F_i^{propulsion}$. We determine which are the neighboring cells from the Voronoi diagram described before. To calculate the cell-cell interaction forces, we use a force derived from an extension of the Lennard-Jones potential:

$$F_{ji}^{cell\text{-}cell}(r) = K^r \left(\frac{r_m^{12}}{r^{13}}\right) - K^a \left(\frac{r_m^6}{r^7}\right) \tag{3.4}$$

Cell-cell interaction forces depend on the distance between both cells ($r = d(\mathbf{p}_i, \mathbf{p}_j)$) as shown in equation 3.4. This force also depends on the equilibrium distance between cells (r_m), that is the sum of the radius associated to each cell ($r_m = R_i + R_j$). We denote by K^r the repulsive force constant and by K^a the attractive force constant. The attractive term of this force represents cell-cell junctions and contractility, and the repulsive term models cytoskeleton reaction when cells are too close. In fact, we can analyze separately how the attractive and the repulsive terms affect the system using this modified Lennard-Jones formulation. Finally, in the case that both constants are equal $K^a = K^r$, the interaction force is exactly the one derived from Lennard-Jones potential:

$$F_{ji}^{cell\text{-}cell}(r) = 12\varepsilon \left[\left(\frac{r_m^{12}}{r^{13}}\right) - \left(\frac{r_m^6}{r^7}\right)\right] \qquad \text{for } K^a = K^r = 12\varepsilon \tag{3.5}$$

where we denote by ε the intensity of the potential well, that is directly related to the magnitude of the force. In this work, we assume that propulsion forces are represented by a vector of constant magnitude and random direction located on the cell centroid:

$$\begin{aligned} F_i^{propulsion} = K^{propulsion}(cos(\varphi^{random})\overrightarrow{x} + sin(\varphi^{random})\overrightarrow{y}) \\ \text{for } \varphi^{random} \sim U(0, 2\pi) \end{aligned} \tag{3.6}$$

We denote by $K^{propulsion}$ the constant force magnitude of the cell propulsion force. The direction of the force is determined by a random angle (φ^{random}) obtained from a uniform distribution U from 0 to 2π. The direction of the cell propulsion force is persistent in time. However, this direction changes periodically during the simulations to avoid artifacts and unrealistic cell motion. We define this time interval as $\tau^{propulsion}$.

3.2.2 Passive mechanics model

To simulate passive mechanics of the epithelial monolayer, we develop a continuum model that overcomes some limitations of the discrete part of our hybrid approach. We assume that the mechanical behavior of the cell layer can be described as a continuum material. In other words, we consider that cells are forming a continuum medium and they can transmit forces through their own bodies and the cell-cell junctional network. We model this material considering a linear elastic behavior:

$$\boldsymbol{\sigma} = \boldsymbol{C} : \boldsymbol{\varepsilon} \tag{3.7}$$

$$\boldsymbol{C} = \lambda \mathbf{1} \otimes \mathbf{1} + G\boldsymbol{I} = \frac{\nu}{(1+\nu)-(1-2\nu)} E\mathbf{1} \otimes \mathbf{1} + \frac{1}{2(1+\nu)} E\boldsymbol{I} \tag{3.8}$$

Let $\boldsymbol{\sigma}$ denote the stress tensor, $\boldsymbol{\varepsilon}$ strain tensor, and $\boldsymbol{C}$ the fourth-order stiffness tensor. In addition, we define the first Lamé parameter by λ, shear stress modulus by G, Poisson's ratio by ν and Young's modulus by E. Finally, let $\mathbf{1}$ be the second-order identity tensor and $\boldsymbol{I}$ the fourth-order identity tensor.

Furthermore, we use the plane stress hypothesis since monolayer thickness is notably lower compared to the other two dimensions. We transform ν and E into ν' and E' to apply this hypothesis:

$$\nu' = \frac{\nu}{1-\nu} \qquad E' = \frac{E}{1-\nu^2} \tag{3.9}$$

First, we develop a dynamic meshing algorithm that connects the agent-based model with the material model geometry. In fact, we generate the mesh used on FEM from the Delaunay triangulation of the cell polygons (V^{cell}) in each step of the simulation. Hence, the geometry of this model is directly related to the Voronoi diagram of the cells that we described earlier. In particular, cell geometry is always associated with the mesh nodes using this approach. This meshing technique offers a high adaptability to strong tissue topology changes derived from cell rearrangements or cell morphology alterations. Moreover, the forces generated by cell-cell interactions and cell propulsion are applied as internal forces on the monolayer material. In particular, we apply forces generated in the discrete model directly on the nodes corresponding to each cell position ($\mathbf{p}_i$).

In the FE analysis, we assume free displacements in the parallel direction of the boundaries and constrained displacements in the normal direction of boundaries. In addition, we assume that the stress generated due to material deformation dissipates from one step to the next. Despite the material model is linear elastic, cell layer presents viscoelastic and plastic properties if we observe its behavior during the whole simulation. These properties emerge from the cell dynamic response and their capacity to rearrange in the monolayer. This behavior has been observed experimentally in previous studies [11, 17]. Also, we assume that material is incompressible considering the results of previous works on mechanical characterization of epithelial monolayers [11].

Lastly, we obtain the cells displacements from the material deformations. These displacements are applied to cell particles in the agent-based model prior to the next simulation step. Hence, the flow of information on our hybrid approach is bidirectional between both continuum and discrete models as Figure 3.1 shows.

3.2.3 Shape index

The analysis of cell morphology and tissue topology is based on an adimensional index commonly used in previous works [66, 88, 109, 110]:

$$q = \frac{P}{\sqrt{A}} \tag{3.10}$$

This adimensional number is usually called shape index (q) and it depends on the cell perimeter (P) and the cell area (A) as shown in equation 3.10. We compute cell perimeter and cell area from the polygonal representation of each cell (V_i^{cell}). It has been demonstrated that shape index is related to the jamming state of the epithelial tissue [66, 88, 109, 110]. In fact, there is a critical value when shape index is equal to 3.81 that denotes the transition from a solid-like behavior of the collective cell motion to a fluid-like one (equation 3.11) The transition from jammed to unjammed state –and viceversa– is defined by this transition point:

$$\begin{aligned} q &< 3.81 \quad \text{solid-like behavior} \\ q &= 3.81 \quad \text{transition point} \\ q &> 3.81 \quad \text{fluid-like behavior} \end{aligned} \tag{3.11}$$

In Figure 3.2B is shown the aspect of the monolayer topology for different collective motion regimes. Moreover, we initialize the system with a lattice cell distribution where most of them present a hexagonal shape. However, we study the shape index after several cycles of propulsion direction changes to minimize the effect of the initial cell distribution in our results. Besides, we keep a constant cell density in all simulations.

3.3 Results

Here we analyze the effect of cell-cell interaction forces and material stiffness on cell motility and tissue topology. In addition, we study the heterogeneity of the collective cell motion and stresses generated in the monolayer. We show in Table 3.1 the default values for model parameters unless other values are explicitly mentioned.

In order to avoid the effect of the boundary proximity, we only consider cells in the internal domain of the monolayer for the topological analysis.

General Parameters	
Number of cells	900
Total simulation time (*steps*)	2000
Layer dimensions (μm)	300x300
Cell-Cell Interaction Forces	
Cell radius - R_i (μm)	5
Interaction constant - ε (μN)	1.0e−4
Attraction constant - K^a (μN)	1.2e−3∗
Repulsion constant - K^r (μN)	1.2e−3∗
Propulsion Forces	
Force magnitude - $K^{propulsion}$ (μN)	1.00e−3
Direction change interval - $\tau^{propulsion}$ (*steps*)	100
Material Properties	
Young's modulus - E ($\mu N/\mu m^2$)	0.02 [11]
Poisson's ratio - ν	0.49**[11]

* This default value is set to match $K = 12\varepsilon$.

** We assume that material is almost incompressible.

Table 3.1: Simulation parameters

3.3.1 The cell-cell interaction forces regulate jamming and collective cell motion

Cell-cell interaction forces are related to tissue topology and cell motility according to previous experimental studies [109–111]. Basically, cells form adhesive structures with their neighbors, and these cell-cell adhesions generate a junctional network at the layer scale. The cell-cell interaction forces are transmitted to the neighboring cells through these junctions.

In our simulations, we find that the magnitude of the cell-cell interaction forces dramatically affects the monolayer topology. To study the cell-cell interaction effects, we vary the interaction constant parameter (ε) that regulates the intensity of the potential well (equation 3.5). This interaction constant is directly related to the interaction force magnitude. We observe that the global shape index decreases when the interaction forces between cells increase. The shape index reaches values even below the critical transition point ($q = 3.81$) for high values of the interaction constant ($\varepsilon > 1.0\text{e}{-3}$), where the cells enter on a jammed state (Figure 3.3A). In addition, we observe that cell shape distribution tends to be hexagonal when the interaction force increases. In fact, this tendency is even more pronounced when cells are clearly in a jammed state ($\varepsilon = 1.0\text{e}{-2}$) (Figure 3.3C).

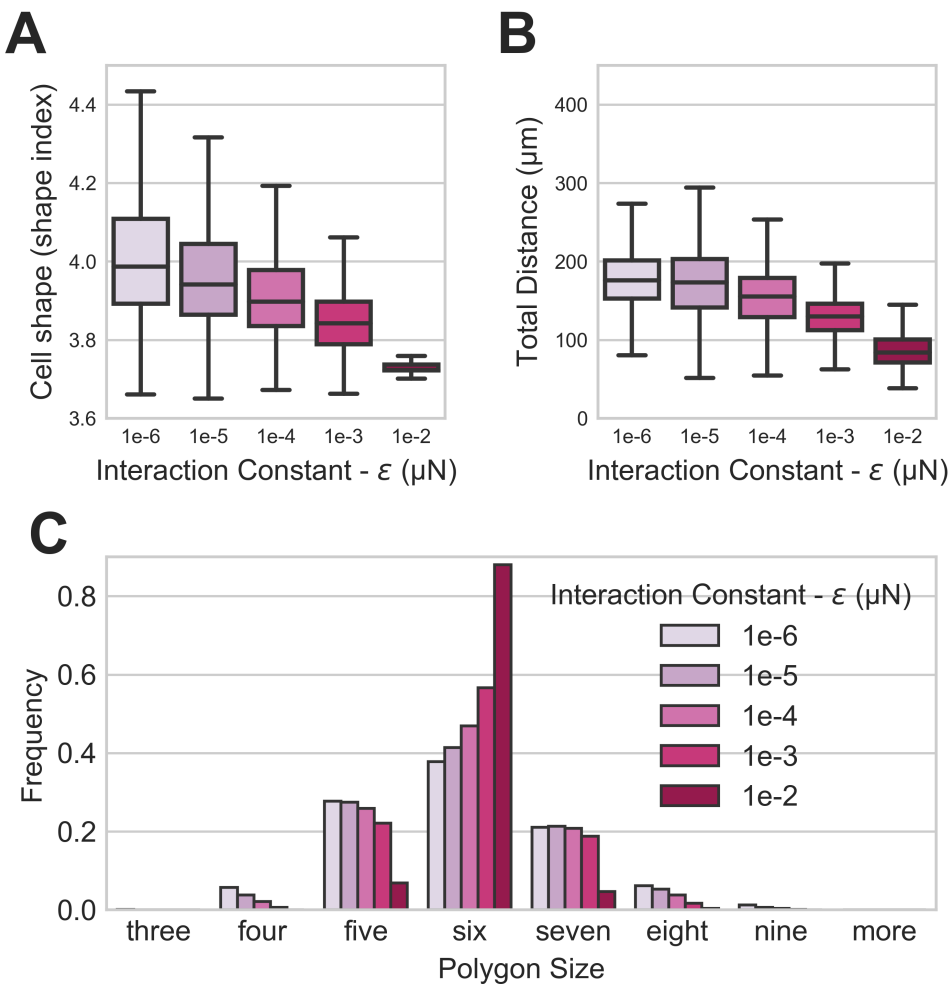

Figure 3.3: Interaction forces are related to jamming and cell motility. Interaction forces are related to jamming and cell motility. We analyze this effect varying the cell-cell interaction constant (ε). In this figure, the boxplot shows median values and quartiles, and the whiskers represent maximum and minimum data values. (A) Stronger interaction forces are predicted to diminish shape index. (B) Stronger interaction forces reduce cell motility and the distance that cells travel. (C) Cell shape tends to a hexagonal geometry when interaction forces increase.

Moreover, we also predict that an interaction constant increment produces a reduction of cell motility. Under strong cell-cell interaction forces, cells travel less distance in the tissue as results show in Figure 3.3B. Collective motion is predicted to be heavily reduced when cells are in jammed state. In particular, we observe that cells in jammed state still move in a 'vibrational-like' manner, however, there is no effective position change in the monolayer (see Video S3.1).

Further, we decompose this cell-cell interaction force to study the effect of the attractive and repulsive terms independently. We use a range of values for K^a and K^r in which the simulation is stable for both cases. Interestingly, the stable range for the repulsion force is wider than the one for the attraction force.

First, we observe that the attraction constant has no effect on the shape index (Figure 3.4A), however, the repulsive constant significantly alters shape index (Figure 3.5A). The shape index is reduced when the repulsion force increases. Thus, the repulsion term favors the transition into a jammed state, at least in a confined space similar to our conditions in the simulations. Further, we do not find any noticeable effect on the cell motility for variations in attraction or repulsion constant (Figure 3.4B and Figure 3.5B). Lastly, the repulsive term affects the tissue topology as shown in Figure 3.5C. Cells tend to a hexagonal shape when we increase the repulsion constant. This effect is similar to what we observe when interaction constant (ε) increases. On the contrary, the attractive term does not show any relevant effect on the topology (Figure 3.4C).

We conclude that, as expected, the magnitude of cell-cell interaction forces plays a key role in the regulation of the jamming process. Our results indicate that cell-cell interactions modulate the tissue topology in the presence of collective cell motion. On the other hand, the effect of the repulsive term on the tissue topology is more pronounced compared to the attractive term. Hence, the simulation results suggest that the effect of the cell-cell interaction force on the topology is mainly caused by the repulsive term.

3.3.2 The passive mechanical properties affect cell motility

The effect of the tissue stiffness on the cell motility has been less investigated than the effect of cell-cell interactions. In fact, it is well-known that a part of the apparent stiffness of the epithelial tissue comes from cell-cell adhesions. However, cell stiffness also contributes to this mechanical property [117]. In our model, we can study these effects separately since stiffness can be modified independently from cell interactions. We vary the tissue material stiffness without modifying the active forces generated between cells to elucidate how cell mechanical properties affect collective cell motion and monolayer topology.

We observe that the material stiffness (E) only affects cell motility. Interestingly, this property does not show any effect on tissue topology in the range we have analyzed. We predict that global cell shape is not affected by changes in tissue material stiffness as shown in Figure 3.6A. In all the simulated cases, cell shape indices correspond to an unjammed state, in which fluid-like behavior dominates.

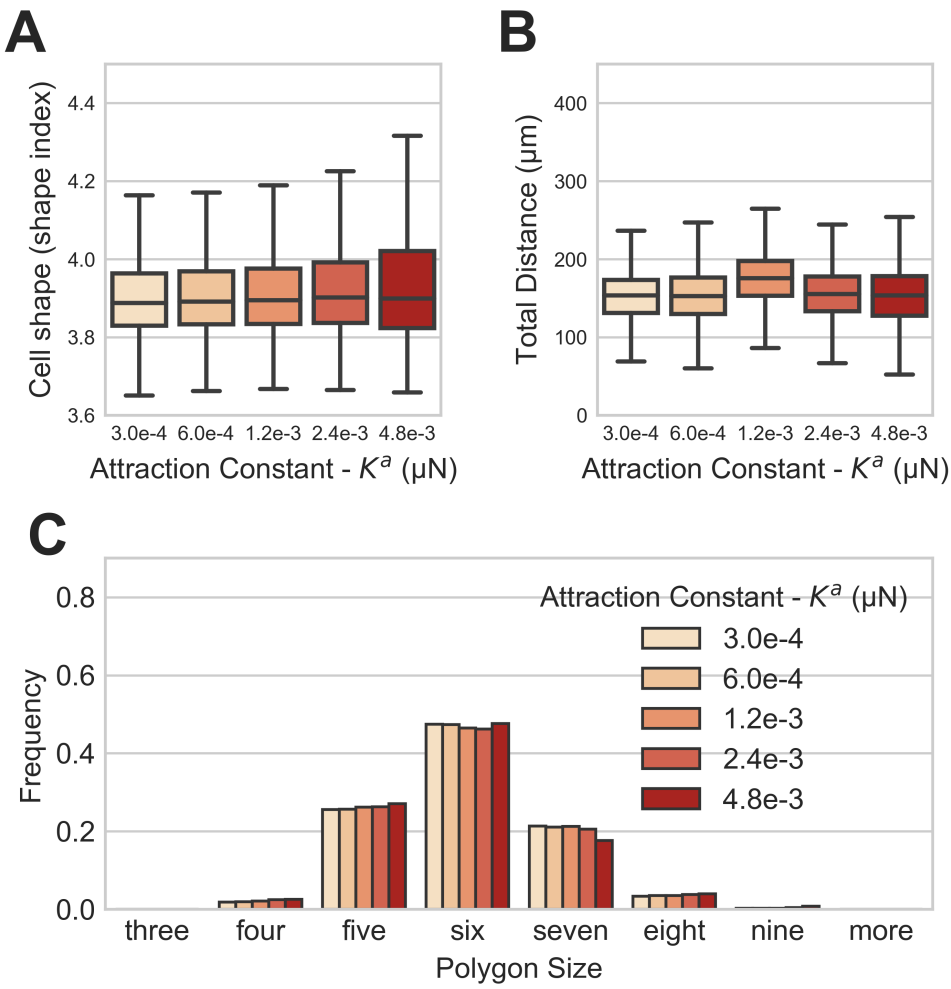

Figure 3.4: Effect of the attractive term of the cell-cell interaction forces. The boxplots show median values and quartiles, and the whiskers represent maximum and minimum data values. (A) The shape index is not affected by the attractive term. We only observe a slight increment on the results variability. (B) The attractive term effect on the cell motility is not relevant for the range analyzed. (C) We do not observe changes in the tissue topology due to the attractive term.

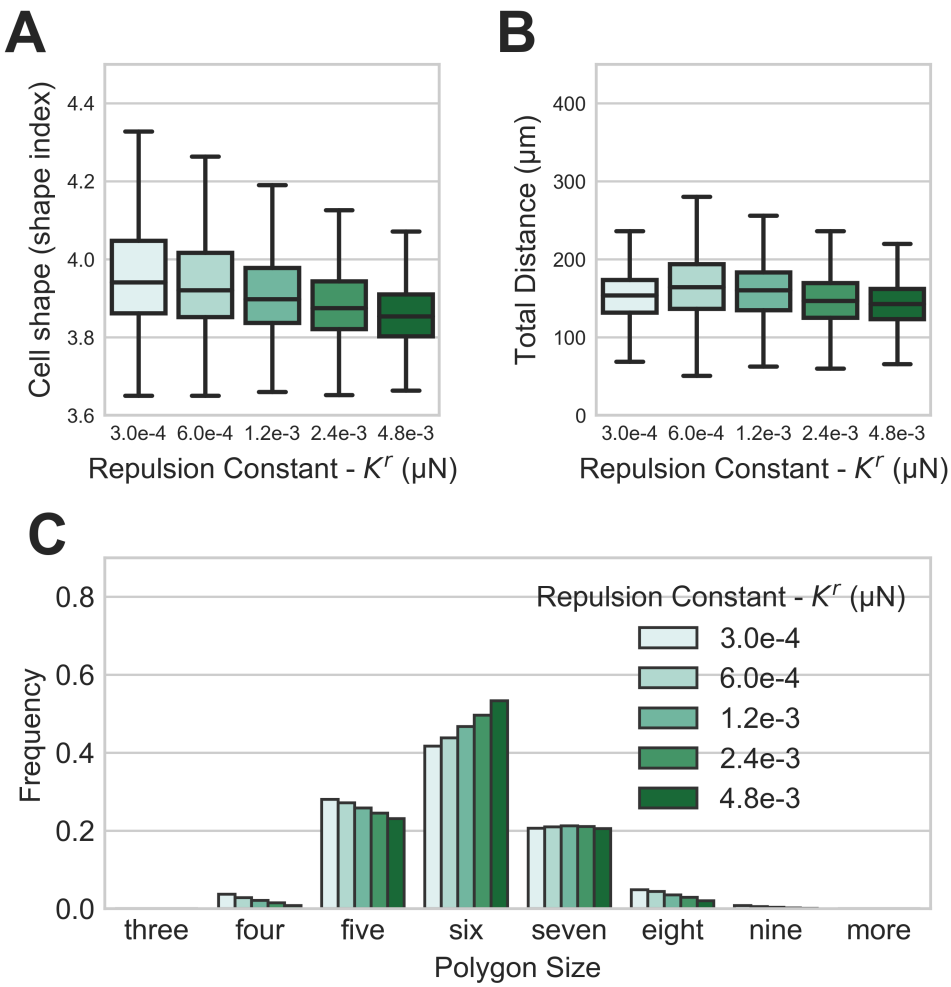

Figure 3.5: Effect of the repulsive term of the cell-cell interaction forces. The boxplots show median values and quartiles, and the whiskers represent maximum and minimum data values. (A) The repulsive term reduces the shape index and favors the transition to a jammed state. (B) We do not observe any relevant effect of the repulsive term on the cell motility. (C) Cells tend to a hexagonal shape when the repulsion forces increase.

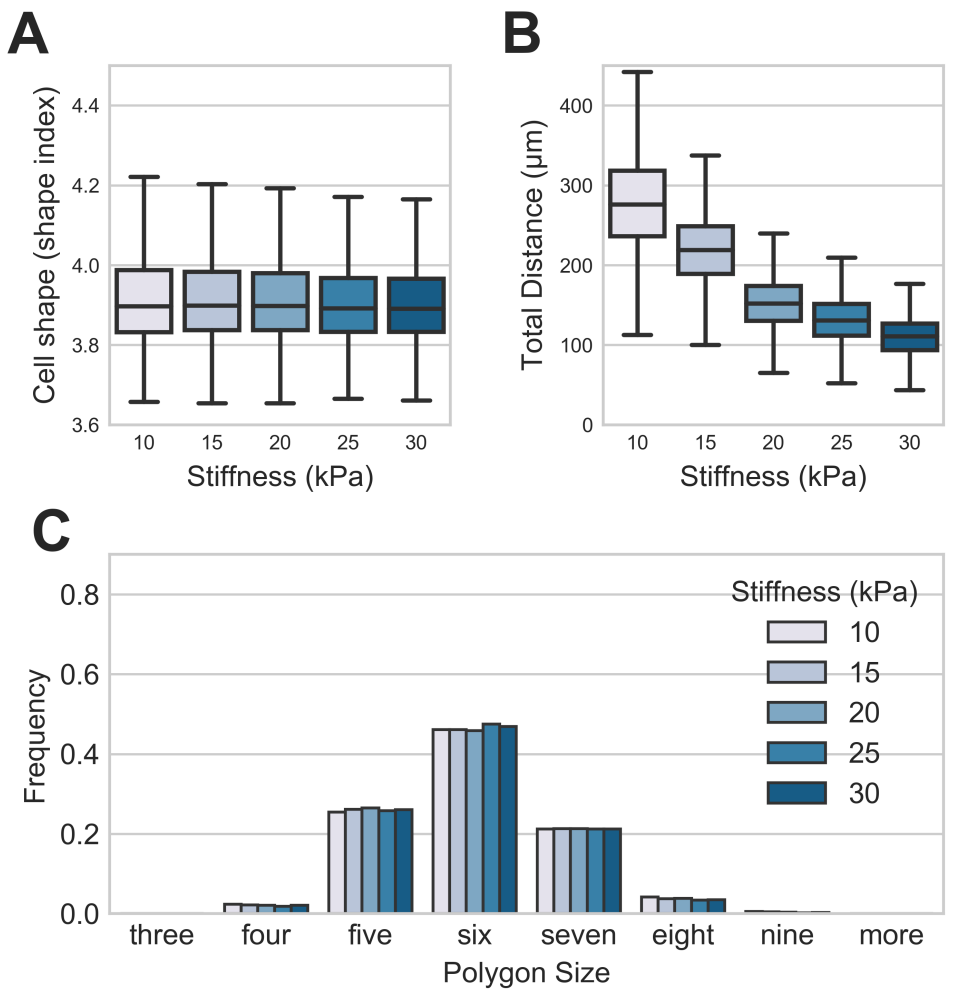

Figure 3.6: Material stiffness is related to cell motility but not to shape index. We analyze this effect varying stiffness modulus of the material. In this figure, boxplot shows median values and quartiles and whiskers show maximum and minimum data values. (A) Cell stiffness does not affect shape index. (B) Higher cell stiffness reduces cell motility and the distance that cells travel. (C) Tissue topology is not affected by material stiffness in the range analyzed.

Nevertheless, material stiffness affects cell motility in the monolayer. In Figure 3.6B, we observe a reduction of the distance that cell traveled when stiffness increases. This effect on the cell motility is even more pronounced compared to cell-cell interaction forces. Finally, we do not find any effect on the polygon distribution either (Figure 3.6C).

In conclusion, these observations suggest that tissue stiffness is not regulating the tissue topology and the cell jamming phenomenon. In contrast to what it is

observed in the cell-cell interaction analysis, cells do not get jammed by increasing the material stiffness. In reality, cells tend to move slower when material stiffness increases and, therefore, they travel less distance. Thus, we only observe a velocity reduction. Here the cell stiffness is acting like a frictional component for the cell movement. These results support the theory that cell jamming is mainly caused by cell-cell interactions and contraction [110, 111].

3.3.3 The collective cell motion produces heterogeneity in the layer topology and the stress distribution

Cells tend to group with other cells with the same motility in the monolayer as shown in previous studies [7, 110]. This generates clusters of cells with the same velocity and, in consequence, global heterogeneity emerges at the monolayer level [88, 109, 111].

Our results also predict this behavior and they show that cells form clusters with the same motility. We observe that they also generate swirls and preferential paths (Figure 3.7 and Video S3.2). This fluid-like motion causes heterogeneity in the tissue topology. Further, the results show that large groups of cells moving in the same direction can drag other cells. In fact, this is true even if they present a propulsion force in a different direction from the collective movement. This phenomenon is probably caused by cell-cell attraction forces and a frictional-like effect generated by surrounding cells.

Additionally, we find that stress distribution in the monolayer is also heterogeneous. Our results show zones of the monolayer that present high compression stresses due to cell motion as shown in Figure 3.7. Although a quantitative validation of monolayer stresses is out of the scope of this work, the stress values of the results are consistent with previous studies on epithelial tissues [109].

3.4 Conclusions

Here we present a novel hybrid approach to simulate cell dynamics in epithelial monolayers. We combine a discrete agent-based model that tracks individual cell information and a continuum material model that simulates tissue level mechanics. This approach allows investigating the effect of the cell-cell interactions, individual cell behavior, and tissue mechanical properties separately. Compared to vertex-based models [87, 88, 109, 110], our hybrid approach does not need to model explicitly the cell rearrangements and vertices transitions because they occur naturally using the Voronoi diagram. The inclusion of propulsion forces is also straightforward since we rely on the agent-based model that represents cells as particles. In addition, there

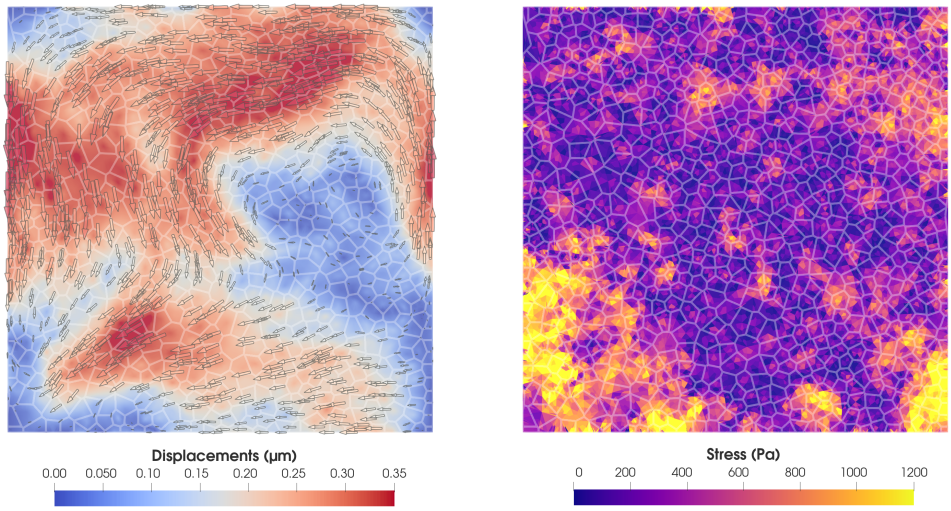

Figure 3.7: The tissue heterogeneity emerges from the clustering of cells with different motility. In the left pane, cells present different displacements and they tend to group together by their motility. This clustering effect generates swirls and preferential paths on the monolayer and, in consequence, heterogeneity at tissue level. In the right pane, we show the absolute value of principal stresses. The stress distribution is also heterogeneous in the tissue. Further, the stress values are compatible with the experimental observed data [109].

are some advantages over pure particle-based methods [7, 111, 114], for instance, we can simulate the tissue as a continuum medium, analyze cell shapes, and obtain monolayer stresses from our results. There are some recent models that also use the Voronoi diagram to simulate cell geometry [66, 89]. Nevertheless, these models rely on energy minimization equations to simulate cell motion and cell mechanical properties depend on cell area. In contrast, we use a material model that offers the possibility of simulating tissue mechanical properties in a continuum medium.

In this work, we focused on understanding how cell-cell interaction forces and epithelial monolayer stiffness affect cell collective motility and topology. First, the cell-cell interactions are widely known to be crucial on cell motility and cell organization on the tissue. We found that stronger interactions between cells were predicted to reduce cell motility and to favor a regular topology on the cell monolayer. Cells reached a jammed stated when the cell-cell interaction forces increased. In the jammed stated, their positions were fixed in the epithelial layer and their movement were limited to a vibration-like one. Also, we found that the repulsive term of the interaction forces has a stronger influence on the tissue topology compared to the attractive term.

Second, our results suggest that tissue passive mechanics affect the collective cellular motion. A material stiffness increment produced a reduction in the cell

motility. Nevertheless, passive mechanics did not affect tissue topology and it was not related to a shape index variation. Although cell velocity was reduced on higher stiffness cases, cells did not enter on a jammed state. We conclude that its effect is rather like a frictional term. These observations reinforce the argument that cell jamming is caused by cell-cell interactions and not by passive cell and tissue mechanics.

Finally, we observed in our results the formation of cell clusters with the same motility during collective cell motion. Thus, this effect favored the heterogeneity in the tissue topology and the stress distribution. These phenomena have been noted previously in other experimental works of epithelial monolayers [109–111].

3.5 Supplementary material

Video S3.1: Collective cell motion for different values of ε.
Video S3.2: Collective cell motion generates heterogeneity in the monolayer.

This document and its supplementary material are accessible from:
`https://m2be-storage.unizar.es/pydio_public/ismael-thesis`

4

Collective Cell Migration in Epithelial Monolayers: Durotaxis and Gap Closure

Contents

This chapter is based on:

Ismael González-Valverde and José Manuel García-Aznar. *Mechanical modeling of collective cell migration: An Agent-based and continuum material approach.* (Submitted)

4.1 Introduction

The mechanical modeling of collective cell migration in epithelial tissues is a complex task since many biophysical phenomena occurs simultaneously. First, the interaction forces between cells and with the extra-cellular matrix need to be modeled [18, 20, 118, 119]. In addition, cell and substrate mechanical properties also affect the system mechanical behavior [11, 16, 17, 119]. Moreover, the tissue morphology suffers considerable changes in these biological processes due to cell proliferation, cell rearrangements and cell shape changes [5]. Finally, to study cell collective behavior and observe the effects at tissue level, we need to have a reasonable number of cells in the simulations.

Previous works on modeling collective migration have engaged this biological problem using very different approaches. We find many models focused on simulating cells as individual units in the tissue [40, 41]. First, center-based and simple particle models offer a straightforward way to track cell information and to calculate their interactions [113, 114, 120]. However, these methods hardly represent tissue morphology and cell shapes inside a monolayer. Vertex-based model is another common modeling strategy to simulate epithelial tissues, and they overcome some limitations of the former type of models [88, 109, 121]. For instance, cell representation is more accurate and cell-cell interfaces are clearly defined. Nonetheless, they are not free of disadvantages. Cell rearrangements and cell proliferation need to be considered carefully and transitions of cell number of vertices and neighboring must be explicitly handled. In recent years, we also find an interesting combination of center-based and vertex-based models that extend the modeling capabilities of both approaches [66, 67, 84]. Recently, some authors are focusing their efforts on developing 3D deformable cells systems [68, 122]. Nevertheless, they are still very computationally expensive and complicated to apply to biomechanical processes with many cells. In constrast, Potts models are very flexible and usually very efficient even simulating a high number of cells [55, 123]. They are often considered to be excessively phenomenological by many authors but, in fact, they have been successfully applied to model cell and tissue mechanical behavior. Furthermore, sub-cellular and molecular-based models have been used to describe the basis of collective migration in epithelial layers [119, 123, 124]. These models are specially useful to simulate and study very specific molecular mechanisms. However, they are limited to simulate only a few cells and not many simultaneous biological processes.

Differently, other researchers focus on the opposite approach, and they reproduce multi-cellular systems using continuum models [78, 125–127]. For example, epithelial

tissue migration can be modeled as a continuum medium and the mechanical problem solved using the finite element method (FEM) [78, 126, 127]. This type of model scales very well for large cell layers but, unfortunately, they do not consider the geometry and behavior of individual cells in the tissue. In addition, some biophysical phenomena are difficult to integrate into this modeling approach.

In this work, we propose a modeling approach that combines an agent-based model and a continuum material model to simulate the mechanical behavior of cells in epithelial tissues. Further, we focus on designing a flexible geometrical representation of the cells and a modular force generation system. In fact, we take some ideas of vertex-based models combined with center-based particle models to represent cells in our modeling approach. Cells are described as discrete particles but they also have a polygonal body associated, that is generated using the Voronoi diagram. In contrast, we model the whole tissue as a continuum media with different domains, basically, cell and substrate domains. The domain properties are defined by the presence of cells and the forces they generate. To solve this mechanical problem, we rely on the finite element method. Therefore, we aim to explore the possibilities that the combination of cell-based models with finite element method can bring to epithelial mechanics modeling, since this approach has not been explored in detail previously. In addition, we present two examples of application of our approach, and we compare them with experimental data taken from previous works of other authors [21, 119, 126]. These examples are based on two extensively studied collective migration processes: durotaxis and gap closure.

4.2 Methods

Our modeling approach is based on three fundamental aspects that are described in Figure 4.1: a discrete cell model, a continuum material model and the interfaces between them. The connection between both models are driven by an adaptable geometry module and several cell force models.

First, we use a discrete cell model in order to track the individual cell information in the tissue. In this way, we are able to characterize individually cell behavior and the direct interaction between each cell and its neighbors and with the substrate. Second, we rely on a continuum material model to create an approximation at the tissue level mechanics. This assumption is supported by the fact that cells in the epithelial tissue are tightly connected by cell-cell junctions [16]. Hence, epithelial monolayer can behave as a continuum media, and some of their mechanical properties can be characterized experimentally [11]. In our continuum material model, we can define several spatial domains in the monolayer and assign them different

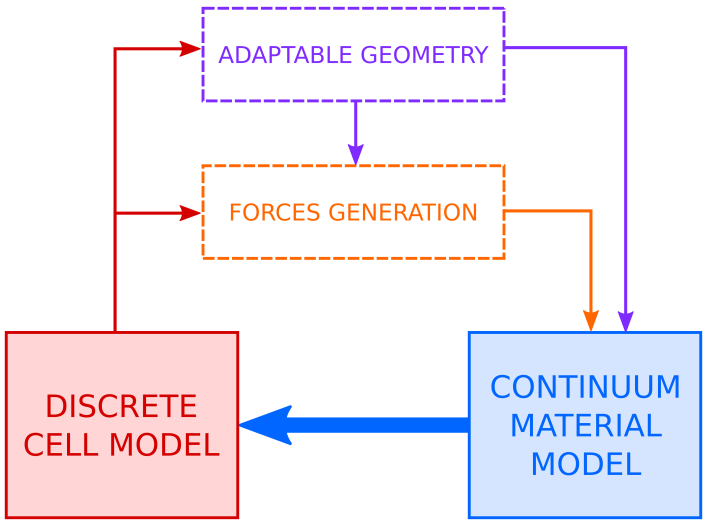

Figure 4.1: Conceptual diagram of the modeling approach. Discrete cell model provides information to geometry and force generation modules. Additionally, to generate the forces used in this approach, forces module also relies on the geometrical representation of the cells. The continuum material model works with the output of geometrical and force modules. Finally, the information generated in the continuum material model is fed back to the discrete cell model.

properties. Moreover, we can specify precise mechanical boundary conditions on our simulations using this continuum approach.

Lastly, to connect both models, we use some geometrical techniques that ease the transition between continuum and discrete representations of cells in the tissue. To tackle cell morphology changes and rearrangements in the monolayer, we must be capable of adapting our representation dynamically to new shapes. To achieve this goal, we combine different tessellation, shape reconstruction and mesh refinement methods. Furthermore, we use several force models based on biophysical phenomena to describe cell behavior in the monolayer.

4.2.1 Discrete cell model

In our modeling approach, we represent each cell of the tissue as a discrete unit. We use an agent-based approach to independently model every cell. Basically, each cell i is defined as a discrete entity $S_i^{cell}(\mathbf{p}_i, R_i, \tau_i)$, whose centroid position is represented by the vector $\mathbf{p}_i$. Every cell has associated a particle virtual radius denoted by R_i and an internal clock denoted by τ_i. The set of all the cells is denoted by $S^{cell} = \{S_1^{cell}, S_2^{cell}, ..., S_n^{cell}\}$. Therefore, we are able to keep separated the

cell information for each unit and associate independent biophyisical processes to them, for instance, its life cycle. In addition, we can track cell position, trajectories and distance traveled directly.

To model cell life cycle, we assume that cells are exclusively in a proliferative state or quiescent. In other words, they can be in an active state of their cycle, that ends up on cell division or, otherwise, in a resting state. We consider that the proliferative state represents both the interphase and the mitotic phase as a simplification of the actual biological process. As shown in equation 4.1, cell internal clock state (τ_i) is incremented in each time step (Δt) if its value is under the cycle division threshold (θ^{cycle}). This process is also regulated by a growing speed parameter (λ^{cycle}). After a cycle is completed, a new daughter cell is generated near its parent cell and both restart their life cycles independently (see Figure S4.1). The duration of the process until cell divides has a slight variability – normal distribution N – to avoid any clustering effect.

$$\begin{aligned} &\text{if } \tau_i(t) < \theta^{cycle} \implies \tau_i(t+\Delta t) = \tau_i(t) + \lambda^{cycle} \\ &\text{if } \tau_i(t) > \theta^{cycle} \implies \tau_i(t+\Delta t) = N(mean = 0.2 \cdot \theta^{cycle}, dev = 0.1 \cdot \theta^{cycle}) \end{aligned} \tag{4.1}$$

This discrete particle-based model is a central part of this work but its cell representation is rather limited. To extend the simulation capabilities of our approach, we generate a more elaborated cell geometry using the information provided by this model as it is described in the following sections. Additionally, the generation of forces depends on some information managed by the discrete model but also on the extended geometrical representation. Hence, the modeling of the forces is tightly related to the discrete model but it can be considered separated from it.

4.2.2 Continuum material model

In contrast to the discrete cell model, our continuum material model represents the mechanical behavior at tissue level. In fact, it is focused on modeling the passive mechanics of the tissue and its properties as a continuum solid [11].

We define a constitutive law for the different materials that can be present in the tissue as shown in equation 4.2 and 4.3. Basically, we consider that tissue can be divided into a cell material (Ω_{cell}) or a substrate material ($\Omega_{substrate}$) considering if cells are present or not. These materials are separated on independent domains with different mechanical properties ($\boldsymbol{C}^{\Omega_n}$), and they interact through their interfaces. In this work, we assume that cell material ($\boldsymbol{C}^{\Omega_{cell}}$) possesses constant properties,

but substrate material stiffness ($\boldsymbol{C}^{\Omega_{substrate}}$) may depend on spatial coordinates ($\boldsymbol{x}$) as illustrated in equation 4.5. This model facilitates the simulation of stiffness gradients in the substrate, that is fundamental to analyze biophysical phenomena such as durotaxis. The stiffness gradient slope is defined by $m(\boldsymbol{x})$, the second-order identity tensor by $\mathbf{1}$, the fourth-order identity tensor by $\boldsymbol{I}$ and the stress and strain tensors by $\boldsymbol{\sigma}$ and $\boldsymbol{\varepsilon}$, respectively. In addition, we define the mechanical properties of the n domain: λ^{Ω_n} as the first Lamé parameter, G^{Ω_n} as the shear modulus, ν^{Ω_n} as Poisson's ratio and E^{Ω_n} as Young's modulus.

$$\boldsymbol{\sigma} = \boldsymbol{C}^{\Omega_n} : \boldsymbol{\varepsilon} \qquad \text{for } n = [substrate, cell] \tag{4.2}$$

$$\begin{aligned} \boldsymbol{C}^{\Omega_n} &= \lambda^{\Omega_n} \mathbf{1} \otimes \mathbf{1} + G^{\Omega_n} \boldsymbol{I} \\ &= \frac{\nu^{\Omega_n}_{PSH}}{(1+\nu^{\Omega_n}_{PSH}) - (1-2\nu^{\Omega_n}_{PSH})} E^{\Omega_n}_{PSH} \mathbf{1} \otimes \mathbf{1} \\ &\quad + \frac{1}{2(1+\nu^{\Omega_n}_{PSH})} E^{\Omega_n}_{PSH} \boldsymbol{I} \end{aligned} \tag{4.3}$$

$$\nu^{\Omega_n}_{PSH} = \frac{\nu^{\Omega_n}}{1-\nu^{\Omega_n}} \qquad E^{\Omega_n}_{PSH} = \frac{E^{\Omega_n}}{1-(\nu^{\Omega_n})^2} \tag{4.4}$$

$$\begin{aligned} &E^{\Omega_{substrate}}(\boldsymbol{x}) = E^{substrate} + m(\boldsymbol{x}) \qquad \text{for } \boldsymbol{x} \in \mathbb{R}^2 \\ &E^{\Omega_{cell}} = E^{cell} \neq E(\boldsymbol{x}) \end{aligned} \tag{4.5}$$

We use the finite element method (FEM) to solve the continuum mechanical problem at tissue level. Each domain considered in the model is represented by independent elements of the FE mesh. To connect these separated domains, we use coincident nodes in their interfaces. Moreover, in order to solve the system in 2D, we assume the plane stress hypothesis (PSH) since one of the monolayer dimensions (thickness) is very small compared to the others. We transform the material parameters as shown in equation 4.4.

Mesh and force generation are explained in detail in their corresponding sections but it is worth noting here their implications in the continuum model. In particular, the mesh used for the FE resolution is generated using cell centroids of the discrete model and the additional polygonal representation of cell bodies. Furthermore, the cell forces are applied to nodes that correspond to either the cell vertices or centroids used to generate the mesh. Hence, these two aspects of our approach are the actual connection between discrete and continuum models.

Finally, after solving the FE problem, we use the deformed mesh to obtain cell displacements from the nodes that represent the cell centroids. These displacements are processed by the discrete model to update cell positions.

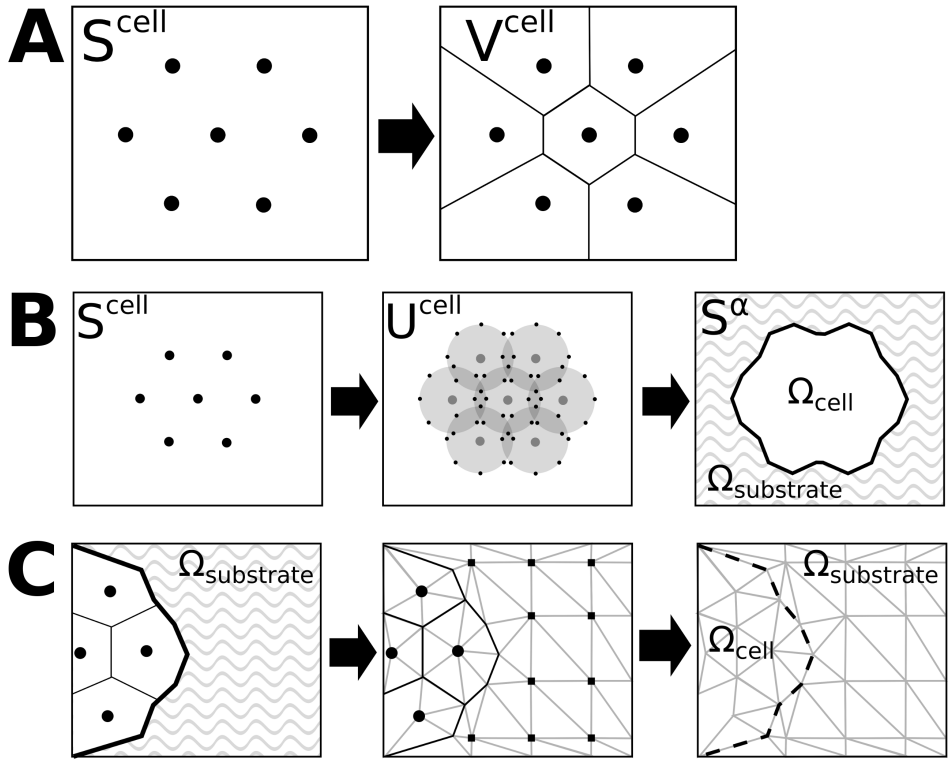

Figure 4.2: Geometry generation. (A) We generate the Voronoi diagram V^{cell} from cell centroids S^{cell} of the discrete model. (B) We create the alpha shapes S^{α} from the virtual circles U^{cell} centered on cell centroids S^{cell}. We use the alpha shapes to differentiate cell domain Ω_{cell} from substrate domain $\Omega_{substrate}$ and, therefore, to define the limits of the epithelial monolayer. (C) We generate the FE mesh (M^{FEM}) from a Delaunay triangulation of the following set of points: cell centroids (S^{cell}), cell vertices (V^{cell}), alpha shapes (S^{α}) and a regular grid in the substrate domain (S^{grid}).

4.2.3 Adaptable geometry

Since tissue morphology changes during cell reorganization, proliferation and migration processes, we need to use a cell geometrical representation flexible enough to adapt to these alterations. Discrete particle model offers a rather limited representation of the cell body. However, we extend cell geometry from a discrete point to a polygon using a Voronoi diagram built from cell centroids. Furthermore, to define the tissue domains, we create alpha shapes that depend on the cell distribution. Lastly, FE mesh is generated using information of the Voronoi diagram and the alpha shapes. Using all these techniques, we effectively connect discrete and continuum models at the geometrical level.

Voronoi diagram

We use Voronoi diagram to generate a representation of cell body using the information from our discrete model (S^{cell}). This tessellation technique divides the plane using an initial set of points into regions (V_i^{cell}) whose distance to its generator point (S_i^{cell}) is less than to any other initial point (S_j^{cell}) as shown in equation 4.6. The resultant convex polygon V_i^{cell} represents the cell body associated to each cell centroid S_i^{cell} as it is shown in Figure 4.2A. We use the function $d(\boldsymbol{x}, \mathbf{p}_i)$ to describe the distance between a point ($\boldsymbol{x}$) and the cell centroid.

$$V_i^{cell} = \{\boldsymbol{x} \in \mathbb{R}^2 : d(\boldsymbol{x}, \mathbf{p}_i) < d(\boldsymbol{x}, \mathbf{p}_j) \quad \text{for } i \neq j\} \tag{4.6}$$

In fact, this cell representation is fundamental to join both continuum and discrete models together. We create a transition from a pure discrete particle-based representation of cells to a partitioned continuum space. In our approach, this tessellation is generated dynamically, in other words, it is a stateless representation of the cell body that it is not stored from one step to the next. It can also be described as a transient vertex-based model since we use this polygonal body to simulate more detailed cell behavior and to map forces. Additionally, Voronoi diagram is a reliable tool to determine neighboring and shared edges between cells in the monolayer ($S^{neighbors} \subset S^{cells}$).

Last, we use this polygonal representation to determine daughter cell position after cell division. We calculate the minimum ellipse that contains the polygon and force the cell cleavage on the minor axis of that ellipse (see Figure S4.1).

Alpha shapes

To differentiate between distinct tissue domains, we generate alpha shapes from our discrete model. These are a family of linear curves associated to a set of points, in our case, to the cells. Alpha shapes are defined by an α parameter that is related to the maximum distance between points for connecting them. In the case of $\alpha \to \infty$, the curve obtained contains all considered points. On the contrary, when $\alpha \to 0$, alpha shapes just degenerates to the set of points. Moreover, more than one curve can be created using this technique. It is even possible to generate 'holes' inside closed curves.

Instead of generating alpha shapes only from cell centroids (S^{cell}), we use virtual circles (U^{cell}) centered on each centroid as shown in equation 4.7 and Figure 4.2B. The virtual circle associated to each cell (U_i^{cell}) is defined by the virtual cell radius (R_i), that it is also used for the cell-cell interactions as it is explained later on

this chapter. In this way, we are able to represent the body of cells located in the monolayer boundary or completely isolated. Hence, we avoid a collapse of the alpha shape to the cell centroid.

$$S^{\alpha} = f(U^{cell}, \alpha) \tag{4.7}$$

We define $f(S, \alpha)$ as the function that generates all possible alpha shapes and S^{α} as the alpha shape for our current set of points for a given α value.

Finally, since Voronoi diagram is a tessellation of an infinite plane by definition, we use these alpha shapes in order to limit the polygonal representation to a finite domain ($S^{\alpha} \cap V^{cell}$). Therefore, we can determine the general location of cells in the tissue. We can conclude if a cell is surrounded only by other cells or it is in direct contact with the substrate.

Dynamic meshing: FE discretization

To generate a mesh for the finite element analysis (M^{FEM}), we create a Delaunay triangulation of a set of points ($DT(P)$) as shown in equation 4.8 and Figure 4.2C. In order to obtain a coherent mesh with coincident nodes, the triangulation is constructed by points of the cell domain and the substrate domain. In the cellular domain, we use cell centroids (S^{cell}), Voronoi polygon vertices (V^{cell}) and points from the alpha shape curves (S^{α}). In the substrate domain, we create a regular grid of points (S^{grid}):

$$\begin{aligned} U^{FEM} &= S^{cell} \cup V^{cell} \cup S^{\alpha} \cup S^{grid} \\ M^{FEM} &= DT(U^{FEM}) \end{aligned} \tag{4.8}$$

The dynamic mesh generation is a key aspect of our approach since, in this process, we map the information from discrete cell model and all the geometrical traits to the continuum model. Here, we keep the relation between centroids and vertices and their corresponding nodes in the mesh. Therefore, we are also able to pass information from the continuum model to the discrete model.

4.2.4 Force generation

To model the cell mechanical behavior, we must consider the forces that generate each one individually and the forces generated on their interactions. First, we describe cell-cell interaction forces using a potential with a repulsive and an attractive term. Second, the contraction force that is generated in each cell by its cytoskeleton. Finally, two different collective migration modes that create forces in the tissue: cell crawling and purse-string [18, 128].

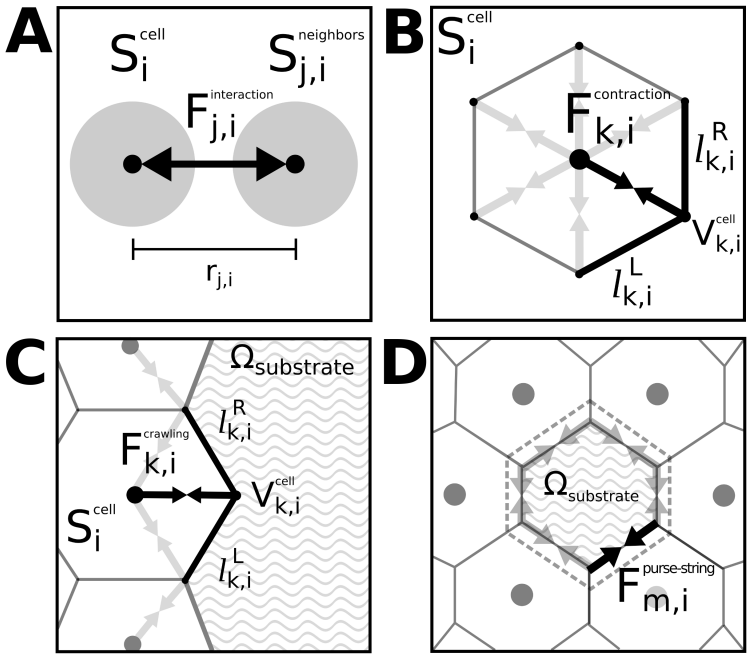

Figure 4.3: Force generation. (A) Cell-cell interaction force $F_{j,i}^{interaction}$ between cell S_i^{cell} and its neighboring cell $S_{j,i}^{neighbors}$. Distance between cells is denoted by $r_{j,i}$. (B) Contraction force in the vertices ($V_{k,i}^{cell}$) of the cell S_i^{cell}. This force depends on the edges lengths $l_{k,i}^R$ and $l_{k,i}^L$ related to the vertex k. We apply the same force with inverted sign to the cell centroid. (C) Cell crawling forces $F_{k,j}^{crawling}$ are similar to contraction forces, but they are only applied to vertices that are on the cell-substrate interface. (D) In purse string migration, we generate a ring around the gap in the monolayer that connects cell vertices m located on the cell-substrate interface. The contraction of the ring generates a force $F^{purse\text{-}string}$.

Cell-cell interaction

To model the direct interaction between cells, we use a potential that approximates several biophysical phenomena. In fact, we consider the average effect of cell adhesion, cytoskeleton interaction and volume exclusion.

We use an interaction force between particles i and j ($F_{j,i}^{interaction}$) that is derived from Lennard-Jones potential as it is shown in equation 4.9. In this work, this potential depends on the distance between cells ($r_{j,i}$) and the sum of cell virtual radii ($r = R_i + R_j$). In addition, there is a parameter ε that modulates the magnitude of the interaction forces. This potential presents a repulsive and an attractive term and, therefore, a distance of equilibrium (r_m) where both effects compensate.

$$F_i^{interaction} = \sum_j F_{j,i}^{interaction}(r) = 12\varepsilon \cdot \sum_j \left[\left(\frac{r_m^{12}}{r_{j,i}^{13}} \right) - \left(\frac{r_m^6}{r_{j,i}^7} \right) \right] \tag{4.9}$$

Unlike other forces in our modeling approach, cell-cell interaction forces depend exclusively on the discrete cell model. These forces are calculated considering all neighboring cells ($S_i^{neighbors}$), and the resultant force is located at the cell centroid position as shown in Figure 4.3A. For each pair of cells, the direction of the force is defined from the cell centroid to the neighbor cell centroid. Finally, the effect of the ε parameter in the monolayer is described in detail in a previous work [116](Chapter 2).

Actomyosin contraction

To model the effect of actomyosin contraction in cell cytoskeleton, we assume a constant net force for the whole cell ($F^{contraction}$). However, we model locally these forces on each vertex k of the polygonal representation of the cell i ($V_{k,i}^{cell}$) as Figure 4.3B illustrates. We show in equation 4.10 that the magnitude of the force on each vertex ($F_{k,i}^{contraction}$) is a constant ($K^{contraction}$) multiplied by a length ratio associated to the vertex. This ratio is equal to the sum of half-lengths of both edges connected by the vertex ($l_{k,i}^R$ and $l_{k,i}^L$) divided by the total cell perimeter (P_i).

$$F_i^{contraction} = \sum_k F_{k,i}^{contraction} = K^{contraction} \cdot \sum_k \left(\frac{l_{k,i}^R + l_{k,i}^L}{2 \cdot P_i} \right) \tag{4.10}$$

These force vectors are directed from cell vertex to the cell centroid. In addition, we apply a similar force with the inverse sign on the cell centroid (S_i^{cell}). The reasoning behind this force model is that cytoskeleton contraction driven by actomyosin is homogeneous in non-polarized cells [129]. Thus, we are assuming that in this particular contraction force there is no polarization beyond the apico-basal one.

Cell Crawling

Cell crawling is a migration mode in which cell extends a protrusion that adheres to the substrate and pulls from it [18, 119, 128]. We model this phenomenon like the actomyosin contraction but only considering cell vertices that are on the cell-substrate boundaries ($\Gamma^{cell\text{-}substrate}$) and its own constant ($K^{crawl}$), as shown in equation 4.11. Hence, these forces (F_i^{crawl}) are not present on the shared faces between cells inside the monolayer as illustrated in Figure 4.3C.

$$F_i^{crawl} = \sum_k F_{k,i}^{crawl} = K^{crawl} \cdot \sum_k \left(\frac{l_{k,i}^R + l_{k,i}^L}{2 \cdot P_i} \right) \quad \text{for } V_{k,i}^{cell} \cap \Gamma^{cell\text{-}substrate} \quad (4.11)$$

In fact, we are assuming here that there is a front-back polarization in the cells that is directed towards substrate domain. Therefore, only cells in direct contact with the interface cell-substrate domain are playing a leading role in the crawling migration mode.

Purse string

Purse string is a migration mode only present in multi-cellular systems with matured cell-cell adhesions [18, 20]. This migration mode is found typically in gap closing and wound healing biological processes. In purse string migration, cells create an actomyosin string that surrounds the gap in the layer. This inter-cellular string contracts and generates forces that, effectively, pull from cells to close the gap.

As Figure 4.3D shows, we model these forces ($F^{purse\text{-}string}$) creating a virtual string that connects cells located around a gap in the tissue. Then, we generate a contraction force on vertices $V_{m,i}^{cell}$ that are shared between cell i and its neighbors j, and also located on cell-substrate interface ($\Gamma^{cell\text{-}substrate}$):

$$F_{m,i}^{purse\text{-}string} = K^{purse\text{-}string} \qquad \text{for } V_{m,i}^{cell} = V_{k,i}^{cell} \cap V_j^{cell} \cap \Gamma^{cell\text{-}substrate} \quad (4.12)$$

We assume that these forces are constant ($K^{purse\text{-}string}$) in our approach.

4.3 Numerical implementation

For the computational implementation of our approach, we use several open-source tools and libraries to extend our own code and to process the results of the simulations. We develop this simulation framework in *C++* using functionality of the *C++11* revision and, in addition, we create some Python tools for the representation and the analysis of the results. In fact, we rely on third party libraries that are demonstrably efficient and well tested. The computational workflow is represented and described in detail in Figure 4.4.

In this work, the discrete cell model is developed completely from scratch including its life cycle model. Additionally, the force generation models are also programmed exclusively for this simulating approach using our own code.

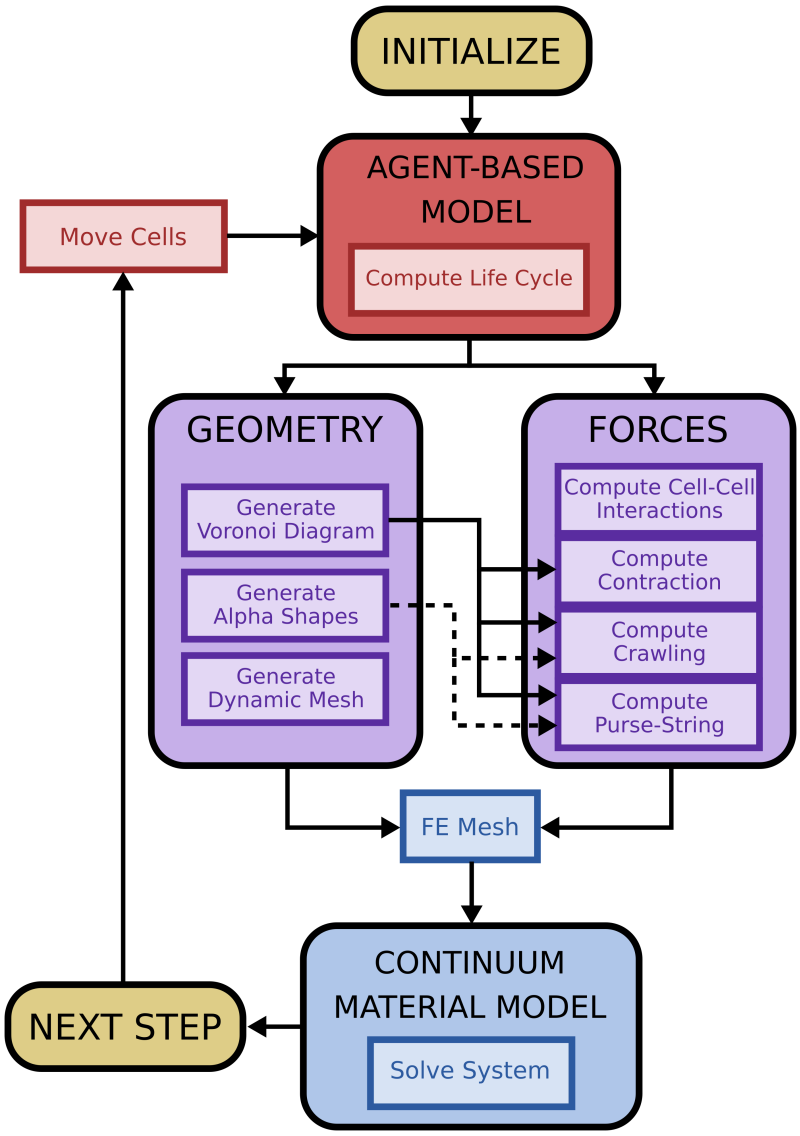

Figure 4.4: Computational workflow. First, we initialize the system variables and, afterwards, we enter the main loop of the calculation. In the agent-based model, we compute the life cycle and cell internal clock is updated. Further, we determine here which cells divide. We use the information of the agent-based model to generate the geometry and the forces in the system. Some forces also depend on the Voronoi diagram representation of the cells and the alpha shapes. Later, we generate the FE mesh and we apply the forces to mesh nodes that correspond to cell centroids and cell vertices. We solve the FE problem after we have defined the material properties of each monolayer domain. Last, we use the deformed mesh to update cells position in the next step.

We use *CGAL* library [2] to compute most of the geometrical algorithms explained before. This library is focused on providing tools for mathematical operations with complex geometries. We use exact predicates and exact constructions kernel to reduce numerical errors in the geometrical operations as much as possible. In addition to the core packages, we use several *CGAL* modules: *2D Triangulation*, *2D Polygons*, *2D Voronoi Diagram Adaptor*, *2D Alpha Shapes* and *Bounding Volumes*.

Moreover, we use *deal.II* library to solve the mechanical problem by the FEM [1]. This library is a very powerful and flexible tool that provides base classes for the basic components to develop a FEM application. In addition, it also provides useful interfaces with external solvers, for instance, *UMFPack* [130] that is the one we use. Additionally, we create a refinement method to convert the triangular mesh in to a quadrilateral mesh since deal.II does not support triangles. We subdivide each triangle into three quadrilaterals as shown in detail in Figure S4.2. We create an intermediate translation layer between geometrical representation and deal.II to manage the mesh and the information associated to it.

Finally, we develop a *legacy VTK* parser to represent results from discrete model and *CGAL* structures. In addition, we visualize these files and generate animations using *Paraview* [4]. We use *seaborn* [3], *pandas* [131] and an in-house python library to perform statistics on the simulation raw data. Moreover, we also rely on *seaborn* to plot the results of the statistical analysis.

4.4 Results

To validate our approach, we present here two examples of application that are found in the literature to describe epithelial tissue mechanics. First, we simulate a cell monolayer over a substrate that presents a stiffness gradient [119, 132]. In this biological scenario, we study cell collective migration to stiffer environments, this phenomenon is also known as durotaxis. Second, we analyze how mechanical interactions between cells and substrate affect gap closing process in epithelial monolayers [20, 126].

For each case shown in the following results, we have run at least $N = 5$ simulations in order to calculate the statistics. In addition, simulation parameters are defined in the tables shown for each example (Table 4.1 and Table 4.2), and we do not change these default values unless it is explicitly indicated.

4.4.1 Collective durotaxis

Durotaxis is the biological process in which cells sense and follow gradients on the extracellular matrix [4]. Cell crawling is the migration mode that predominates in the case of collective durotaxis. Therefore, cells located at the edges of the layer extend protrusions that adhere to the substrate. Afterwards, the contraction of this protrusion produces a deformation of the cell and the substrate. This deformation depends on the rigidity of extracellular matrix and defines the net displacement of the cell center of mass. In softer matrices, substrate deformations are larger and cell center of mass movement is reduced for the same contraction force. On the contrary, cells are effectively displaced larger distances on stiffer matrices since substrate deformations are smaller. Therefore, a cell monolayer will effectively migrate over a substrate that presents a stiffness gradient.

Moreover, it has been observed experimentally that force transmission to the substrate in collective cell migration is mostly concentrated at the monolayer edges [119]. Thus, we assume that interaction between cell monolayer and substrate can be modeled applying forces only on the interface that separates both domains as it is shown in Figure S4.3. To simulate this process using our modeling approach, we consider forces that are generated by cell-cell interactions, cell contraction and cell crawling models explained in the previous sections. In this case, we do not use purse string forces since it is not relevant for this phenomenon. Purse string migration mechanism is mainly found in gap closure or wound healing processes and not in the case of monolayer expansion shown in this example [18, 20].

Finally, we simulate three different scenarios to study collective durotaxis changing substrate properties: uniform stiffness, steep stiffness gradient and shallow stiffness gradient. For two later cases, we use a linear stiffness gradient where the softer side is always on the left of the simulated substrate and the stiffer side is on the right. The difference between steep and shallow gradient is just the slope of the linear function that defines the stiffness of the substrate.

Results and Discussion

We calculate the angular distribution of cell trajectories on the three substrates to understand how substrate stiffness gradients affect cell migration. This distribution is obtained using the angle between cell velocity vector direction and X axis. Instantaneous cell velocity vector is computed from the cell trajectories for every 50 simulation steps. This metric let us understand if cells show a preferential direction during migration. In Figure 4.5A, we observe that cells present durotaxis only when a stiffness gradient is present (see Video S4.4 and Video S4.6), as it was described

General parameters	
Cell radius - R_i (μm)	10
Cell layer size (μm)	500x1000
Substrate size (μm)	2500x1000
Alpha shapes parameter - α	150
Proliferation parameters	
Growth rate - λ^{cycle}	0.05*
Proliferation threshold - θ^{cycle}	100*
Cell domain mechanical properties	
Cell domain Young's modulus - E^{cell} ($\mu N/\mu m^2$)	0.02 [11]
Cell domain Poisson's ratio - $\nu^{\Omega_{cell}}$	0.49**[11]
Substrate domain mechanical properties	
Substrate domain Young's modulus - $E^{substrate}$ ($\mu N/\mu m^2$)	0.02 [11, 119]
Substrate domain Poisson's ratio - $\nu^{\Omega_{substrate}}$	0.49**[11]
Uniform stiffness slope - m (kPa/mm)	0
Shallow stiffness gradient slope - m (kPa/mm)	15 [119]
Step stiffness gradient slope - m (kPa/mm)	57 [119]
Force generation parameters	
Cell-cell interaction parameter - ε (μN)	1.0e−4 [116]
Cell contraction constant - $K^{contraction}$ (μN)	5.0e−4 [119, 129]
Cell crawling constant - K^{crawl} (μN)	1.5e−3
Purse-string constant - $K^{purse\text{-}string}$ (μN)	0

* Approximately a 2% of cells proliferating

** Approximately incompressible

Table 4.1: Collective durotaxis parameters

in previous experimental studies [119]. In addition, the cell motion persistence is intensified by using steeper stiffness gradients. Therefore, cell migration over substrates with a steep stiffness gradient is more polarized than over substrates with a shallow stiffness gradient.

Furthermore, we analyze the displacement of the monolayer center of mass over substrates with different average stiffness. These results let us determine how durotaxis phenomenon is affected by extracellular matrix rigidity. Hence, we calculate the displacement of center of mass using the average distance from left border to right border of the monolayer. We predict that durotaxis is reduced when substrate global stiffness increases as shown in Figure 4.5B. On the other hand, on lower stiffness substrates within the stiffness range analyzed, the durotaxis is more pronounced when the gradient is stronger.

On Figure 4.6A,B, we can observe how cell displacements are distributed during

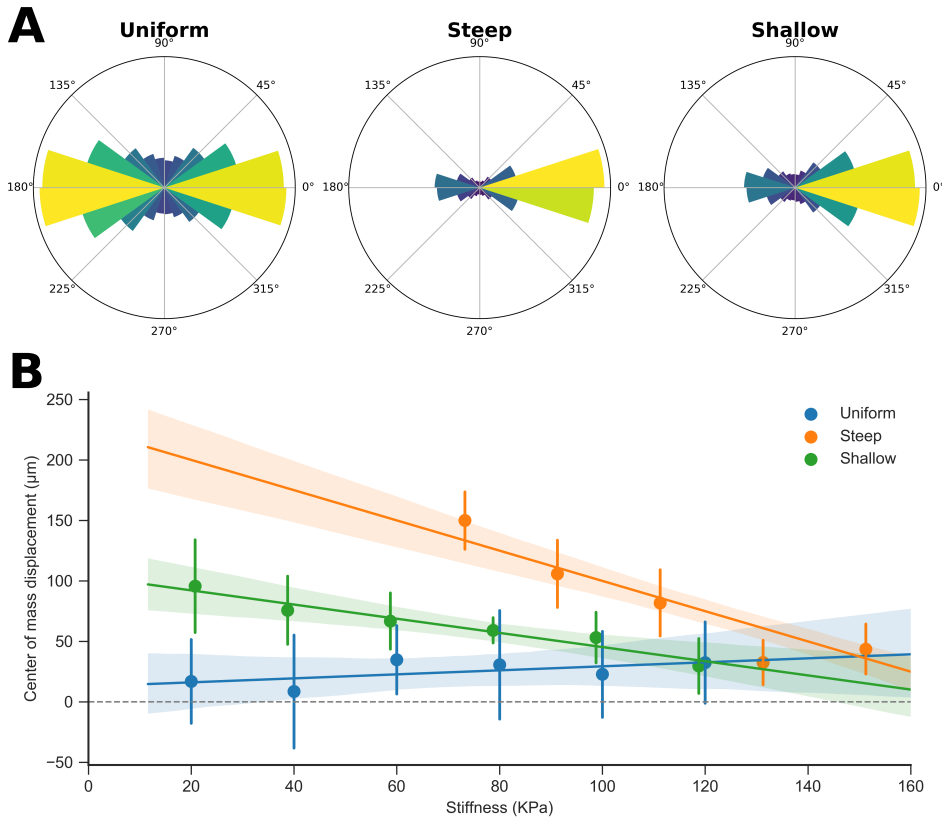

Figure 4.5: Cell migration direction and collective durotaxis. (A) Angular distribution of cell trajectory for the three different substrates. Cells only shows a preferential direction to migrate when a stiffness gradient is present. (B) Displacements of monolayer center of mass depending on the initial substrate stiffness. Collective durotaxis is reduced on stiffer substrates.

the simulation. In the case with a substrate stiffness gradient, cells are moving to the stiffer side of the substrate and the displacements are higher in gradient direction. In the uniform stiffness case, cell displacements are distributed without a preferential direction. Finally, stresses in the monolayer accumulate on the interface between the substrate and the monolayer in both cases as seen in Figure 4.6C,D (see Video S4.5 and Video S4.7).

These simulation results are compatible with the experimental data from Sunyer et al.[119]. Moreover, they validate several of our model considerations about collective cell migration and cell interaction with the substrate. In particular, the assumption that force transmission between cell monolayer and substrate occurs exclusively in the monolayer borders. Further, we predict that durotaxis effectiveness

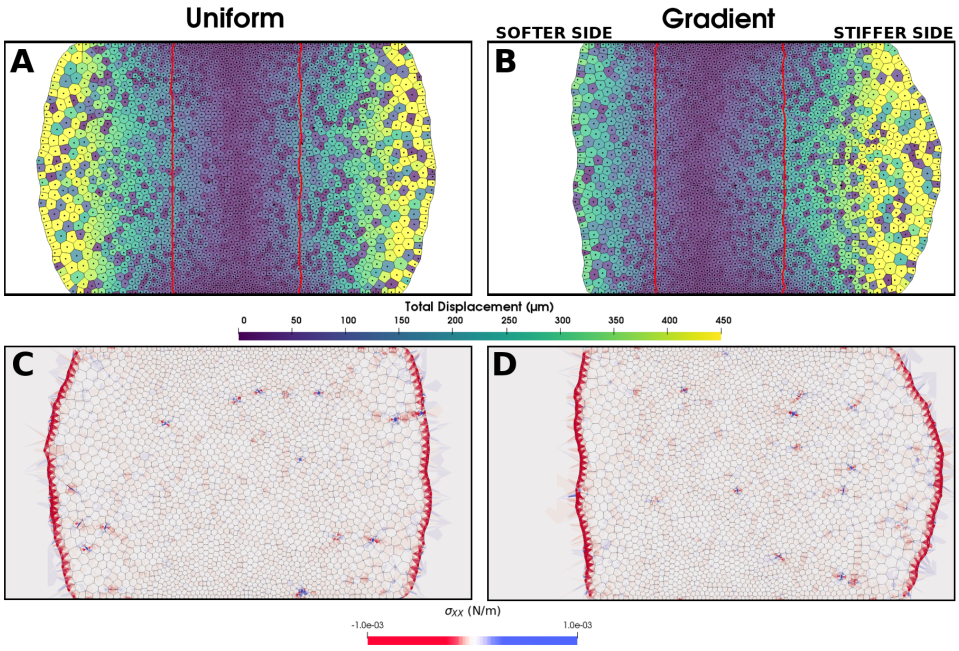

Figure 4.6: Displacement and stress map in collective durotaxis. (A, B) Total distance traveled by cells. The initial shape of the monolayer is shown in red. We observe that when stiffness gradient is present cells show a preferential direction to migrate. (C, D) Principal stresses in the material. We observe that in both uniform and gradient substrates stresses are accumulated in the monolayer/substrate interface.

decreases when average stiffness of the substrate increases, that is also one of the main conclusions of Sunyer et al.[119] work.

Finally, it is also demonstrated here that using a transient vertex model combined with a continuum material model is a reliable option to simulate complex mechanical phenomena in cell monolayers.

4.4.2 Gap closure

In contrast to monolayer expansion, epithelial cells can present several migration modes during gap closing. It has been observed that depending on gap size, tissue type and environmental conditions the way to close a gap in the tissue may change, however, cell crawling and purse string contraction are the most common migration modes [18, 20, 21, 126]. Moreover, these modes can even be present at the same time and compete between them to dominate the closing process.

Here, we aim to analyze how these migration modes affect a gap closing process using our modeling approach. We generate a confluent monolayer and then remove

General parameters	
Cell radius - R_i (μm)	10
Cell layer size (μm)	1000x1000
Substrate size (μm)	1000x1000
Gap size (μm)	180x180
Alpha shapes parameter - α	150
Proliferation parameters	
Growth rate - λ^{cycle}	0*
Proliferation threshold - θ^{cycle}	0*
Cell domain mechanical properties	
Cell domain Young's modulus - E^{cell} ($\mu N/\mu m^2$)	0.02 [11]
Cell domain Poisson's ratio - $\nu^{\Omega_{cell}}$	0.49**[11]
Substrate domain mechanical properties	
Substrate domain Young's modulus - $E^{substrate}$ ($\mu N/\mu m^2$)	0.02 [11]
Substrate domain Poisson's ratio - $\nu^{\Omega_{substrate}}$	0.49**[11]
Force generation parameters	
Cell-cell interaction parameter - ε (μN)	1.0e−4 [116]
Cell contraction constant - $K^{contraction}$ (μN)	5.0e−4 [119, 129]
Cell crawling constant - K^{crawl} (μN)	5.0e−4
Purse-string constant - $K^{purse\text{-}string}$ (μN)	1.5e−3

* No proliferation

** Approximately incompressible

Table 4.2: Gap closure parameters

some cells from the center to create a gap. In this case, we consider all the forces explained before: cell-cell interaction, contraction, cell crawling and purse string. We focus our efforts on studying the effect of cell crawling and purse string forces in this phenomenon.

Results and Discussion

To understand the effect of cell forces in gap closing, we quantify the area of the tissue gap using the alpha shapes and the cell average velocity. We compare how cells close the gap using purse string and crawling migration mode in Figure 4.7A,B. In fact, we observe different cell velocity profiles between migration modes. Purse string migration presents a high initial velocity that decays rapidly. In contrast, cell crawling migration shows an almost constant velocity profile. Moreover, we observe a reduction of the curvature and a smoothing of the gap morphology in the case of purse string migration as shown in Figure 4.7E (see Video S4.8). However,

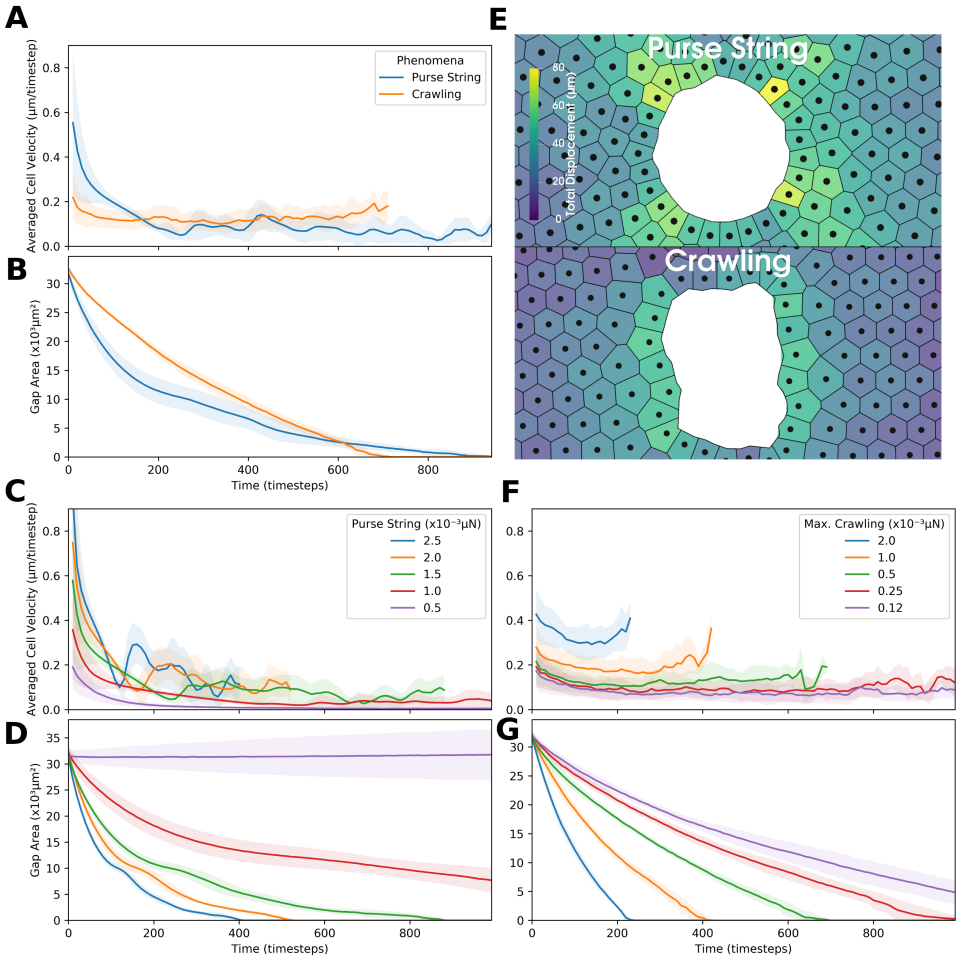

Figure 4.7: Collective migration during gap closure. (A, C, F) Average cell velocity during the simulation under different conditions. (B, D, G) Gap area during the simulation under different conditions. (A, B) Comparison between purse string and crawling migration mode. (C, D) Parametric analysis of purse string forces. (F, G) Parametric analysis of crawling forces. (E) Gap morphology with purse string migration mode (top) and crawling migration mode (bottom).

this curvature reduction is not observed in crawling migration mode. These results are in agreement with the experimental results found in [126].

On Figure 4.7C,D, we show a parametric analysis of the purse string force effect in gap closing (see Video S4.9). The cell velocity presents a high initial value for all the cases followed by a notable velocity drop. In addition, gap area evolution during the simulation is highly non-linear. Moreover, we observe that gap closes faster for higher purse string forces. However, cells never fill the gap using when purse string forces are too low ($0.5\text{e}{-3}\,\mu N$).

Furthermore, we show a parametric analysis of cell crawling forces in Figure 4.7F,G (see Video S4.10). We predict that for all cases gap closes faster when we increase crawling force. In contrast to purse string, cells fill the gap even when we are using very low crawling forces and gap area profile is almost linear.

It has been previously reported that larger gaps are dominated mostly by cell crawling [18, 20, 21, 126]. If we observe the results from our simulations, purse string mechanism creates a very fast migration that decays quickly. Hence, our results are compatible with these observations since closing a large gap in a monolayer needs a constant migration force to complete the process. The initial peak of cell velocity during purse string migration may facilitate the closure when the gap is small. In addition, the reduction of curvature and the gap border smoothing could also be beneficial in combination with cell crawling. In fact, exclusive cell crawling migration does not produce a homogeneous closure as it is shown in the work of Ravasio et al. [126] and Brugués et al. [20]. Therefore, purse string may not be the main driving force in some gap closure cases, but it can help to smooth and homogenize the process.

In conclusion, we successfully reproduce here another collective migration phenomenon from a mechanical perspective. In our approach, we can study the effect of the two migration mechanisms separately. Moreover, we observe their effects at monolayer scale and we can still track the individual cell velocities and trajectories (see Videos S4.8, S4.9 and S4.10).

4.5 Conclusions

We present here a novel approach to model collective migration in epithelial cell monolayers. In fact, we combine a discrete agent-based model that let us keep individual cell information with a continuum material model that can simulate tissue and substrate mechanical behavior. In this modeling approach, we also aim to build a framework from modular models. This design facilitates the inclusion of independent force models and decoupling some biophysical phenomena.

We demonstrate that our modeling approach is able to reproduce a variety of experimental results for durotaxis and gap closure processes. First, we analyze the assumption that force transmission between cell layer and substrate occurs right on the interface. This is valid for cases where monolayer is expanding, and, therefore, it is also applicable to durotaxis phenomenon. Further, our results predict the behavior of collective cell migration on substrate stiffness gradients [119]. Second, we reproduce and compare the effect of the principal migration mechanisms in gap closing process: cell crawling and purse string contraction. We observe a very

different response and gap morphology for the two migration modes. In fact, these results are compatible with the experimental results obtained by other authors that have extensively analyzed gap closure [18, 20, 21, 126].

Unlike the classic vertex-based model, we can not control the shape of the cells explicitly since its generation is given by the cell centroids positions on the Voronoi diagram. Despite this can be considered a drawback of our approach, cell morphology is an emergent property of the system that depends on the cell spatial distribution. In fact, we are not really interested in controlling individual cell morphology, but in using the cell shape to more accurately distribute the forces generated in the layer.

In this work, we have assumed that stress dissipation in the monolayer due to cytoskeleton and cell-cell junctions restructuring is several orders of magnitude faster than cell rearrangements and migration on the layer [5, 11, 15, 17]. Thus, we do not accumulate stresses in the monolayer material from one step to the next under this assumption. Although we would need to accumulate these stresses to simulate very fast mechanical changes in the epithelial layer, this simplification is still valid for 'slow' migration and rearrangement processes shown here as examples of application. In any case, we could accumulate stress in the material and model a non-instantaneous stress dissipation during the simulation, but it is out of the scope of this study.

We believe that this modeling approach here presented offers a great flexibility and new possibilities to simulate cell layer mechanics which were not considered before. The combination of particle, transient vertex representation and continuum model may open new strategies to model other inherently 2D biological processes where cell and tissue mechanics are fundamental. For instance, it would be possible to apply this approach to simulate processes where cells are driven by patterns on the substrate, cell transition between solid-like to fluid-like behavior or collisions between migrating cell monolayers.

4.6 Supplementary material

Figure S4.1: Cell division using the minimum ellipse.

We model an oriented cell division over its shortest axis. To simulate this division, we generate an ellipse that is circumscribed in the cell polygonal representation. Since polygonal representation of the cells is generated using Voronoi diagram, we locate parent (S_i^{cell}) and daughter (S_j^{cell}) centroids on the ellipse major axis separated by a distance d. Therefore, cell will be effectively divided by the shortest ellipse axis.

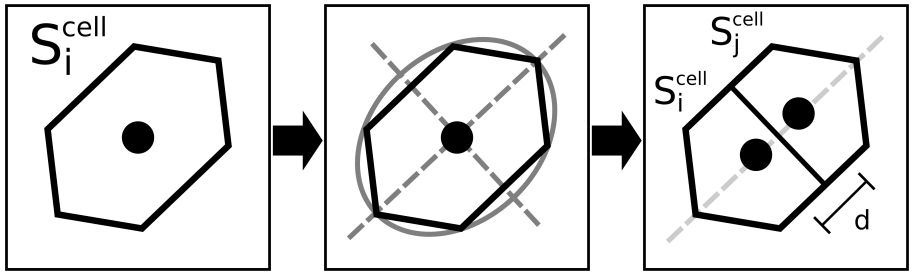

Figure S4.2: Mesh refinement.

Our original FE mesh generated from the Delaunay triangulation is, by definition, composed by triangles. However, we use *deal.II* library to solve FE problem and, unfortunately, it does not support triangles. Hence, we must convert triangular elements to quadrilaterals. To overcome this issue, we refine each triangular element E of the mesh into three quadrilaterals E'_A, E'_B and E'_C. The vertices of these quadrilaterals are defined by the vertices of the triangle E, the midpoints of E edges (M_A, M_B and M_C) and the center of mass of E (C_E).

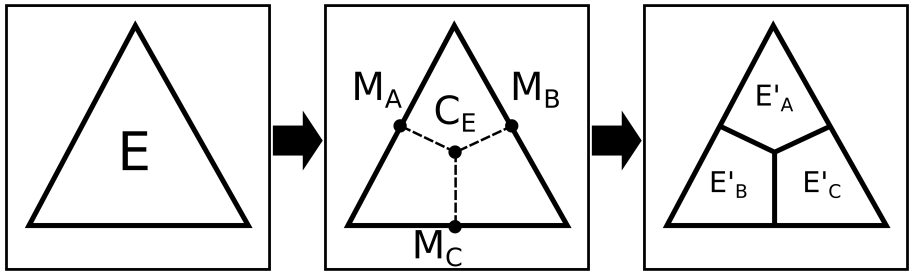

Figure S4.3: Force transmission between the monolayer and the substrate.

The force transmission between expanding cell monolayer and substrate is mainly concentrated at the limits of the monolayer. Basically, forces are transmitted through the cell monolayer by the cell-cell junctions and to the substrate by cell-substrate adhesions. These cell-substrate adhesions are notably stronger at the monolayer limits. Therefore, we do not model the substrate under the cell monolayer since its role in the force transmission is negligible during collective migration.

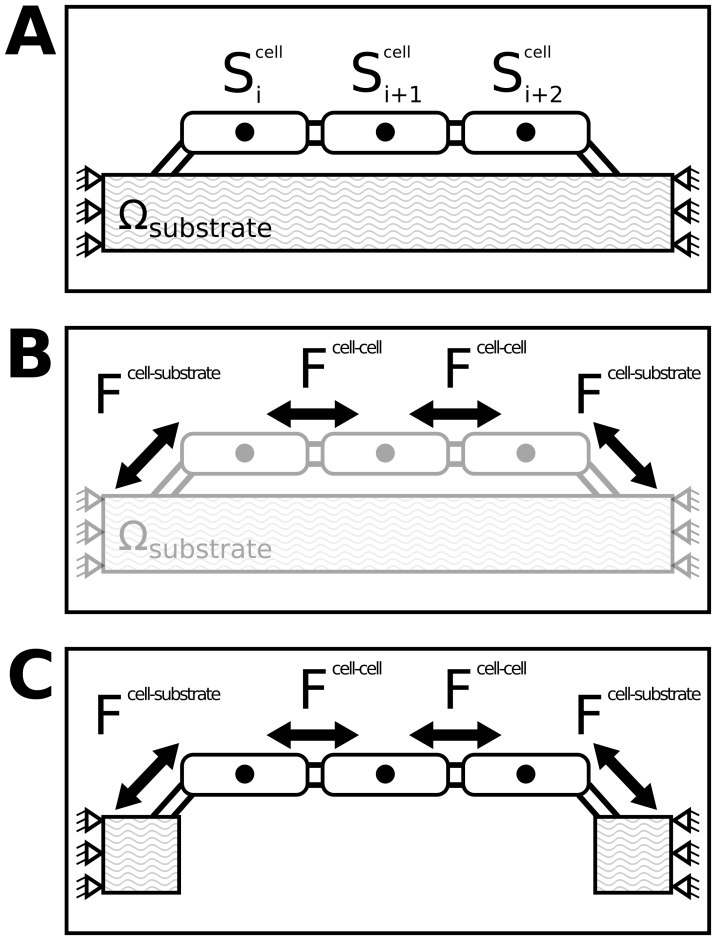

Video S4.4: Cell displacements in a uniform substrate.
Video S4.5: Monolayer stresses in a uniform substrate.
Video S4.6: Cell displacements in a substrate with a stiffness gradient.

Video S4.7: Monolayer stresses in a substrate with a stiffness gradient.
Video S4.8: Comparison between purse-string and cell crawling forces.
Video S4.9: Parametric analysis of purse-string force.
Video S4.10: Parametric analysis of cell crawling force.

This document and its supplementary material are accessible from:
`https://m2be-storage.unizar.es/pydio_public/ismael-thesis`

5

Cell Clusters in 3D Environments

Contents

This chapter is published as:

Ismael González-Valverde, Carlos Semino and José Manuel García-Aznar. *Phenomenological modelling and simulation of cell clusters in 3D cultures.* Computers in Biology and Medicine, Vol. 77, 249-260. August (2016).

5.1 Introduction

Cell clustering is described as the formation of multi-cellular aggregates from individual cells via the creation of adherent junctions [22]. Cellular aggregation has been shown to be fundamental in certain biological processes, such as tissue formation during different stages of embryonic development. Mesenchymal progenitor cells migrate and condensate, forming high-density cell aggregates that will differentiate into several tissue lineages at early stages [25, 26]. Furthermore, cell-cell interactions play an important role in the formation of these aggregates and the collective cell behavior. It is well known that the behaviors of cells are completely different if they are in direct contact with other cells rather than being isolated [23]. Moreover, some biological processes, such as differentiation, do not occur in the absence of these interactions [24].

Cluster formation is directly influenced by cell movement, but cell contacts inside an aggregate also regulate the cell migratory pattern [133, 134], which inhibits individual movement in most cases. Cell movement can be regulated by chemotaxis, haptotaxis and mechanotaxis [26–29, 135], determining the micro-tissue morphology and cell density of aggregates.

Cell clustering has been widely used in tissue engineering to develop micro-tissues [136–139]. It also influences cell differentiation [30, 140] and protein expression, for example, on pancreatic cells [36] or bone marrow stromal cells [25]. Furthermore, this cellular aggregation is a key factor in the production of extracellular matrix (ECM) [31].

There is one type of cell cluster, known as spheroid, that presents a typical spherical shape [141]. These aggregates can be created in *in vitro* cultures of different cell types, including adipose cells [30], endothelial cells [31] or fibroblasts [22, 32]. Fusion of spheroids occurs in the presence of adjacent similar structures, and some 3D printing tissue techniques are focused on this phenomenon [39].

However, one of the limiting factors for *in vitro* tissue cultures is the low oxygen levels that exist in the core of the cellular aggregates when they reach a specific size. Poor oxygen and nutrient diffusion due to the lack of vascularization must be taken into account in these procedures to achieve a viable *in vitro* tissue [33–35].

Cell clustering also plays an important role in several diseases, notably in cancerous tumor formation and spreading of the disease to other tissues; additionally, the dimensions of these aggregates will affect drug penetration [37, 38].

To advance the understanding of how environmental conditions regulate the biological behavior of cell cluster formation, mathematical modeling and simulations

are playing an essential role. Indeed, we find many studies that model collective cell movement on 2D substrates based on a discrete [61, 133, 142] or continuum approach [125, 127, 143–145]. In addition, there are other numerical models that simulate individual cell movement using a discrete [146–148] or continuum approach [149, 150]. Interestingly, hybrid approaches that combine discrete and continuum strategies are less frequent [151]. However, hybrid models can overcome some of the limitations of discrete or continuum approaches. Recently, the number of studies that model collective cell movement in 3D environments has been increasing [41, 44, 58, 62, 152–157]. In addition, we take into account some models focused on the collective cell morphology [158, 159], particularly those that simulate cell clusters [59, 92, 160–164].

Despite the high number of modeling works focused on simulating cell clusters, there are not many works that consider the influence of oxygen concentration on cell proliferation and cell death. In this paper, we present a discrete-continuum hybrid framework that is able to simulate the formation of 3D cell clusters and predict the oxygen concentration profile in *in vitro* cultures. A multi-physics approach is developed considering several mechanical and chemical phenomena: interaction forces between cells, oxygen diffusion through cells and ECM, cellular oxygen consumption, cell proliferation and cell death. The discrete model allows each individual cell to be tracked in the culture, and the FE-based approach simulates the oxygen diffusion-consumption phenomena along the culture domain.

To validate our computational approach, we have qualitatively compared the results obtained from our numerical simulations with some experimental data found in the literature regarding the formation of cell clusters. For this purpose, different variables have been analyzed and quantified: cluster diameter growth [38], oxygen distribution in the clusters [165, 166] and the effect of the initial cell distribution on cluster formation [137].

5.2 Methods

We use a multi-physics approach to simulate *in vitro* 3D cultures; particularly, we have focused on cell cluster formation and its effect on the oxygen concentration in the scaffold.

Our approach is based on four coupled simple models, as shown in Figure 5.1. First, a cell movement and mechanical interaction model that is based on a force equilibrium is used to compute cell movement; this equilibrium takes cell-cell interaction forces and matrix drag forces into account. Second, the oxygen concentration is determined by a reaction-diffusion model that considers variations in the diffusion coefficient and oxygen consumption due to the presence of cells.

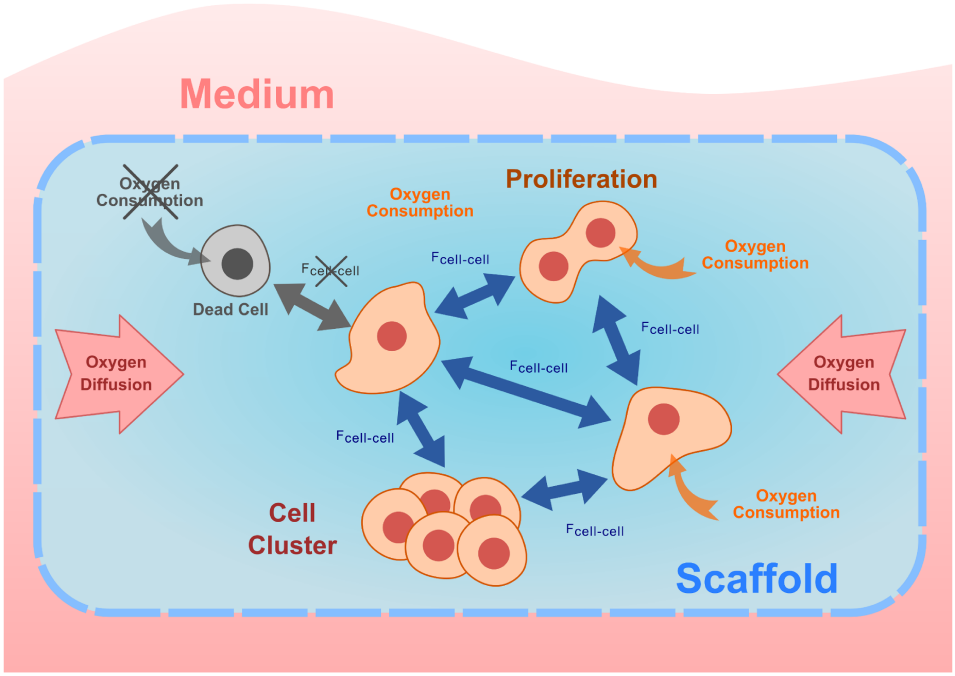

Figure 5.1: Multi-physics model that represents a 3D culture. We have considered a culture scaffold where cells are seeded surrounded by culture media. Cell-cell interaction in this work represents implicit chemical and mechanical attraction forces, and it is a key factor in the development of aggregates along with cell proliferation. Cell repulsion is also modelled when two cells are attempting to occupy the same space, simulating the mechanical response of the cell cytoskeleton and cytoplasm. Cell movement is determined by these interaction forces and by the ECM drag force as a resistive term opposing the cell displacement. Additionally, the oxygen concentration will be analyzed in the system, and it will directly depend on the cell density and distribution in the scaffold. Cell density and position determine the oxygen diffusion coefficient and cell oxygen uptake in the simulations. Finally, we consider cell death due to a low level of oxygen concentration. Dead cells do not consume oxygen but do modify the local diffusion properties. These cells only present repulsive forces in the cell-cell interaction model.

Third, a cell death model is employed that determines the cell status, namely, alive or dead, using an internal health variable, which depends on the oxygen concentration. Finally, the cell population in the simulation is defined by a proliferation model that is based on an exponential growth, as proposed by other authors [35, 58, 161], and it is also influenced by the local oxygen concentration.

5.2.1 Cell-cell mechanical interactions: a discrete approach

We propose a particle-based approach to describe individual cell movement, in which each cell is simulated as a particle. The discrete model allows tracing each

cell in the pool, analysing their properties and tracking their positions.

Cells are considered to be spherical in our model for computation purposes, where each cell is characterized by its own radius. Force equilibrium is calculated on the cell centroid, as shown in equation 5.1, and it dictates its new cell position.

$$\sum_{j=1}^{N} (F_{ji,c-c}) + F_{i,drag} = 0 \qquad \forall_i = 1, ..., N \tag{5.1}$$

Basically, we assume that there are two types of forces exerted on the cells: cell-cell interaction forces and cell drag forces [1]. Cell-cell interaction forces are calculated by derivation of the Lennard-Jones 12-6 potential (equation 5.2), as shown in equation (5.3):

$$V_{ji,c-c}(r) = 4\varepsilon \left[\left(\frac{\sigma}{r}\right)^{12} - \left(\frac{\sigma}{r}\right)^{6} \right] \tag{5.2}$$

$$F_{ji,c-c}(r) = -\frac{dV}{dr} = 24\varepsilon \left[\left(\frac{2\sigma^{12}}{r^{13}}\right) - \left(\frac{\sigma^6}{r^7}\right) \right] \tag{5.3}$$

where the variable (r) represents the distance between centroids of the cells. Furthermore, there are two additional parameters in the potential: ε, which represents the intensity of the interaction (or depth of the potential well), and σ, which is the distance where the potential is zero. In fact, the second parameter (σ) can be replaced by the distance where the potential is minimum (r_m). This is obtained by solving equation 5.3 when the force is equal to zero:

$$F_{ji,c-c}(r_m) = 0 \quad \Rightarrow \quad r_m = 2^{1/6} \cdot \sigma \tag{5.4}$$

Therefore, r_m represents the equilibrium distance between two cells where interaction forces are zero, and this parameter is easier to obtain from experimental data than is σ. We obtain equation 5.5 after substituting σ by r_m in equation 5.3 to determine the interaction force:

$$F_{ji,c-c}(r) = 12 \cdot \varepsilon \left[\left(\frac{r_m^{12}}{r^{13}}\right) - \left(\frac{r_m^6}{r^7}\right) \right] \tag{5.5}$$

[1] As a first approach, we do not consider explicit cell-ECM interactions, which could be included as in [61], for example. The inertial terms are also underestimated in this model.

Consequently, this force shows that two cells are attracted until a certain distance, or they are repulsed if they are too close. The attractive actions correspond to mechano-chemical signalling between cells that derives a migratory response, as well as from the adherent junctions formed when the cells are adjacent. The repulsive term represents forces generated when cells are attempting to occupy the same space. This reaction is due to the cell stiffness associated with the cell cytoskeleton and cytoplasm. Regardless, we have to keep in mind that we selected this potential as a simplified and phenomenological approach to model cell-cell interactions.

The drag force term in the force equilibrium represents the resistance of the ECM to cell movement (equation 5.1). This resistance is considered to be proportional and opposite to the velocity of the cell [148]:

$$F_{i,drag} = -f_d * \mathbf{v}_i \tag{5.6}$$

where the parameter f_d is equal to the viscous drag of a sphere in a medium with infinite viscosity.

Finally, we solve the equilibrium of forces (equation 5.1) and obtain velocities for each cell from equation 5.6. The new position of the cell is calculated from its former position, the current velocity and the time increment.

This model is implemented as part of a discrete particle-based approach. Each cell is considered to be an individual particle that retains its own information (position, radius,...). Consequently, global effects such as cell clustering arise from the interaction of these particles.

5.2.2 Reaction-diffusion model: a continuum approach

We use a continuum description to model oxygen diffusion in the culture based on Fick's second law of diffusion (equation 5.7). We consider the culture to be a heterogeneous medium, in which we distinguish between the cell domain (Ω_{cell}) and the extracellular matrix domain (Ω_{ECM}), for which have different oxygen transport properties:

$$\frac{dC_{O_2}}{dt} = \begin{cases} D_{O_2}^{ECM} \nabla^2 C_{O_2} & \text{in} \quad \Omega_{ECM} \\ D_{O_2}^{cell} \nabla^2 C_{O_2} - k & \text{in} \quad \Omega_{cell} \end{cases} \tag{5.7}$$

In the ECM domain, the rate of change of the oxygen concentration depends exclusively on the ECM diffusion coefficient ($D_{O_2}^{ECM}$) and the oxygen concentration. In contrast, the oxygen concentration in the cell domain is determined by the

cell diffusion coefficient constant ($D_{O_2}^{cell}$) and by the oxygen consumption of the cell (k). Oxygen consumption is considered to be constant and independent of the oxygen concentration. Therefore, the oxygen transport in the entire domain is described as a reaction-diffusion model.

The oxygen diffusion coefficient in the ECM ($D_{O_2}^{ECM}$) is considerably higher than the oxygen diffusion coefficient in cells ($D_{O_2}^{cell}$). Thus, the volume that is not occupied by cells has ECM diffusive properties and no oxygen consumption. In contrast, the volume occupied by cells has a lower oxygen diffusion coefficient and presents oxygen consumption.

5.2.3 Modelling cell death

In this work, we consider that each individual cell can present one of two possible states: alive or dead. First, live cells consume oxygen, and they mechanically interact with the remainder of the cells, as described in the previous sections. In contrast, dead cells do not consume any oxygen but retain their oxygen transport properties. Additionally, these cells still mechanically interact with the other cells, but this interaction generates only repulsive forces. In other words, the material of the dead cells remains in the culture, but it does not present any active cell behavior.

The health of the cell (λ_i) is evaluated separately for each individual cell, and it is modelled as an internal variable that takes values from 0 to 1. In the case that the cell health is zero, the cell is considered to be dead. Otherwise, the cell is considered to be alive.

These states are determined by the health of the cell (λ_i), as shown in equation 5.8:

$$\begin{cases} \textit{Alive} & \text{if} \quad 0 < \lambda_i^n \leq 1 \\ \textit{Dead} & \text{if} \quad \lambda_i^n = 0 \end{cases} \tag{5.8}$$

Moreover, cell health (λ_i) also depends on the local oxygen concentration (C_{O_2}). Hence, the temporal evolution of the cell health variable is as described in equation 5.9:

$$\dot{\lambda}_i = \begin{cases} -\phi_{damage} & \text{if} \quad C_{O_2} < \alpha_{O_2} \\ \phi_{healing} & \text{if} \quad C_{O_2} > \alpha_{O_2} \end{cases} \qquad \text{and} \qquad \lambda_i \neq 0 \tag{5.9}$$

The health of live cells is reduced by a damage rate (ϕ_{damage}) if the oxygen concentration decreases below the damage threshold (α_{O_2}). We assume that the cell damage is only due to hypoxic conditions. In addition, live cells present the

capacity to recover health if they are above the damage threshold. In this case, the increment of the cell health is driven by a healing rate ($\phi_{healing}$).

Finally, we assume that dead cells are not able to recover from this state. Therefore, we consider that when one cell is dead, it does not recover health and the health value remains zero.

5.2.4 Modelling cell proliferation

To simulate cell proliferation, we assume that live cells can present one of two possible states: proliferating or resting. The main difference between these two phases is that proliferating cells are able to duplicate.

We consider that the cell is in the proliferating phase if the local oxygen concentration is above the proliferation threshold (β_{O_2}). In contrast, the cell is in the resting phase if the oxygen concentration is below this threshold. This model is described as follows:

$$\begin{cases} Proliferating & \text{if} \quad C_{O_2} > \beta_{O_2} \\ Resting & \text{if} \quad C_{O_2} < \beta_{O_2} \end{cases} \tag{5.10}$$

We assume that proliferating cells follow an exponential growth law that is normally used in the biological literature [167, 168]. The population of proliferating cells (CP) directly depends on the initial population of proliferating cells (CP_0), time (t) and doubling time (T_d):

$$CP(t) = CP_0 \cdot 2^{\frac{t}{T_d}} \tag{5.11}$$

Note that cells in the resting phase and dead cells are not considered in the proliferating population (CP) when we model the proliferation.

Additionally, considering that our cell model is discrete, we adapt this exponential growth law to be estimated for every step in the simulation (see section 5.3).

5.3 Numerical implementation

We can clearly divide the framework into two parts: discrete approach, which represents the cells using a particle-based model, and FE-based approach to approximate the oxygen transport in the continuum medium. In Figure 5.2, a simplified system flowchart is presented. The models are fully coded in C++ using the Standard Template Library (STL) and inSilico library [105].

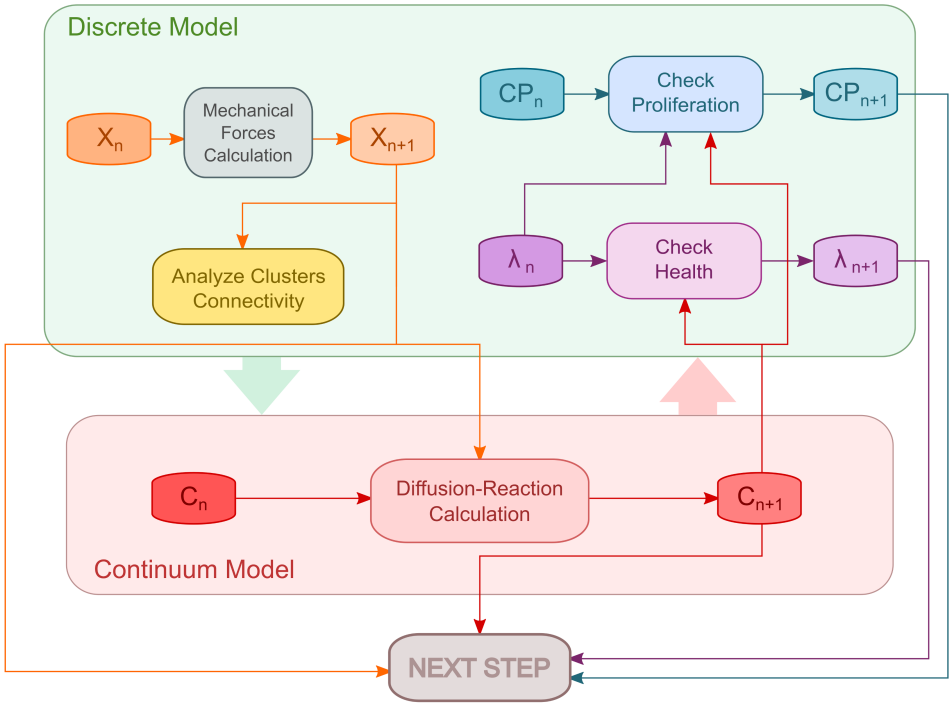

Figure 5.2: Numerical implementation flowchart. First, we calculate the mechanical interaction forces between cells knowing the current cell positions (X_n). From these forces and the current cell positions, we obtain new positions of the cells (X_{n+1}) using our cell-cell mechanical interaction model. We use these new positions to analyze the cluster connectivity to determine how many clusters are in the culture and their size. In the continuum model, we compute the new oxygen concentration (C_{n+1}) with our diffusion-reaction model using the current oxygen concentration distribution (C_n) and the cell positions (X_{n+1}). In fact, cells determine the local diffusion coefficient and oxygen consumption in this analysis. We update the health of each cell (λ_{n+1}) using the calculated oxygen concentration (C_{n+1}) and the current cell health (λ_n). Additionally, we determine the status of the cell (alive or dead). Finally, using the local oxygen concentration (C_{n+1}) and the cell health (λ_{n+1}), we determine the proliferation phase (proliferating or resting) of each live cell. Knowing the current population of proliferating cells (CP_n), we compute the new cell population (C_{n+1}) using our proliferation model. All information obtained in this step after calculations is updated for the next step.

In our numerical implementation, we can easily initialize the main fundamental variables to adapt the computational framework to the specific *in vitro* experiments, for instance, number of cells, scaffold dimensions, oxygen concentration or initial cell distribution. To analyze the results, we use VTK format (open source visualization toolkit) to export the data and Paraview to visualize them.

Cell behavior is fully described by the particle-based approach, in which each cell is represented by a particle with its associated radius. The cell interaction and proliferation models are merged together and implemented using object-oriented programming, where each cell is an unique object that belongs to a global class, sharing some properties but maintaining its individuality. Moreover, the cell health model is also described using this approach.

In addition, we approximate the solution of the oxygen transport phenomena using the finite element method (FEM) in our implementation. The oxygen diffusion coefficient and consumption in each mesh element are determined by the number of discrete cells that are present in each specific finite element. As described in equation 5.12, the volume ratio occupied by cells ($U^{element}$) is the sum of the volume of all cells in the element divided by the element volume:

$$U^{element} = \frac{\sum_{i=1}^{N} \int_{\Omega_{cell}} dV_i}{\int_{\Omega_{element}} dV} \qquad \text{where } 0 \leq U^{element} \leq 1 \tag{5.12}$$

In the case where the volume ratio is zero ($U^{element} = 0$), we assume that there are no cells in the reference volume. Otherwise, in the case where the volume ratio is one ($U^{element} = 1$), we consider that the reference volume is fully occupied by cells. We obtain the volume ratio occupied by cells from the particle-based cell model. Subsequently, we use this volume ratio in our continuum reaction-diffusion model to obtain the oxygen diffusion coefficient. Likewise, the oxygen consumption rate is obtained similarly to how we calculate the oxygen diffusion coefficient in the element. To avoid negative oxygen concentration values, we also considered that cells consume oxygen only if there is oxygen in the current cell location. Moreover, we assume two additional considerations: the oxygen concentration in the surrounding media is constant as a boundary condition, and the mesh elements in the calculations are always larger than the cells.

In the implementation of our reaction-diffusion model, we assume that the diffusion coefficient is dependent on this volume ratio occupied by the cells ($U^{element}$). We use a mixture law (equation 5.13) to determine the oxygen diffusion coefficient in each element:

$$D_{O_2}^{element}(U) = D_{O_2}^{ECM} + U^{element} \cdot (D_{O_2}^{cell} - D_{O_2}^{ECM}) \tag{5.13}$$

Hence, we link the discrete and the continuum approaches. In fact, we establish how the discrete approach determines the evolution of the continuum field corresponding to the oxygen concentration. Additionally, the continuum approach provides the spatio-temporal distribution of the oxygen concentration, which allows the discrete evolution for each individual cell to be calculated. In other words, the local oxygen concentration regulates the cell health and the proliferation phase.

The diffusion model uses the inSilico Cell library in its core. This is a software library designed to serve as a code development platform to solve the finite element method (FEM). This library is programmed in C++ and makes heavy use of templates, which provides the library user the ability to fit the system solver to their own needs [169]. The robustness and flexibility of inSilico Cell make it the perfect choice for creating a complex biological system connecting a particle-based model to a finite element approach.

Finally, the workflow of the framework can be divided in two different parts. The first is the initialization of the system, where we initialize all the variables for the computations. The second is the calculation loop of the framework, where we run the actual simulation (see Figure 5.2).

Initialization

In this step, we initialize several variables in the cell mechanical interaction model, such as the number of cells and their sizes. We initialize the cell positions to random values during the system configuration step. Random numbers are obtained using a uniform distribution from tools provided by STL (Standard Template Library). Moreover, the POSIX time of the machine since epoch (January 1th, 1970) is used as the seed for the random number generator. Additionally, initial cell aggregates can be generated from random positions of cells, thus expanding the model flexibility to simulate different experiments from a specific starting point.

The scaffold size and initial oxygen concentration values are also initialized at this point; these will limit the cell position to the boundaries of the selected volume. The diffusion coefficient of the oxygen in the ECM and in the cell is also stored. A mesh is created considering the scaffold size and number of elements per dimension. This mesh presents elements with the same shape and will be used to calculate oxygen diffusion through the scaffold of the simulation (ECM or ECM+cells). The medium oxygen concentration is constant on the boundary in the model. These boundaries represent scaffold surfaces in direct contact with culture media.

Without taking the particle-based model into consideration, the initial oxygen concentration inside the scaffold is assumed to be zero, and the diffusivity is fixed to a constant value for all elements. The diffusion model will reach steady state during the early steps of the simulation with scaffold dimensions commonly found in the literature ($< 50mm^3$) due to its fast dynamics. Therefore, these initial conditions will not affect the cell-cell mechanical interaction model or the proliferation model. The particle-based model will change diffusivity values and incorporate oxygen consumption into the elements wherever cells are present.

Calculation loop

At this point, different parts of the systems are sequentially connected inside a time loop, whose parameters are defined at the previous configuration step. First, cell displacement is calculated considering interaction forces; then, taking the magnitude of the time step into account, the new cell positions are updated based on the previous cell positions and current velocities. The cell displacement should be smaller than the cell radius to achieve proper cell movement behavior; this can be indirectly manipulated by modifying the time increment. Positions are stored in each cell object every step after computation. Note that a cell population increment produces a quadratic increase in the computation time of the interaction forces. Consequently, force computation is implemented using parallel computation techniques (OMP library, multi-threading for loops) because of the considerable reduction of time spent in these massive operations.

In the proliferation model, the proliferating cell population and doubling time are taken into account to determine how many cells replicate in this step. After computing how many cells replicate, cells are randomly selected from the proliferating cell population, and they are duplicated. These cells are selected using the same algorithm that was used to determine the initial cell positions. A new cell is located in a random position near the cell selected to replicate, never farther than the original cell radius. Additionally, these new cells also retain some properties from their progenitors, such as radius.

Cell clusters are now analyzed to determine how many of them are in the culture and to quantify the number of cells that they contain. An algorithm has been implemented that checks whether cells are in contact to determine whether they belong to a certain cluster. Cells are considered to be in contact if the distance between them is lower than the sum of their radii. If a cell is considered to be in contact, it is stored in that aggregate and will look for cells in contact in the next time step. This process is repeated until the entire cell population is sorted.

At this point, the oxygen diffusion coefficient and the consumption rate are determined for each element using equations 5.12 and 5.13. The oxygen concentration is computed using the inSilico library. After every step in the computation loop, concentration values will be stored in each element for use in the next step. We must note that this oxygen concentration model is time dependent and that it will only solve the time increment defined previously. In other words, this model does not reach the steady state in each step of the calculation loop. This dynamic behavior is necessary due to the integration with the particle-based model, which modifies the oxygen transport properties of the mesh elements in every step. Consequently, a detailed oxygen concentration profile in the entire culture is obtained.

Knowing the local oxygen concentration, we determine the state of the cell. We update the health of each cell in the simulation by evaluating the oxygen concentration on the corresponding mesh element in which the cell is located. In addition, we use this oxygen concentration to determine the cell proliferation phase, as described in the proliferation model.

When the calculation loop is completed, all relevant information from all models will be written into output files in VTK format.

5.4 Results

We compare our numerical results (Figure 5.3) with some experimental data taken from the literature to assess the predictive potential of the model under specific conditions. We have chosen two major simulation examples to test our numerical framework: the simulation of the growth of a single cluster and the simulation of the growth and interaction of multiple initial clusters.

In the first example, we simulate only one cluster of cells (see Video S5.1). We analyze the cluster growth and the oxygen transport phenomenon in the culture under these conditions. In the second example, we begin the simulation considering multiple initial clusters (see Video S5.2). We study the growth and the interactions between the clusters; additionally, we observe how different parameters affect these interactions and the oxygen distribution in the culture.

The numerical framework proposed here presents numerous configurable parameters to predict several physical and biological effects. Regardless, we have attempted to keep these parameters sufficiently close to measurable experimental data (Table 5.1). Nevertheless, some of these parameters are difficult to quantify directly from experiments due to the phenomenological design of our framework. This is the case of ε in the Lennard-Jones potential; this parameter represents the

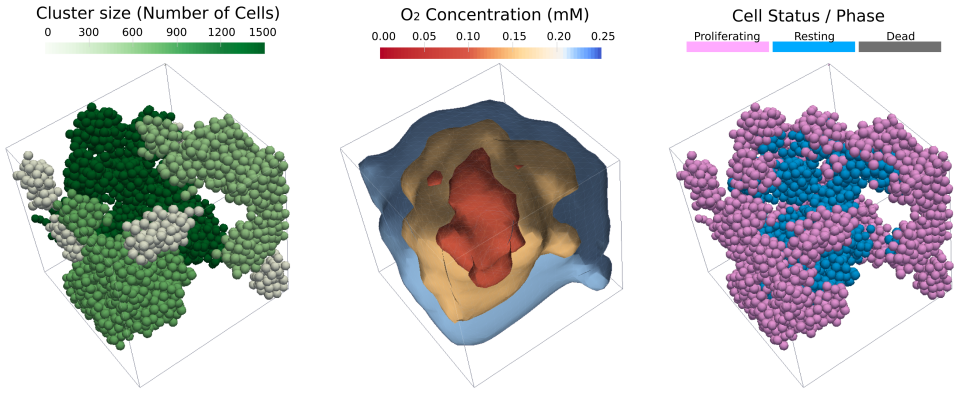

Figure 5.3: Representation in 3D of the simulated data. On the left, we show the size of the cell clusters in the computed volume. Each cell is represented as a sphere using its cell radius. At the center, we show isosurfaces of the oxygen concentration to represent the oxygen distribution on the simulation volume. On the right, we present the status of each cell in the 3D culture.

depth of the potential well and is related to the strength of the cellular interaction. Consequently, we should analyze this parameter to understand how it affects the emergent behavior of the framework.

5.4.1 Example I: Analysis of a single cluster

We analyze the cluster growth and the oxygen distribution in a single cluster simulating the conditions shown in [38]. Specifically, we use a single cluster with an initial population of 500 cells in all the simulations. Cluster growth is described by both the number of cells contained in the cluster and the diameter. Additionally, we analyze how the oxygen diffusion coefficient and the oxygen consumption rate affect the oxygen distribution in the cell culture.

Cluster Growth

We compare a single cluster growth embedded in a gel (which represents the extracellular matrix) with the experimental data obtained in [38] (Figure 5.4). In that work, Ong *et al.* studied tumour growth -as a single cell cluster- for *in vitro* drug penetration experiments. In our case, we start the simulation with a single cluster of 500 cells centered in the volume and we allow it to grow. Furthermore, the cluster size has been represented in a percentage of the initial diameter along 14 days of cell culture.

The model results show a linear increase in the cluster diameter that fits with data taken from [38] in the first fourteen days of the cell culture. Note that the

Time Step Parameters	
Number of steps	5000
Step size (h)	0.1
Total simulation time (h)	500[a]
Cell Population Parameters	
Initial clusters	50
Cells per initial cluster	10
Doubling time (h)	50
Proliferation rate ($cell^{-1} \cdot h^{-1}$)	0.02
Proliferation threshold $[\beta_{O_2}](mM)$	0.15
Damage threshold $[\alpha_{O_2}](mM)$	0.08
Cell Interaction Parameters	
Radius (μm)	[50, 60][b]
Lennard-Jones $[\varepsilon](dyne \cdot \mu m)$	0.1[c]
Drag parameter $[f_d](dyne \cdot s/\mu m^2)$	10^{-2} [d]
Oxygen Parameters	
Scaffold diffusion coefficient $[D_{O_2}^{ECM}](\mu m^2/h)$	500[e]
Cell diffusion coefficient $[D_{O_2}^{cell}](\mu m^2/h)$	0.001[f]
Boundary oxygen concentration (mM)	0.25[g]
Cell consumption rate (mM/h)	0.05[h]
Simulation Volume Parameters[i]	
Scaffold dimensions (μm)	3000x3000x3000
FEM - Elements per dimension	20
FEM - Total elements	8000

[a] The ratio of the computation time to simulation time is approximately 1:350 with the given parameters. The entire simulation took between 1 and 2 hours to simulate 500 hours of the culture.

[b] We consider cells of different sizes with diameters from 100 to 120 μm.

[c] Selected after parameter analysis.

[d] From references [146] and [61].

[e] Derived from [170] and [171].

[f] Taken approximately 1:100000 ratio of the scaffold diffusion coefficient value.

[g] Considering 20% of oxygen in air and the Henry constant from [172].

[h] Derived from [173].

[i] The volume ratio of the largest cell in the pool to element volume is approximately 1:4. In other words, each element can contain up to 4 cells of the largest size.

Table 5.1: Default parameter values.

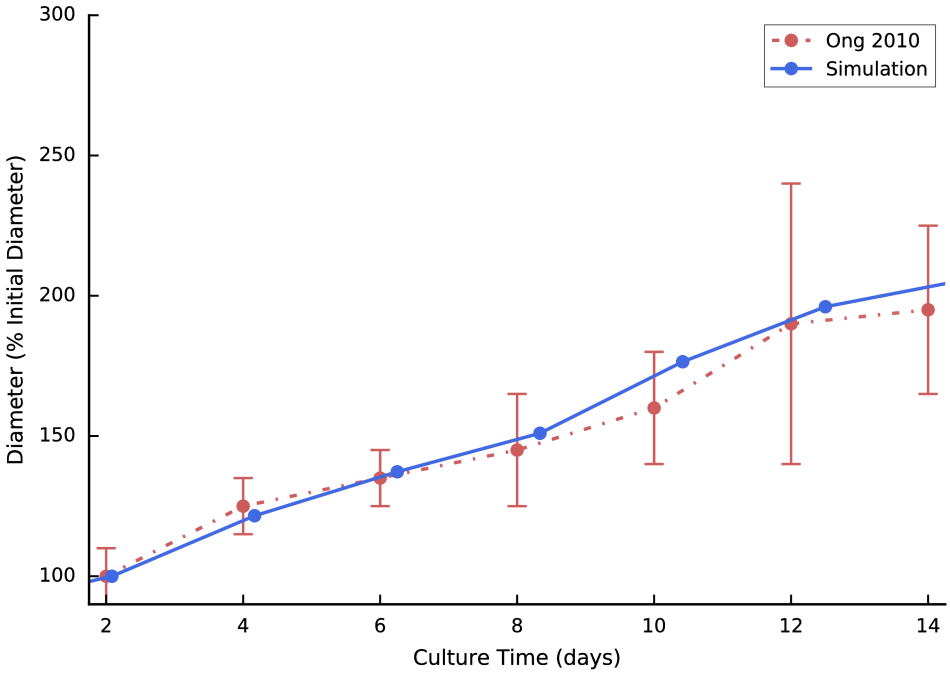

Figure 5.4: Time-dependent growth of a single cell cluster. Experimental measurements taken from [38], which are presented along with model output for similar conditions during 14 days of culture. Cluster dimensions are represented as the ratio of the initial cluster diameter.

cluster growth and cell population growth do not exhibit a linear relationship. In this example, cluster growth is associated with cell proliferation, which is affected by the local oxygen concentration.

Oxygen Profile and Cell Viability

Here, we analyze the oxygen profile in a single cluster and how the oxygen concentration affects the cell proliferation and viability. Moreover, we study the effect of the ECM diffusion coefficient (Figure 5.5) and the cell consumption rate (Figure 5.6) on the dynamics of the cluster growth. Note that the oxygen concentration is taken from the center of the cluster to the boundary of the gel volume. Therefore, the oxygen concentration is analyzed in both the cluster and extracellular matrix domains. In addition, the medium oxygen concentration that is surrounding the gel volume has been considered to be 0.25 M, which is approximately the oxygen equilibrium concentration in water at 298 K taking 20% of oxygen content in air.

Analysis of the diffusion coefficient of the ECM. In Figure 5.5b, we observe that the reduction of the diffusion coefficient of the ECM is related to lower oxygen

concentrations in the cluster core. Moreover, note that the oxygen concentration abruptly decreases in the interphase of the cell cluster domain and the ECM domain. Due to these low concentrations, cells enter the resting phase, and they even die in extreme cases where the diffusion coefficient is very low ($D_{O_2}^{ECM} < 100$), as shown in Figure 5.5a. Consequently, the results show a clear progression from the highest diffusion coefficient ($D_{O_2}^{ECM} = 1000$), where all cells are in the proliferating phase, to the lowest diffusion coefficient ($D_{O_2}^{ECM} = 10$), where all the cells die. At the intermediate values of the diffusion coefficient, we can find cells that are in the proliferating state as well as in the resting phase. In fact, resting cells reside in the core of the cluster and proliferating cells reside at the edge since the oxygen concentration is lower in the core and higher at the edge.

Analysis of the cell oxygen consumption. Figure 5.6b shows that the oxygen concentration reaches its minimum value when the oxygen consumption rate of the cells is maximum ($k = 0.5$). The oxygen concentration in the cluster increases if the oxygen consumption is reduced. Interestingly, the entire cell population is in the proliferating phase with low consumption rates ($k < 0.025$), as shown in Figure 5.6a. However, part of the cell population is in the resting phase when we increase the consumption rate of the cells since the oxygen concentration is lower in these cases ($k > 0.05$). In fact, in cases where the consumption rate is very high ($k > 0.25$), cells begin to die due to the hypoxic conditions produced in the center of the cluster.

5.4.2 Example II: Analysis of multiple clusters

In the following results, we analyze the evolution of the size of different cell clusters when the simulations begin with multiple initial clusters. Additionally, we investigate how several model parameters, namely, initial cell distribution, cell density and cell size, affect the cluster sizes and their influence on the oxygen distribution in the culture.

We also compare our results with the experimental data presented in [137]. In that case, two phenomena occur that determine the cluster size: cell population growth due to cellular division and cluster fusion, which occurs when two different clusters join together. Note that in all the cases in which we simulate multiple clusters, the average size of the clusters may suddenly change when two large clusters are merged or split. This effect can be appreciated in some of the figures shown in this section.

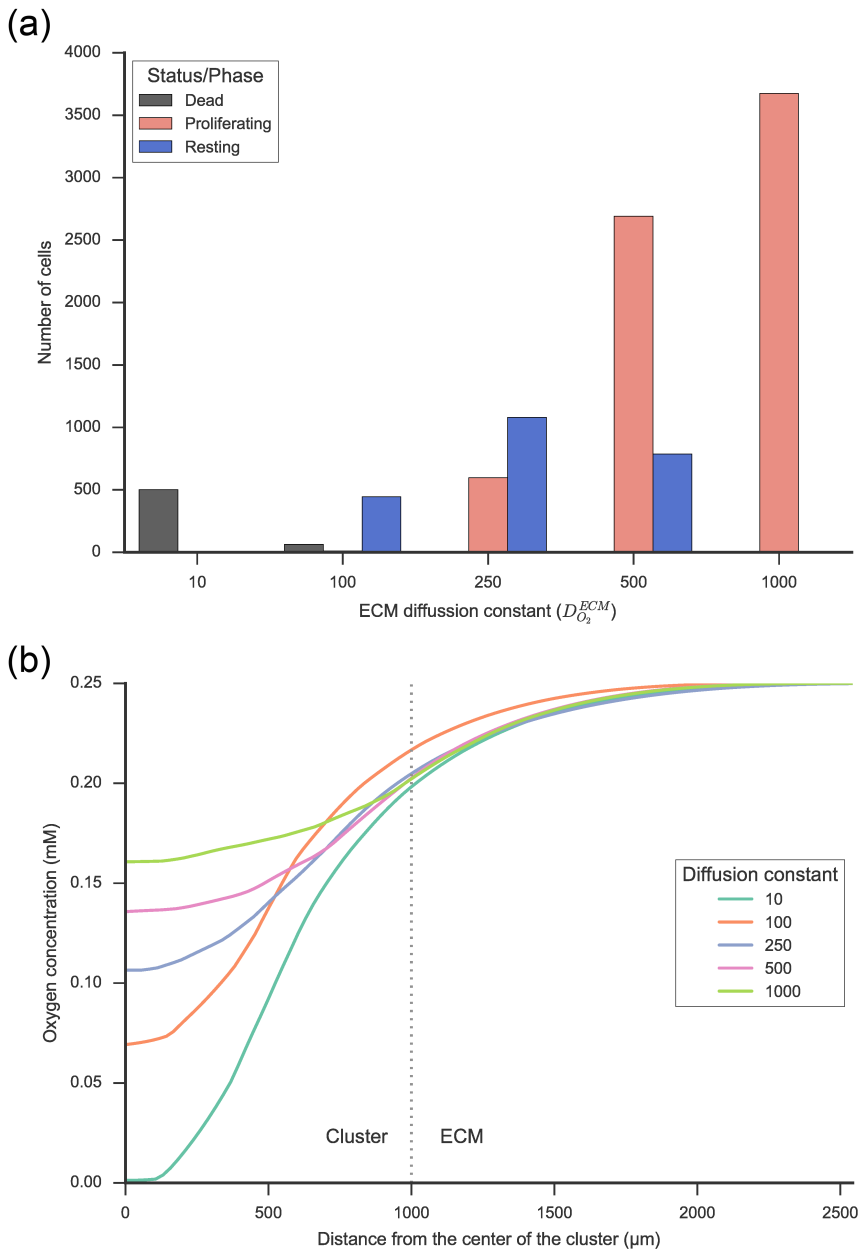

Figure 5.5: Analysis of the diffusion coefficient of the ECM. Analysis of $D_{O_2}^{ECM}$ on (a) the number of cells and their status and (b) the spatial oxygen concentration profile. (a) The number of cells and their status/phase are represented for different $D_{O_2}^{ECM}$ values. Low values produce more cells in the resting phase and even dead cells due to low oxygen concentrations. (b) The oxygen concentration distribution in the culture is represented in this figure for different $D_{O_2}^{ECM}$ values. Lower diffusion coefficients reduce the oxygen level in the core of the cluster. To clarify the separation of the two different domains (cluster and ECM), a vertical line is drawn at the average radius of the clusters (1000 μm).

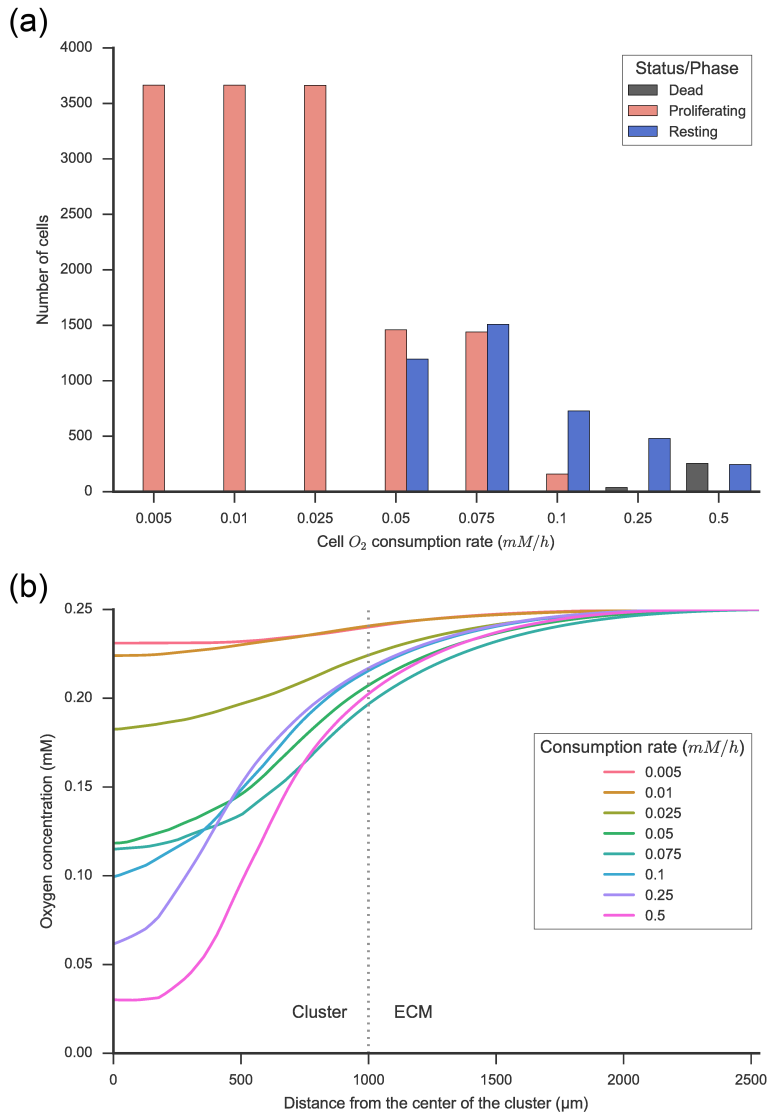

Figure 5.6: Analysis of the effect of the consumption rate of the cells. Effect of the cell consumption rate on (a) the number of cells and their status and on (b) the oxygen distribution profile. (a) The number of cells and their status/phase are presented for different oxygen consumption rates of the cells. All cells are in the proliferation phase at low consumption rates. Nevertheless, increasing the consumption rate is related to an increase of resting and dead cells in the culture. (b) The oxygen concentration distribution in the culture is presented in this figure for different consumption rates. High oxygen consumption rates produce lower oxygen concentrations in the core of the clusters. A vertical line is drawn at the average radius of the clusters (1000 μm).

Influence of the initial cell distribution

We find that the initial cell distribution is one of the key factors that alters the final cluster size, which is measured as the number of cells contained in each cluster. We simulate several initial cell distributions to analyze its influence on cluster formation. Nevertheless, we assume the same cellular density, that is, the same number of initial cells, in all these cases.

As shown in Figure 5.7-a, we observe an increase in the cluster size that is directly related to the initial cell distribution. The cases in which the clusters initially contain more cells produce larger clusters at the end of the simulation.

These results are consistent with the experimental measurements from [137] (Figure 5.7-b). In that work, they experimented with micro-carrier beads with different initial cell loads, and they analyzed their temporal evolution. They concluded that initial conditions where the bead contained more cells resulted in clusters with more cells. We have presented the first 14 days of culture data, where our model correctly predicts the effect of the initial distribution of the cells.

Influence of the initial cell density

To investigate how the cell density affects the cluster formation, we simulate the same culture volume with different quantities of initial cells. The evolution of the average cluster size under several cell density cases is shown in Figure 5.8a. We observe that increasing the cell density produces larger clusters. This is an expected result considering that the proliferation law is exponential and that it depends on the cell population. Consequently, a higher cell density implies a faster growth of the cell population.

Therefore, the oxygen concentration is lower when the cell density increases, as shown in Figure 5.8b. The reduction in the oxygen concentration at higher cell densities is due to the presence of a greater number of cells in the culture and consequently a higher oxygen consumption. Additionally, the effective diffusion coefficient in the culture decreases since there is more volume occupied by cells, which presents a lower diffusion coefficient than the ECM. In conclusion, the cell density has a strong effect on the oxygen distribution in the culture.

Influence of the cell size

We analyze the effect of the cell size on the dimensions of the clusters and the oxygen concentration on the culture. To modify the cell size, we change the cell radius in our framework. The volume of the computation domain and the number

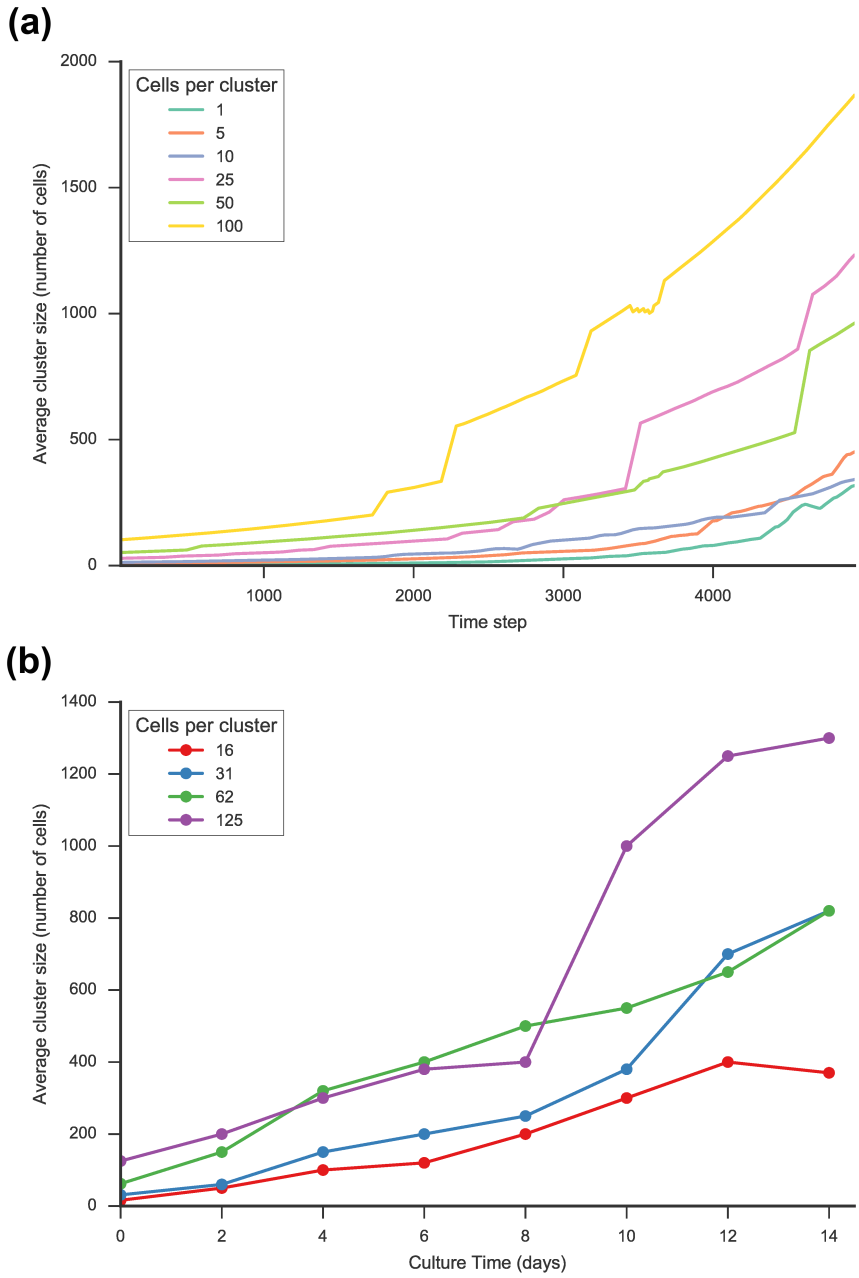

Figure 5.7: Influence of the initial cell distribution on the cluster size. (a) We show the temporal evolution of the average cluster size for different initial cell distributions. In the cases where the initial cell clusters are more populated, the final average cluster size is notably greater. (b) We show the temporal evolution of the average cluster size during the first 14 days of the experimental data from [137].

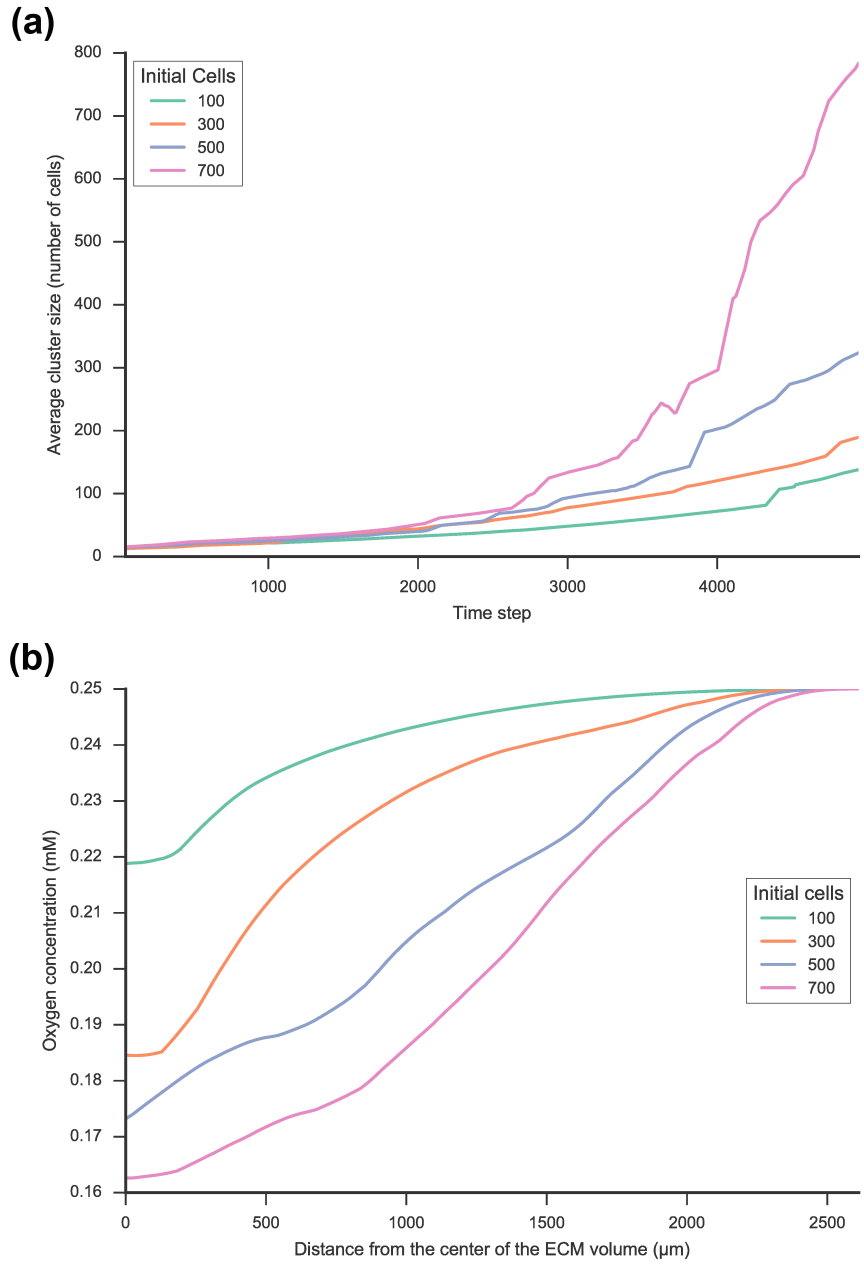

Figure 5.8: Effect of the initial cluster density on the cluster formation and the oxygen concentration. (a) The average size of the clusters is plotted for different initial cell densities; the same volume has been used for the simulation while we vary the initial number of cells. We observe that a high cell density is related to larger clusters. (b) The oxygen concentration is presented from the center of the computed volume to the boundary considering several cell densities. We predict that a high cell density is related to low oxygen concentrations.

of initial cells remain constant in these simulations. We observe that the average cluster size increases with the cell radius, as shown in Figure 5.9a. Otherwise, small cells tend to form clusters with a smaller number of cells. This behavior is due to the fact that clusters of small cells are separated by longer distances in the volume, and consequently, the fusion of the cluster is less probable.

In addition, we show in Figure 5.9b the oxygen concentration distribution for several cell radii. Large cells clearly reduce the oxygen concentration in the core of the culture compared to smaller cells. Because cells with larger radii occupy a larger volume, the effective diffusion coefficient of the culture is notably lower in these cases since the cell diffusion coefficient is considerably lower than the ECM one.

5.4.3 Analysis of the Lennard-Jones $\mathcal{E}$ parameter

The effect of the epsilon parameter (ε) of the Lennard-Jones potential on cluster formation is presented in Figure 5.10. In these simulations, we analyze different values of the epsilon parameter considering a random initial distribution of the cells in the culture. Individual cells group themselves to from clusters, and eventually, some of these clusters may join together.

In fact, high values of this parameter create highly compact clusters. Under these conditions, cell interactions with other cells that are not in the same cluster are notably reduced. This is because the long-range interactions are notably lower compared to the forces generated by close cells. Otherwise, low values of the epsilon parameter generate loose clusters. Moreover, they also diminish long-range interactions, but in this case, it is due to the direct reduction of the attractive forces. A reduction in the epsilon parameter generates a decrease in the force intensity between two distant cells.

These results suggest that this parameter can be determined to reach an *optimal* value where cell clusters present their maximum size. We find that cell clusters reach the maximum size when the value of epsilon parameter is in the range of $[0.01, 0.1]$. Therefore, we use an epsilon value equal to *0.1* for the remainder of the simulations since it appears to be optimal for the cluster formation.

5.5 Conclusions

In this work, we present a hybrid (continuum-discrete) computational framework for simulating 3D cultures focused on cell cluster formation. This framework has been designed as a modular system composed of several coupled models to represent physical and chemical phenomena. In our framework, we connect these models

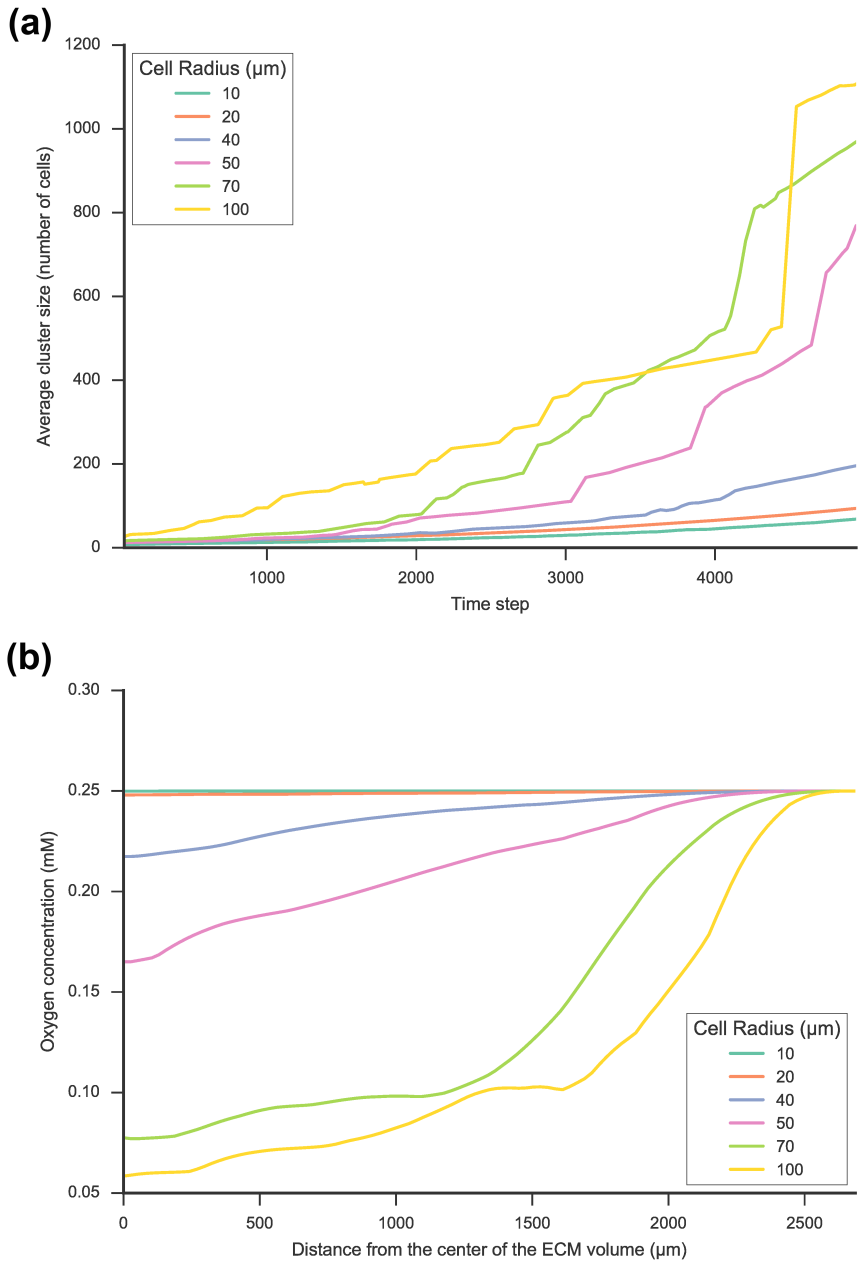

Figure 5.9: Effect of cell size on cluster formation and the oxygen concentration. (a) The average size of the clusters is presented for several cell radius ranges. We observe that larger cells produce larger cell clusters. Note that we use the same culture volume and number of cells in all these simulations. (b) We show the oxygen concentration in the computed volume for several cell radii. The oxygen concentration is presented from the center of the computed volume to its boundary. We observe that a larger cell size is related to a lower oxygen concentration in the culture.

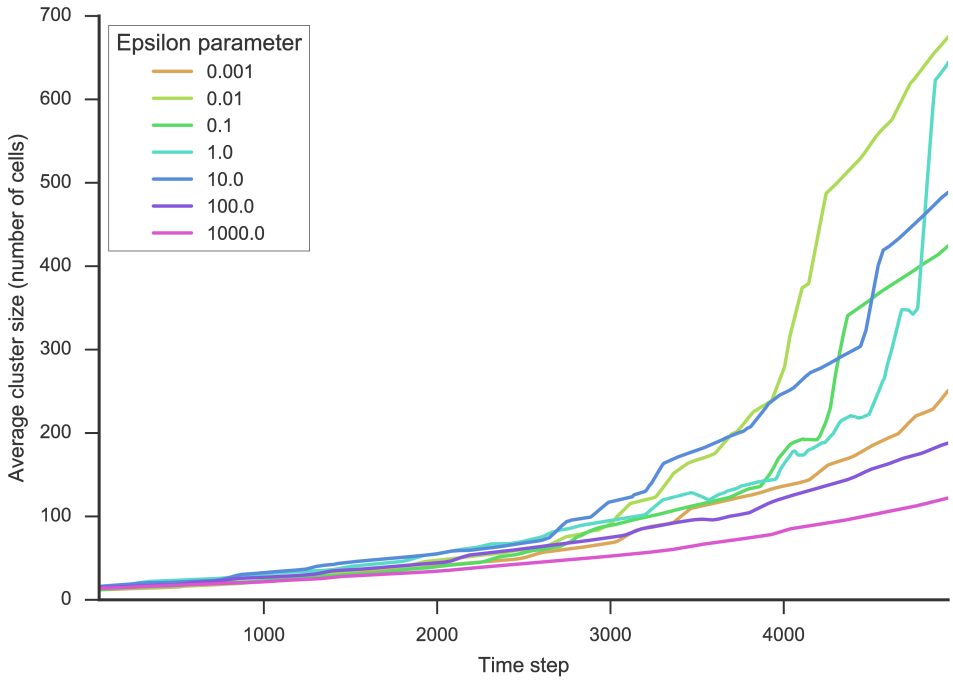

Figure 5.10: Lennard-Jones ε effect on cluster formation. The average cell size is presented for different values of this parameter through simulation time. We find the maximum size of the cell clusters when the epsilon parameter is between 0.01 and 0.1.

to reproduce the emergent behavior of cells in 3D cultures. In particular, our proliferation model is coupled with both the oxygen reaction-diffusion model and cell-cell interaction discrete approach to determine the spatio-temporal oxygen profile of the culture. Moreover, we are able to predict the cell distribution in the clusters and the effect of the oxygen concentration on the cell viability and proliferation. Interestingly, this framework presents a multi-time emergent behavior, where oxygen transport, cell movement and cell proliferation occur at different time scales. In fact, oxygen transport is a considerably faster process, and it reaches a pseudo-stationary regime during the simulation. The pseudo-stationary regime is altered by the cell proliferation and the variations of the cell positions in the culture. Moreover, cell movement presents faster dynamics compared to cell proliferation, which is the slowest process.

First, our numerical results reproduce the growth of a single cluster in the early days of the culture, although some effects are not captured in later days. The growth of the cluster size increase rapidly after several days of culture, and this behavior deviates from the linear growth predicted by the model. This divergence may be caused by some phenomena that affect the cluster dimensions, such as

cell volume changes or ECM formation, which have not been considered in this model. In fact, cell spheroids generally develop some characteristics such as ECM production and morphology changes in long-duration cultures, as shown in [38]. In addition, our numerical approach is able to predict the oxygen concentration profile in a single cluster. The simulation results exhibit a clear oxygen concentration decrease near the cluster core, and this expected behavior is directly related to the cell oxygen consumption. It reaches an equilibrium state, creating zones of permanent low oxygen levels with the cluster acting as an oxygen sink. Additionally, the diffusion coefficient determines both the minimum oxygen concentration and its spatial profile. In fact, it can be observed in Figures 5.5 and 5.6 that a change in the curve gradient occurs when passing from one domain to the other (ECM and cell cluster). Despite not being exactly the same case [2], the data observed in [165] and [166] are very similar with the results that we have obtained in our simulations. Moreover, we find that the diffusion coefficient of the ECM and the cell oxygen consumption have an intense effect on the oxygen concentration in the cluster.

Additionally, we find that the initial distribution is fundamental in the evolution of the cell culture with multiple clusters. In fact, the average cluster size is higher in the cases where the initial cell clusters have more cells. We suggest that this effect is caused by a localized concentration of forces on the initial clusters with more cells. Furthermore, proliferation is more concentrated in the case of fewer clusters with a higher number of cells, and consequently, large initial clusters grow faster in terms of the number of cells in comparison with less populated ones. Otherwise, we observe that the cell density also determines the evolution of the cultures with multiple clusters. At higher cell densities, the cells are nearer to their neighbors, generating more intense attraction forces between them. Due to these interactions, cell clusters are larger in the cases with higher cell density since it is easier for the cells to aggregate. A higher cell density also means a higher oxygen consumption and lower diffusion coefficient of the culture. Consequently, a high cell density is related to a low oxygen concentration in the culture. Finally, cell size is another fundamental parameter that determines the size of the clusters on cultures with multiple clusters. The increase of the cluster size with the cell radius is caused by a reduction in cell-cell distance; actually, larger cells in the same volume result in less available space. This situation generates more intense interactions between cells and thus higher force values. Additionally, the cell radius affects the Lennard-Jones potential equilibrium distance (r_m in equation 5.2).

Moreover, cell cluster growth is not limited to cell proliferation; cell displacements also play an important role in this process. Note that the cell-cell interaction effect

[2] Our cluster is not in direct contact with the medium, and consequently, the diffusion coefficients may vary. Nevertheless, the process dynamics appear to match in both cases.

is not only limited to cells in the same cluster. Cells that do not belong to any cluster are noticeably attracted by clusters that have already formed. Therefore, individual cells present a migratory-like behavior in the culture due to this attraction. Additionally, cell clusters also interact with other clusters. Small clusters tend to join larger clusters, and clusters of similar size tend to fuse if they are sufficiently close to each other. Therefore, there is a range of values where the Lennard-Jones ε creates optimal conditions for cluster formation. For each set of simulation parameters, this range may vary, and different configurations may need their own adjustment to match experimental data.

Despite the good agreement that we found between numerical predictions and experimental measurements, we have to keep in mind that our approach presents some limitations and simplifications that have to be analyzed. First, cell resistance and response to hypoxic conditions strongly differ from one cell type to another. For instance, endothelial cells could increase their proliferation rate under low oxygen pressure levels [174]; in contrast, cells from other tissues, such as kidney or intestinal tissues, need high oxygen concentrations to be viable [175]. Second, some long-term effects may not be captured by our model that would affect the fitting on long-lasting cultures, for instance, reduction of proliferation rate, culture quiescence or cell differentiation. These phenomena have a direct impact on the cell population in the culture and thus on cluster dimensions and distributions.

Another controversial aspect of our framework is that we decided to use a phenomenological cell-cell interaction model based on the Lennard-Jones potential, which is typically used to simulate pairs of atoms or neutral molecules. In our simple approach, we assume that the attraction term is due to cell migratory response and cell adhesion. The migratory response is caused by chemotaxis and mechanotaxis phenomena, which occur when a pair of cells are separated by a large distance. The cell adhesion effect arises at shorter distances, and this represents the anchoring junctions that mechanically attach the cytoskeleton of one cell to the cytoskeletons of other cells. The repulsion term represents Pauli repulsion, and in our case, this repulsion represents a passive cytoskeleton interaction. Additionally, the cell-cell friction phenomenon is also neglected using this interaction model. Although this cell-cell interaction law may appear oversimplified, we are able to phenomenologically recreate the collective cell migration, and its numerical implementation is easy with a very low computational cost. In addition, this simplification is consistent with the conclusions reached by Drasdo and Hoehme in [92], where they simulated growing cell populations using particle contact models (Johnson-Kendall-Roberts and Hertz) and other simpler force models. After comparing their results, they suggested that the precise form of the interaction model used may have no significant impact on the simulation of multi-cellular dynamics.

Therefore, due to the simplifications assumed in this work, we have to keep in mind that this framework cannot in its current state represent the formation of complex structures –tissue or organ development, for instance– or cell collective migration that implies large movements. However, it successfully predicts the 3D cluster formation and the oxygen distribution in the cell cultures quite well. The framework also is able to simulate the effect of the oxygen transport on the clusters and the cell viability and proliferating behavior. In conclusion, this framework can recreate diverse effects that occur on cluster formation in 3D cultures using a simplified approach, which is very flexible for recreating the experimental conditions. Certainly, the approach presented here will be improved in future works by including additional phenomena, such as cell differentiation, more complex cultures (e.g., bioreactors), matrix formation/degradation or deformable cell geometry. In addition, we will implement random events to extend the flexibility of this framework.

5.6 Supplementary material

Video S5.1: Simulation of a single cluster. On the left, we show the cluster size considering the number of cells in the cluster. At the centre, we show the isosurfaces of the oxygen concentration on the simulation volume. On the right, we present the status of the cells.

Video S5.2: Simulation of multiple clusters. On the left, we show the cluster size considering the number of cells in the cluster. At the centre, we show the isosurfaces of the oxygen concentration on the simulation volume. On the right, we present the status of the cells.

This document and its supplementary material are accessible from:
`https://m2be-storage.unizar.es/pydio_public/ismael-thesis`

6 Discussion

Contents

6.1 General conclusions

We present in this thesis two novel hybrid approaches to model and simulate epithelial monolayer mechanics and 3D cell clustering respectively. They share a common design characteristic: they combine an agent-based model with a continuum model that is solved using the Finite Element Method. Here we summarize the main conclusions of each model and, finally, we provide a general discussion about our modeling proposal.

Epithelial monolayer model

In our epithelial monolayer model, we combine an agent-based model with a continuum material model. A fundamental aspect of this work is the emergence of continuum mechanical properties from the interaction of discrete cells. Interestingly, we observe that, even when we are using a linear elastic constitutive law in the continuum material model, the global behavior that emerges from the system is closer to a viscoplastic material. This behavior is due to the effect of cell-cell interaction forces and to the stress dissipation assumptions, which are discussed in detail in previous chapters. Furthermore, the modeling techniques presented in this work let us study separately how tissue mechanics are affected by active cell forces (cell-cell interactions, migration forces, ...) and the passive mechanical properties (p.e. material stiffness).

To understand the possibilities that this model offers, we quantitatively compare our numerical results with previous experimental studies taken from the current literature. We analyze the epithelial tissue mechanics focused on different aspects and phenomena in each chapter of this thesis. First, we analyze the topology of proliferating epithelial tissue in chapter 2. We consider a variety of variables and processes that can alter tissue topology such as cell life cycle, division cleavage-plane or cell-cell interaction forces. Second, we add random propulsion forces to cells to study collective motion and cell jamming in chapter 3. We observe how cell motion is affected by cell-cell interaction forces and material stiffness in an epithelial layer. Lastly, we simulate two different collective migration processes in chapter 4: collective durotaxis and wound healing. In contrast to the previous collective motion study, here we do not impose propulsion forces to cells. In fact, cell migration occurs due to cell-substrate and cell-cell interaction forces, in particular, cell crawling and purse-string. In conclusion, we successfully reproduce biological phenomena related to epithelial monolayer mechanics with our hybrid approach.

In chapter 4, the distinction between center-based and vertex-based model becomes blurred in our agent-based approach. Although we use cell centers to

define cell positions, we also apply different contraction forces to cell vertices. We may define this modeling approach as a 'transient vertex-model' since the information of cell vertices is not stored from one step to the next. However, we explicitly use these vertices to compute cell forces and to solve tissue mechanics. In fact, Voronoi diagram has been used to represent cell body in center-based models before but, usually, only to associate an area to the cell center. We believe that the center-based approach combined with a dynamic polygonal representation of the cells offer interesting modeling possibilities, as we have shown in this work.

Remarkably, we find that Alpha Shapes are a key tool that greatly expands modeling capabilities of our approach. To begin with, we use them to limit the Voronoi diagram representation that is unbounded by definition. In addition, we use Alpha Shapes to distinguish between different domains in the tissue. We can assign different mechanical properties and behavior to these domains in the continuum model. Moreover, we can easily distinguish and locate cells that are in the monolayer borders, completely surrounded by other cells or even in contact with the system boundaries. Hence, our hybrid model is able to represent the interface between cells and substrate, but also gaps and discontinuities in the layer. In fact, it could simulate indifferently both confluent and non-confluent epithelial tissues. Particularly, our hybrid approach is able to naturally represent individual cells detached from the rest, different cell groups that join together or cell clusters that split into separated groups. For this reason, we think that this modeling approach is also applicable to other processes such as angiogenesis, epithelial-mesenchymal transition, pattern formation or monolayer collision.

We are aware that our approach presents some limitations. Despite results indicate that our model is able to simulate long duration processes, it may fail to recreate short term phenomena where tissue accumulates mechanical stress. We have assumed that tissue stress dissipates between simulation steps. This assumption is only acceptable in processes in which cells have enough time to restructure their cytoskeletons and the adhesive junctions with their neighbors. On the contrary, we would need to consider stress accumulation to simulate the tissue reaction to sudden external forces. A good example would be the experiments to characterize epithelial monolayer that Harris and Charras developed [11]. Although the implementation of accumulative stresses should not be excessively complicated, this is out of the scope of this work.

3D cell clustering model

In Chapter 5, we combine a center-based discrete model with a continuum oxygen reaction-diffusion model. In addition, we also implement a cell life cycle and health model that depends on oxygen levels in the cell environment.

Our hybrid framework accurately predicts the size of a single cell cluster in a 3D culture. Moreover, we determine that oxygen concentration drops very fast in the cluster core during cell aggregate growth as it was observed in previous experimental studies. However, this framework is not limited to single cluster simulations. We also reproduce experiments with multiple clusters in which we study its effect on the oxygen distribution and cell viability.

We observe that cell distribution may dramatically change proliferation and viability given the same culture volume and cell density. Thus, the analysis of cell density is not enough to predict how a 3D culture evolves. Since our hybrid approach represents cells individually, we are able to study how cell distribution affects these biological systems. In addition, the agent-based model let us simulate cell-cell interactions in detail. Interestingly, we can observe that not only individual cells are attracted by others due to these cell-cell interactions, but clusters show a similar behavior as a collective structure. This emergent phenomenon is responsible of the fusion of aggregates that are close to each other. The fusion of aggregates generates larger cell clusters.

We have demonstrated that this approach is valid to simulate biological phenomena that are in different time scales. First, we find that the fastest process is the oxygen transport in the 3D culture. We assume that the reaction-diffusion is uncoupled from other phenomena. In fact, this means that we can solve this problem in each time step assuming that cell positions and life cycle have not changed. Similarly, we can consider that the oxygen concentration is in a pseudo-stationary regime when we analyze the other biophysical processes since the equilibrium is reached much faster. Second, cell movement and migration are slower than the reaction-diffusion events. On the other hand, cell movement is faster than cell life cycle. In reality, cell position only affects cell life cycle and health indirectly. Cells can migrate to zones with different oxygen concentration in the culture and, in addition, alter oxygen distribution. However, there are no other coupled variables between these models. Therefore, the slowest process is cell life cycle. We can measure a complete cell cycle in hours or days. Cell life cycle is directly affected by oxygen concentration. Also, this model determines the population in the 3D culture and, in consequence, it will indirectly affect both cell-cell interaction and oxygen reaction-diffusion models. In conclusion, although these models operate in different time scales, they are connected by their emerging effects.

Nevertheless, this modeling approach presents some limitations. We observe that our results do not match with the experimental data in long-lasting cultures (more than 15 days). This may be caused by the lack of some phenomena such as cell differentiation, cell quiescence or proliferation rate reduction when a certain

cluster size is reached. Further, we used a simple cell-cell mechanical interaction model that represents different processes at the same time. We demonstrated that this phenomenological approach is valid to simulate cases of cell clustering that includes cell migration and simple interactions, but it may fail to predict more complex structures. Although this framework is not currently adapted to simulate organs or structured tissues, we believe that it is an interesting approach to model oxygen transport in multi-cellular systems. In fact, the modeling approach could be implemented in more elaborated and detailed cell mechanical models.

Finite Element and agent-based hybrid approach

It is important to note that the objective behind this thesis is to explore how to combine continuum models (in particular those which are usually solved using Finite Element Method) and discrete agent-based models. In fact, we show how this idea can drive to different modeling applications. Each hybrid approach presented here is focused on a different biological problem and, in consequence, the integration of their individual models has its own particularities. Evidently, they share some common aspects, but they offer insight into the numerous possibilities of this hybrid schema and the biological problems that they can reproduce.

We believe that these hybrid modeling approaches are flexible tools to fill the gap between cell discrete representation and continuum behavior of some biological structures. Furthermore, we have tried as much as possible to use simple models and define clear interfaces between them. Obviously, the work presented here is just a step in this direction. We think that these hybrid approaches can be further extended and applied to other biomechanical problems.

Currently, there are no open source modeling platforms that support these hybrid approaches. The only implementation of our models is done with in-house code. This fact may be regarded as an important drawback to extend the use of these hybrid models. However, we have explained in detail how to implement the models and interfaces. Also, we have tried to rely exclusively on open source libraries and standard technical specifications.

In the next section, we will summarize some possible improvements and future biological applications. To conclude, we hope that the modeling community find this proposal useful to study new aspects of multi-cellular systems.

6.2 Future work

In this section, we describe some proposals to improve these modeling approaches and possible additional applications. Moreover, we aim to provide some ideas to overcome some limitations.

Epithelial monolayer model

We believe that this hybrid approach can be applied to other biological phenomena without many changes. For instance, it could easily simulate monolayer collisions or pattern formation in epithelial layers. We only need to add different cell types as cell property in the agent-based model, and make cell-cell interaction forces dependent on these cell types. Also, we could add cell death to the life cycle. This addition is really simple to implement and our framework would be able to simulate new processes such as homeostatic equilibrium in mature tissues and cell extrusion.

As we discussed in the previous section, stress in the tissue is not stored from one step to the next. We think this is one of the most important points for future enhancement. To add this feature, it would require some additional work and the creation of new interfaces. However, we believe that it should not be too complicated to extend it. Here we offer a draft of a possible implementation in our framework:

1. Compute the first calculation loop as described in the previous sections.
2. Store stress map of the current solution.
3. Generate the new mesh for the next step.
4. Transfer the previous stress map to the new mesh.
5. Use mapped stresses in the FE analysis in this step.
6. Continue to the next iteration using this new simulation workflow.

With this workflow, we would be able to simulate the work of Harris and Charras [11], in which they developed an experimental technique to characterize the mechanical properties of epithelial monolayers. In particular, they culture a cell monolayer over a system with two test rods. In that experimental setup, one rod is mobile and the other is static. They study the material properties under different displacement conditions by controlling and monitoring both rods with micromanipulators. In our case, it is trivial to apply external forces to the system in the FE analysis. We would just need to impose fixed displacements or other required boundary conditions on the relevant mesh nodes.

In addition, cells could react to the stress or the strain in the tissue material. For example, cells could stop proliferating or even die if compressive stress is too high in the layer. Otherwise, cells could be forced to divide in a high tensile stress condition.

Furthermore, it would be interesting to analyze the viability of extending this modeling approach to 3D cases. Also, it would be necessary to detect possible computational performance issues and bottlenecks that were not present in the 2D implementation.

3D cell clustering model

We think that our 3D cell clustering model can be applied to a wide variety of biological phenomena after implementing some enhancements.

Currently, the modeling of cell movement is purely phenomenological. A more detailed description of cell-cell and cell-matrix interactions would significantly improve the modeling scope of this hybrid approach. With these changes, we could study migration processes that were driven by different factors, or the formation of more complex structures beyond cell clusters.

Further, we could extend the agent-based model from a center-based to a deformable cell one. Here we could use some ideas of the previous monolayer model. For instance, cell geometry could be generated combining Voronoi diagram and alpha shapes in a 3D environment.

Also, extracellular matrix formation and degradation could be included in this approach. This process could be modeled both mechanical and chemically extending the current reaction-diffusion model. In fact, it would be interesting to study how these changes in the matrix could alter the diffusive properties of the cell environment.

Finally, we could expand the cell life cycle and health models. For example, we could add cell differentiation to simulate cultures with several cell types and longer duration. Otherwise, these models could also depend on mechanical stimuli in addition to oxygen levels.

General enhancements

As it was discussed before, these hybrid approaches are implemented using an in-house code and they are not available in any open-source framework. We believe that the better solution to overcome this issue is to personally collaborate with open-source projects to include this modeling approach. This would benefit the whole community providing additional tools to simulate multi-cellular systems.

Finally, despite we find that the current performance of the code is acceptable, code parallelization should be studied and considered as future improvement. All simulations presented in this work took approximately from some minutes to several hours in a standard PC. We think that the computational cost of this technique is reasonable. However, this cost could increase after implementing some ideas proposed in this section. That would make parallelization more necessary that it currently is.

6.3 Contributions

6.3.1 Articles in peer-review journals

Published work:

- Ismael González-Valverde, Carlos Semino and José Manuel García-Aznar. *Phenomenological modelling and simulation of cell clusters in 3D cultures.* Computers in Biology and Medicine, Vol. 77, 249-260. August (2016).
- Ismael González-Valverde and José Manuel García-Aznar. *A hybrid computational model to explore the topological characteristics of epithelial tissues.* International Journal for Numerical Methods in Biomedical Engineering, Vol. 33, Issue 11, e2877. February (2017).

Submitted work under review:

- Ismael González-Valverde and José Manuel García-Aznar. *An agent-based and FE approach to simulate cell jamming and collective motion in epithelial layers.*
- Ismael González-Valverde and José Manuel García-Aznar. *Mechanical modeling of collective cell migration: An Agent-based and continuum material approach.*

In preparation:

- Ismael González-Valverde and José Manuel García-Aznar. *A hybrid computational approach to model angiogenesis and cell self-organization.*

6.3.2 Collaborations

I have collaborated with Dirk Drasdo and Paul Van Liedekerke during a research stay in the Drasdo group (INRIA-Paris). We developed a command-line tool to generate 3D meshes using implicit surfaces called *TiMesh*. This application will be integrated into a larger modeling project (*CellSys/TiSim*). In addition, we reconstructed a 3D vascular network using this tool. We ran some simulation with a deformable cell model using *CellSys/TiSim* to observe cell interactions with that vascular network. We also used *TiMesh* to generate a 3D environments and reproduce gap closure phenomena.

Despite this work is not included in this thesis, it has been a unique opportunity to acquire a wider vision of different model approaches. This experience has provided us a deeper understanding of the multi-cellular modeling and it has helped to enrich this document in many ways.

6.3.3 Presentations in conferences

The work shown in this thesis has been presented in the national and international conferences listed below.

- Oral presentations:
  - *Modeling and simulation of the dynamics of epithelial/endothelial monolayers.* IV International Conference on Particle-Based Methods. PARTICLES 2015 Barcelona
  - *Modelado y simulación del comportamiento mecánico de una monocapa celular.* Spanish Chapter of the European Society of Biomechanics. Madrid 2017 (Award Session finalist)
  - *Modelling the mechanical behaviour of the epithelial monolayers: a hybrid approach.* XXXIV Annual Conference of the Spanish Society of Biomedical Engineering. CASEIB 2016 Valencia
  - *Computational modeling of cell dynamics in epithelial tissues.* V International Conference on Computational and Mathematical Biomedical Engineering. CMBE 2017 Pittsburgh *****
  - *Particle-based modeling and simulation in cell mechanics: from adhesion and contraction to migration.* V International Conference on Particle-Based Methods. PARTICLES 2017 Hannover (Plenary Session) *****
  - *A hybrid approach to model epithelial tissue mechanics.* 23rd Congress of the European Society of Biomechanics. CESB 2017 Seville
  - *Mechanical regulation of collective cell migration: simulating from cell dynamics to layer topology on densely packed tissues.* Barcelona BioMed Conference: Morphogenetic Engineering. Barcelona 2017 *****
- Poster presentations:
  - *A hybrid framework to simulate the topology and the mechanics of epithelial tissues.* ESM-EMSTB Summer School: Mathematical Biology of Tissue Mechanics. Leiden 2016
  - *Modeling the mechanics of epithelial cell monolayers using a hybrid approach.* VII European Cell Mechanics Meeting. CellMech 2017 Windermere
  - *A hybrid framework for simulating the dynamics of epithelial monolayers* I Biology for Physics Conference. Barcelona 2017 *****

***** José Manuel García Aznar presented the work in these sessions.

Appendices

A
Resumen

Muchas de las propiedades biomecánicas de los organismos multicelulares surgen directamente de las interacciones entre células. Las células de los órganos y tejidos interactúan entre sí y con su entorno de diferentes formas. Debido a este hecho, es fundamental analizar cómo estas interacciones se traducen como propiedades mecánicas a nivel del tejido. Por ejemplo, las adhesiones entre células determinan la rigidez aparente de una capa epitelial. Las interacciones célula-matriz pueden además determinar la formación de muchas estructuras biológicas y su morfología. Estos sistemas multicelulares no se pueden considerar como estructuras estáticas ya que sufren constantes cambios causados por la proliferación, la reorganización o la migración celular. Por lo tanto, es necesario estudiar la dinámica de la célula y las interacciones individuales para comprender plenamente cómo funcionan los fenómenos a escalas superiores, desde el desarrollo de tejidos hasta el crecimiento de tumores.

Recientemente, el uso de enfoques *basados en agentes* se ha vuelto muy popular para modelar sistemas multicelulares. Los modelos *basados en agentes* representan células como entidades individuales. Estos modelos son especialmente adecuados para estudiar fenómenos biofísicos que ocurren a nivel celular. Aquí las interacciones célula-célula se pueden simular directamente de forma mecanicista. Además, estos modelos capturan realmente bien las heterogeneidades presentes en las estructuras biológicas. Por otra parte, los modelos continuos se utilizan comúnmente en problemas de escalas mayores. A diferencia de los modelos *basados en agentes*, en estos no representan células como entidades individuales, sino que se definen

leyes constitutivas para modelar procesos biológicos, físicos y químicos. Por lo tanto, las propiedades celulares se promedian usando parámetros macroscópicos, y estos modelos a menudo trabajan con la densidad celular en lugar de entidades celulares separadas. En cualquier caso, los modelos continuos presentan una buena escalabilidad y una excelente representación de fenómenos físicos particulares como el transporte masivo y las transmisiones de fuerza en medios continuos.

En esta tesis, se exploran las posibilidades que los enfoques híbridos pueden ofrecer para desarrollar nuevos modelos de sistemas multicelulares. Se presentan dos modelos híbridos diferentes que combinan un modelo *basado en agentes* y un modelo continuo. Ambos enfoques tienen en común que el modelo continuo se resuelve utilizando el método de los elementos finitos. También se muestra, siguiendo este patrón de diseño, cómo resolver varias de las limitaciones intrínsecas de cada tipo individual de modelo.

En primer lugar, se presenta un modelo híbrido para simular la mecánica epitelial monocapa. Este modelo se centra en el modelado de las interacciones mecánicas célula-célula y célula-sustrato, pero también en la topología y morfología de los tejidos. Con este enfoque se reproducen tejidos epiteliales proliferativos, movimientos celular colectivo y procesos de migración. El segundo modelo presentado en esta tesis se ha diseñado para simular agregados celulares en entornos tridimensionales. Se estudian las interacciones mecánicas entre células, pero este modelo se centra especialmente en analizar cómo afecta el transporte de oxígeno a las células en un proceso de agrupamiento en 3D.

Finalmente, se comparan los resultados de ambos modelos con datos experimentales de otros autores y se discuten los beneficios de combinar diferentes tipos de modelos. Se demuestra que los enfoques híbridos que se proponen en este trabajo son capaces de simular una amplia variedad de sistemas multicelulares. De hecho, son particularmente útiles para estudiar cómo algunos fenómenos emergen de las interacciones celulares individuales a escalas biológicas más grandes.

B
Conclusiones

En esta tesis se presentan dos diseños híbridos para modelar y simular la mecánica epitelial monocapa y la agregación de células 3D respectivamente. Estos modelos comparten una característica de diseño común: combinan un modelo *basado en agentes* con un modelo continuo que se resuelve mediante el método de los elementos finitos. Aquí se resumen las principales conclusiones de cada modelo y, finalmente, se presenta una discusión general sobre esta propuesta de modelado.

Modelo de monocapa epitelial

En el modelo monocapa epitelial, se combina un modelo *basado en agentes* con un modelo de material continuo. Un aspecto fundamental de este trabajo es la aparición de propiedades mecánicas macroscópicas a partir de la interacción de células discretas. Curiosamente, se observa que, incluso cuando se usa una ley constitutiva elástica lineal en el modelo de material continuo, el comportamiento global que emerge del sistema está más cerca de un material viscoplástico. Este comportamiento se debe al efecto de las fuerzas de interacción entre células, y a las consideraciones de disipación de las tensiones en la monocapa que se discuten en detalle en capítulos anteriores. Además, las técnicas de modelado que se presentan en este trabajo permiten estudiar por separado cómo la mecánica de los tejidos se ve afectada por las fuerzas celulares activas (interacciones célula-célula, fuerzas de migración,...) y las propiedades mecánicas pasivas (por ejemplo la rigidez del material).

Para entender las posibilidades que ofrece este modelo, se compara cuantitativamente los resultados numéricos con estudios experimentales previos tomados

de la literatura actual. En cada capítulo de esta tesis se analiza la mecánica del tejido epitelial centrándose en diferentes aspectos y fenómenos. En primer lugar, se analiza en el Capítulo 2 la topología del tejido epitelial proliferativo. Se consideran diversas variables y procesos que pueden alterar la topología de los tejidos, como por ejemplo el ciclo de vida de la célula, el plano de división de las células o las fuerzas de interacción entre células. En segundo lugar, se añaden fuerzas de propulsión aleatorias a las células para estudiar el movimiento colectivo y el *jamming* celular en el Capítulo 3. Se estudia cómo el movimiento de la célula se ve afectado por las fuerzas de interacción entre células y la rigidez del material en una monocapa epitelial. Por último, se simulan dos procesos de migración colectiva diferentes en el Capítulo 4: la durotaxis colectiva y la cicatrización de heridas. A diferencia del anterior estudio de movimiento colectivo, aquí no se imponen fuerzas de propulsión a las células. En concreto, la migración celular se produce debido a las fuerzas de interacción célula-substrato y célula-célula, en particular, *crawling* y *purse-string*. En conclusión, en este trabajo se consigue reproducir con éxito fenómenos biológicos relacionados con la mecánica epitelial monocapa con un enfoque híbrido.

En el Capítulo 4, la distinción entre el modelo *basado en los centros de las células* y el *basado en los vértices* se vuelve borrosa con el enfoque de diseño híbrido presentado. Aunque se utilizan los centros de las células para definir sus posiciones, también se aplican diferentes fuerzas de contracción a los vértices de las células. Se puede definir este enfoque de modelado como un "*modelo de vértices transitorio*", ya que la información de los vértices de las células no se almacena de un paso a otro. Sin embargo, se usan explícitamente estos vértices para calcular las fuerzas celulares y resolver la mecánica tisular. El diagrama de Voronoi ya se había usado en estudios anteriores para representar el cuerpo de la célula en modelos basados en el centro de la célula, pero, por lo general, sólo para asociar un área a la célula. El diseño que se usa en este modelo combina los centros de las células con una representación poligonal dinámica de las mismas, esto ofrece interesantes posibilidades de modelado como se muestra en este trabajo.

Sorprendentemente, encontramos que las *alpha shapes* son una herramienta clave que expande enormemente las capacidades de modelado de nuestro trabajo. En primer lugar, se usan para limitar la representación del diagrama de Voronoi, que es infinita por definición. Se utilizan también las Alpha Shapes para distinguir entre varios dominios en el tejido, por lo que se pueden asignar diferentes propiedades mecánicas y comportamiento a estos dominios en el modelo continuo. Además, estas permiten distinguir y localizar fácilmente las células que se encuentran en los bordes de una sola capa, completamente rodeadas por otras células o incluso en contacto con los límites del sistema. Por lo tanto, este modelo híbrido es capaz de representar

la interfaz entre las células y el sustrato, pero también los huecos y discontinuidades en la monocapa celular. De hecho, se podría simular indiferentemente tejidos epiteliales confluentes y no confluentes. Este diseño híbrido es capaz de representar naturalmente células individuales separadas del resto, diferentes grupos celulares que se unen o grupos de células que se dividen a su vez en distintos grupos separados. Por esta razón, creemos que este enfoque de modelado también es aplicable a otros procesos como la angiogénesis, la transición epitelial-mesenquimal, la formación de patrones en los tejidos o la colisión de monocapas.

Somos conscientes de que este modelo de agregados celulares presenta algunas limitaciones. A pesar de que los resultados indican que nuestro modelo es capaz de simular procesos de larga duración, este puede no ser tan preciso al recrear fenómenos a corto plazo donde el tejido acumula estrés mecánico. Se asume que en este trabajo que las tensiones en el tejido se disipan entre los pasos de simulación. Esta suposición sólo es aceptable en procesos en los que las células tienen tiempo suficiente para reestructurar sus citoesqueletos y las uniones adhesivas con las células vecinas. Por parte, se tendría que considerar la acumulación de estrés para simular la reacción del tejido a las fuerzas externas repentinas. Un buen ejemplo serían los experimentos para caracterizar la monocapa epitelial que Harris y Charras desarrollaron [11]. Aunque la introducción de la acumulación de tensiones no es excesivamente complicada a nivel técnico, esto no se ha abordado en este trabajo.

Modelo de agregados celulares en 3D

En el Capítulo 5, se combina un modelo discreto basado en el centro de las células con un modelo continuo de reacción-difusión de oxígeno. Además, también se implementa un modelo de ciclo de vida y salud celular que depende de los niveles de oxígeno en el ambiente celular.

Esta aproximación híbrida predice con precisión el tamaño de un agregado celular aislado en un cultivo 3D. Además, se reproduce que la concentración de oxígeno cae muy rápidamente en el núcleo del agregado durante el crecimiento del mismo como se observó en estudios experimentales previos. Sin embargo, este trabajo no se limita a simulaciones de agregados individuales. También se representan experimentos con múltiples agregados, en los que se estudian su efecto sobre la distribución de oxígeno y la viabilidad celular.

Se observa que la distribución celular puede alterar enormemente la proliferación y viabilidad dado el mismo volumen de cultivo y densidad celular. Por lo tanto, el análisis de la densidad celular no es suficiente para predecir cómo evoluciona un cultivo celular en 3D. Dado que nuestro enfoque híbrido representa las células

individualmente, se puede usar para estudiar cómo la distribución celular afecta a estos sistemas biológicos. El modelo *basado en agentes* nos permite además simular interacciones células-células en detalle. Curiosamente, se puede observar que no sólo las células individuales son atraídas por otras debido a estas interacciones células-células, sino que los grupos muestran un comportamiento similar a nivel colectivo. Este fenómeno emergente es responsable de la fusión de agregados celulares cercanos entre sí, y como consecuencia, esta fusión genera agregados celulares más grandes.

Se demuestra en este trabajo que este enfoque es válido para simular fenómenos biológicos en diferentes escalas de tiempo. Primero, se observa que el proceso más rápido es el transporte de oxígeno en el cultivo 3D. Se asume en consecuencia que la reacción-difusión está desacoplada de otros fenómenos. De hecho, esto significa que se puede resolver este problema en cada paso de tiempo de la simulación asumiendo que las posiciones de las células y el ciclo de vida no han cambiado en ese intervalo de tiempo. Del mismo modo, se puede considerar que la concentración de oxígeno se encuentra en un régimen *pseudo-estacionario* cuando se analizan los otros procesos biofísicos, dado que este equilibrio se alcanza mucho más rápido que el resto. En segundo lugar, el movimiento y la migración celular son más lentos que los eventos de reacción-difusión. Por otro lado, el movimiento celular es considerablemente más rápido que el ciclo de vida celular. En particular, la posición celular sólo afecta indirectamente al ciclo de vida celular y a la salud. Las células pueden migrar a zonas con diferentes concentraciones de oxígeno en el cultivo y, además, alterar la distribución de oxígeno. Sin embargo, no existen otras variables acopladas entre estos modelos. En conclusión, el proceso más lento es el ciclo de vida celular, se puede asumir que un ciclo celular tarda entre horas o días en completarse. En este trabajo, el ciclo de vida de las células se ve afectado directamente por la concentración de oxígeno. La población celular en el cultivo 3D afectará tanto a la interacción célula-célula como a los modelos de reacción-difusión de oxígeno. Finalmente, aunque estos modelos funcionan en escalas temporales diferentes, están conectados por los efectos emergentes derivados de cada uno de ellos.

Somos conscientes que este diseño presenta algunas limitaciones. Se observa que los resultados no coinciden con los datos experimentales en cultivos de más de 15 días. Esto puede ser causado porque algunos fenómenos no se han considerado, como, por ejemplo, la diferenciación celular, el estado de reposo en el ciclo celular o la reducción de la tasa de proliferación cuando se alcanza un cierto tamaño de agregado celular. Por otra parte, se usa un modelo simple de interacción mecánica célula-célula que representa diferentes procesos al mismo tiempo. Se demuestra que este enfoque fenomenológico es válido para simular casos de agrupamiento celular que incluye migración celular e interacciones simples, pero es posible que

no sea capaz predecir estructuras más complejas. Aunque este diseño híbrido no está actualmente adaptado para simular órganos o tejidos estructurados, creemos que es interesante para simular el transporte de oxígeno en sistemas multicelulares. Realmente este enfoque podría implementarse con modelos mecánicos celulares más elaborados y detallados para solventar los problemas mencionados.

Conclusiones sobre los modelos basados en agentes y elementos finitos

El objetivo de esta tesis es explorar cómo combinar modelos continuos (en particular los que se resuelven habitualmente con el método de elementos finitos) y modelos discretos *basados en agentes*. En concreto, se muestra cómo esta idea puede conducir a diferentes aplicaciones de modelado. Cada modelo híbrido presentado en este documento se centra en un problema biológico diferente y, en consecuencia, la integración de sus modelos individuales tiene sus propias particularidades. Evidentemente, comparten algunos aspectos comunes, pero ofrecen una visión global de las numerosas posibilidades de este esquema híbrido y sobre que tipo de problemas biológicos que se pueden reproducir.

Estos modelos híbridos son herramientas flexibles que permiten unir la representación discreta de células y el comportamiento continuo de algunas estructuras biológicas. Se ha intentado en la medida de lo posible utilizar modelos sencillos y definir interfaces claras entre ellos. Obviamente, el trabajo presentado aquí es sólo un paso en esta dirección, pero estos diseños híbridos pueden extenderse y aplicarse a otros problemas biomecánicos de forma sencilla.

No existen actualmente plataformas de modelado de código abierto que soporten estos modelos híbridos. La única implementación de nuestros modelos se realiza con código interno del grupo de investigación. Este hecho puede considerarse como un importante inconveniente para extender el uso de estos diseños híbridos. Sin embargo, se ha explicado en detalle cómo implementar los modelos e interfaces y, se ha intentado además utilizar exclusivamente en bibliotecas de código abierto y especificaciones técnicas estándar.

References

[1] Daniel Arndt et al. “The deal.II Library, Version 8.5”. In: *Journal of Numerical Mathematics* (Jan. 2017). ISSN: 1569-3953. DOI: 10.1515/jnma-2017-0058.

[2] The CGAL Project. *CGAL User and Reference Manual*. 2017.

[3] Michael Waskom et al. *seaborn*. 2016. DOI: 10.5281/zenodo.54844.

[4] Utkarsh Ayachit. *The ParaView Guide: A Parallel Visualization Application*. Kitware, 2015. ISBN: 978-1930934306.

[5] Charlène Guillot and Thomas Lecuit. “Mechanics of Epithelial Tissue Homeostasis and Morphogenesis”. en. In: *Science* 340.6137 (June 2013), pp. 1185–1189. ISSN: 0036-8075. DOI: 10.1126/science.1235249.

[6] S. R. K. Vedula et al. “Emerging modes of collective cell migration induced by geometrical constraints”. In: *Proceedings of the National Academy of Sciences* 109.32 (2012), pp. 12974–12979. ISSN: 0027-8424. DOI: 10.1073/pnas.1119313109. arXiv: 1404.7111 [cond-mat.soft].

[7] Thomas E Angelini et al. “Glass-like dynamics of collective cell migration”. In: *Proceedings of the National Academy of Sciences* 108.12 (Mar. 2011), pp. 4714–4719. ISSN: 0027-8424. DOI: 10.1073/pnas.1010059108.

[8] Guillermo A. Gomez, Robert W. McLachlan, and Alpha S. Yap. “Productive tension: force-sensing and homeostasis of cell–cell junctions”. In: *Trends in Cell Biology* 21.9 (Sept. 2011), pp. 499–505. ISSN: 09628924. DOI: 10.1016/j.tcb.2011.05.006.

[9] Thomas Lecuit and Pierre-François Lenne. “Cell surface mechanics and the control of cell shape, tissue patterns and morphogenesis”. In: *Nature Reviews Molecular Cell Biology* 8.8 (Aug. 2007), pp. 633–644. ISSN: 1471-0072. DOI: 10.1038/nrm2222. arXiv: 34547191723.

[10] Shigenobu Yonemura. “Cadherin–actin interactions at adherens junctions”. In: *Current Opinion in Cell Biology* 23.5 (Oct. 2011), pp. 515–522. ISSN: 09550674. DOI: 10.1016/j.ceb.2011.07.001.

[11] Andrew R Harris et al. “Characterizing the mechanics of cultured cell monolayers”. In: *Proceedings of the National Academy of Sciences* 109.41 (Oct. 2012), pp. 16449–16454. ISSN: 0027-8424. DOI: 10.1073/pnas.1213301109.

[12] Matthew C Gibson et al. “The emergence of geometric order in proliferating metazoan epithelia”. In: *Nature* 442.7106 (Aug. 2006), pp. 1038–1041. ISSN: 0028-0836. DOI: 10.1038/nature05014. arXiv: 33748313224.

[13] Reza Farhadifar et al. “The Influence of Cell Mechanics, Cell-Cell Interactions, and Proliferation on Epithelial Packing”. In: *Current Biology* 17.24 (Dec. 2007), pp. 2095–2104. ISSN: 09609822. DOI: 10.1016/j.cub.2007.11.049.

[14] T Aegerter-Wilmsen et al. “Exploring the effects of mechanical feedback on epithelial topology”. In: *Development* 137.3 (Feb. 2010), pp. 499–506. ISSN: 0950-1991. DOI: 10.1242/dev.041731.

[15] Tom Wyatt, Buzz Baum, and Guillaume Charras. "A question of time: tissue adaptation to mechanical forces". In: *Current Opinion in Cell Biology* 38 (Feb. 2016), pp. 68–73. ISSN: 09550674. DOI: 10.1016/j.ceb.2016.02.012.

[16] Andrew R Harris, Alicia Daeden, and Guillaume T Charras. "Formation of adherens junctions leads to the emergence of a tissue-level tension in epithelial monolayers". In: *Journal of Cell Science* 127.11 (June 2014), pp. 2507–2517. ISSN: 0021-9533. DOI: 10.1242/jcs.142349.

[17] Tom P J Wyatt et al. "Emergence of homeostatic epithelial packing and stress dissipation through divisions oriented along the long cell axis". In: *Proceedings of the National Academy of Sciences* 112.18 (May 2015), pp. 5726–5731. ISSN: 0027-8424. DOI: 10.1073/pnas.1420585112.

[18] Simon Begnaud et al. "Mechanics of epithelial tissues during gap closure". In: *Current Opinion in Cell Biology* 42 (Oct. 2016), pp. 52–62. ISSN: 09550674. DOI: 10.1016/j.ceb.2016.04.006.

[19] M. Behrndt et al. "Forces Driving Epithelial Spreading in Zebrafish Gastrulation". In: *Science* 338.6104 (Oct. 2012), pp. 257–260. ISSN: 0036-8075. DOI: 10.1126/science.1224143.

[20] Agustí Brugués et al. "Forces driving epithelial wound healing". In: *Nature Physics* 10.9 (Aug. 2014), pp. 683–690. ISSN: 1745-2473. DOI: 10.1038/nphys3040.

[21] Ester Anon et al. "Cell crawling mediates collective cell migration to close undamaged epithelial gaps". In: *Proceedings of the National Academy of Sciences* 109.27 (July 2012), pp. 10891–10896. ISSN: 0027-8424. DOI: 10.1073/pnas.1117814109.

[22] Bruno da Rocha-Azevedo and Frederick Grinnell. "Fibroblast morphogenesis on 3D collagen matrices: The balance between cell clustering and cell migration". In: *Experimental Cell Research* 319.16 (Oct. 2013), pp. 2440–2446. ISSN: 00144827. DOI: 10.1016/j.yexcr.2013.05.003.

[23] Pernille Rørth. "Collective Cell Migration". In: *Annual Review of Cell and Developmental Biology* 25.1 (Nov. 2009), pp. 407–429. ISSN: 1081-0706. DOI: 10.1146/annurev.cellbio.042308.113231.

[24] Ulf Dahl, A Sjodin, and Henrik Semb. "Cadherins regulate aggregation of pancreatic beta-cells in vivo". In: *Development* 2902 (1996), pp. 2895–2902.

[25] Hideyuki Suenaga et al. "Cell Condensation and 3-Dimensional Dynamic Environment in a Rotation Culture Upregulates Osteogenic Differentiation of Mesenchymal Stromal Cells". In: *Asian Journal of Oral and Maxillofacial Surgery* 20.4 (Dec. 2008), pp. 177–183. ISSN: 09156992. DOI: 10.1016/S0915-6992(08)80022-2.

[26] Tadanori Mammoto et al. "Mechanochemical Control of Mesenchymal Condensation and Embryonic Tooth Organ Formation". In: *Developmental Cell* 21.4 (Oct. 2011), pp. 758–769. ISSN: 15345807. DOI: 10.1016/j.devcel.2011.07.006.

[27] O Moreno-Arotzena et al. "Inducing chemotactic and haptotactic cues in microfluidic devices for three-dimensional in vitro assays". In: *Biomicrofluidics* 8.6 (Nov. 2014), p. 064122. ISSN: 1932-1058. DOI: 10.1063/1.4903948.

[28] Tetsuya Hiraiwa et al. "Relevance of intracellular polarity to accuracy of eukaryotic chemotaxis". en. In: *Physical Biology* 11.5 (Aug. 2014), p. 056002. ISSN: 1478-3975. DOI: 10.1088/1478-3975/11/5/056002.

[29] James E Bear and Jason M Haugh. "Directed migration of mesenchymal cells: where signaling and the cytoskeleton meet". In: *Current Opinion in Cell Biology* 30.Figure 1 (Oct. 2014), pp. 74–82. ISSN: 09550674. DOI: 10.1016/j.ceb.2014.06.005.

[30] Yan-Hsiung Wang et al. "Characterization and evaluation of the differentiation ability of human adipose-derived stem cells growing in scaffold-free suspension culture". In: *Cytotherapy* 16.4 (Apr. 2014), pp. 485–495. ISSN: 14653249. DOI: 10.1016/j.jcyt.2013.07.015.

[31] T.R. Olsen et al. "Manipulation of cellular spheroid composition and the effects on vascular tissue fusion". In: *Acta Biomaterialia* 13 (Feb. 2015), pp. 188–198. ISSN: 17427061. DOI: 10.1016/j.actbio.2014.11.024.

[32] Bruno da Rocha-Azevedo, Chin-Han Ho, and Frederick Grinnell. "Fibroblast cluster formation on 3D collagen matrices requires cell contraction dependent fibronectin matrix organization". In: *Experimental Cell Research* 319.4 (Feb. 2013), pp. 546–555. ISSN: 00144827. DOI: 10.1016/j.yexcr.2012.10.005.

[33] Christopher S. Szot et al. "3D in vitro bioengineered tumors based on collagen I hydrogels". In: *Biomaterials* 32.31 (Nov. 2011), pp. 7905–7912. ISSN: 01429612. DOI: 10.1016/j.biomaterials.2011.07.001.

[34] Dennis Lambrechts et al. "Fluorescent oxygen sensitive microbead incorporation for measuring oxygen tension in cell aggregates". In: *Biomaterials* 34.4 (Jan. 2013), pp. 922–929. ISSN: 01429612. DOI: 10.1016/j.biomaterials.2012.10.019.

[35] Tristan I. Croll et al. "Modelling oxygen diffusion and cell growth in a porous, vascularising scaffold for soft tissue engineering applications". In: *Chemical Engineering Science* 60.17 (Sept. 2005), pp. 4924–4934. ISSN: 00092509. DOI: 10.1016/j.ces.2005.03.051.

[36] Renjitha Gopurappilly and Ramesh Bhonde. "Transcriptional profiling and functional network analyses of islet-like clusters (ILCs) generated from pancreatic stem cells in vitro". In: *Genomics* 105.4 (Apr. 2015), pp. 211–219. ISSN: 08887543. DOI: 10.1016/j.ygeno.2015.01.003.

[37] Daniela Loessner et al. "Bioengineered 3D platform to explore cell–ECM interactions and drug resistance of epithelial ovarian cancer cells". In: *Biomaterials* 31.32 (Nov. 2010), pp. 8494–8506. ISSN: 01429612. DOI: 10.1016/j.biomaterials.2010.07.064.

[38] Siew-Min Ong et al. "Engineering a scaffold-free 3D tumor model for in vitro drug penetration studies". In: *Biomaterials* 31.6 (Feb. 2010), pp. 1180–1190. ISSN: 01429612. DOI: 10.1016/j.biomaterials.2009.10.049.

[39] Vladimir Mironov et al. "Organ printing: Tissue spheroids as building blocks". In: *Biomaterials* 30.12 (Apr. 2009), pp. 2164–2174. ISSN: 01429612. DOI: 10.1016/j.biomaterials.2008.12.084.

[40] B A Camley and W-J Rappel. "Physical models of collective cell motility: from cell to tissue". In: *Journal of Physics D: Applied Physics* 50.11 (Mar. 2017), p. 113002. ISSN: 0022-3727. DOI: 10.1088/1361-6463/aa56fe.

[41] P. Van Liedekerke et al. "Simulating tissue mechanics with agent-based models: concepts, perspectives and some novel results". In: *Computational Particle Mechanics* 2.4 (Dec. 2015), pp. 401–444. ISSN: 2196-4378. DOI: 10.1007/s40571-015-0082-3.

[42] Jorn Starruß et al. “Morpheus: A user-friendly modeling environment for multiscale and multicellular systems biology”. In: *Bioinformatics* 30.9 (2014), pp. 1331–1332. ISSN: 14602059. DOI: 10.1093/bioinformatics/btt772.

[43] Maciej H. Swat et al. “Multi-Scale Modeling of Tissues Using CompuCell3D”. In: 2012, pp. 325–366. DOI: 10.1016/B978-0-12-388403-9.00013-8.

[44] Gary R. Mirams et al. “Chaste: An Open Source C++ Library for Computational Physiology and Biology”. In: *PLoS Computational Biology* 9.3 (Mar. 2013). Ed. by Andreas Prlic, e1002970. ISSN: 1553-7358. DOI: 10.1371/journal.pcbi.1002970.

[45] Stefan Hoehme and Dirk Drasdo. “A cell-based simulation software for multi-cellular systems”. In: *Bioinformatics* 26.20 (2010), pp. 2641–2642. ISSN: 13674803. DOI: 10.1093/bioinformatics/btq437.

[46] Florian Milde et al. “SEM++: A particle model of cellular growth, signaling and migration”. In: *Computational Particle Mechanics* 1.2 (June 2014), pp. 211–227. ISSN: 2196-4378. DOI: 10.1007/s40571-014-0017-4.

[47] M. Radszuweit et al. “Comparing the growth kinetics of cell populations in two and three dimensions”. In: *Physical Review E - Statistical, Nonlinear, and Soft Matter Physics* 79.5 (2009). ISSN: 15393755. DOI: 10.1103/PhysRevE.79.051907.

[48] Alexander R.A. Anderson et al. *Tumor Morphology and Phenotypic Evolution Driven by Selective Pressure from the Microenvironment*. 2006. DOI: 10.1016/j.cell.2006.09.042.

[49] D.-S. Lee, H. Rieger, and K. Bartha. “Flow Correlated Percolation during Vascular Remodeling in Growing Tumors”. In: *Physical Review Letters* 96.5 (Feb. 2006), p. 058104. ISSN: 0031-9007. DOI: 10.1103/PhysRevLett.96.058104. arXiv: 0507043 [q-bio.TO].

[50] M. Block, E. Schöll, and D. Drasdo. “Classifying the Expansion Kinetics and Critical Surface Dynamics of Growing Cell Populations”. In: *Physical Review Letters* 99.24 (Dec. 2007), p. 248101. ISSN: 0031-9007. DOI: 10.1103/PhysRevLett.99.248101. arXiv: 0610146 [physics].

[51] A R Kansal et al. “Cellular automaton of idealized brain tumor growth dynamics.” In: *Bio Systems* 55 (2000), pp. 119–127. ISSN: 0303-2647. DOI: 10.1016/S0303-2647(99)00089-1.

[52] René F. M. van Oers et al. “Mechanical Cell-Matrix Feedback Explains Pairwise and Collective Endothelial Cell Behavior In Vitro”. In: *PLoS Computational Biology* 10.8 (Aug. 2014). Ed. by Anand R. Asthagiri, e1003774. ISSN: 1553-7358. DOI: 10.1371/journal.pcbi.1003774. arXiv: 1308.3721.

[53] François Graner and James A. Glazier. “Simulation of biological cell sorting using a two-dimensional extended Potts model”. In: *Physical Review Letters* 69.13 (Sept. 1992), pp. 2013–2016. ISSN: 0031-9007. DOI: 10.1103/PhysRevLett.69.2013. arXiv: 0000135489.

[54] Amy L. Bauer, Trachette L. Jackson, and Yi Jiang. “Topography of Extracellular Matrix Mediates Vascular Morphogenesis and Migration Speeds in Angiogenesis”. In: *PLoS Computational Biology* 5.7 (July 2009). Ed. by András Czirók, e1000445. ISSN: 1553-7358. DOI: 10.1371/journal.pcbi.1000445.

[55] Margriet M. Palm and Roeland M H Merks. “Vascular networks due to dynamically arrested crystalline ordering of elongated cells”. In: *Physical Review E - Statistical, Nonlinear, and Soft Matter Physics* 87.1 (2013). ISSN: 15393755. DOI: 10.1103/PhysRevE.87.012725. arXiv: 1210.7164.

[56] Sabine Dormann and Andreas Deutsch. "Modeling of self-organized avascular tumor growth with a hybrid cellular automaton." In: *In silico biology* 2.3 (2002), pp. 393–406. ISSN: 1386-6338. arXiv: 1542344734.

[57] Marco Tektonidis et al. "Identification of intrinsic in vitro cellular mechanisms for glioma invasion". In: *Journal of Theoretical Biology* 287.1 (Oct. 2011), pp. 131–147. ISSN: 00225193. DOI: 10.1016/j.jtbi.2011.07.012.

[58] Jörg Galle, Markus Loeffler, and Dirk Drasdo. "Modeling the Effect of Deregulated Proliferation and Apoptosis on the Growth Dynamics of Epithelial Cell Populations In Vitro". In: *Biophysical Journal* 88.1 (Jan. 2005), pp. 62–75. ISSN: 00063495. DOI: 10.1529/biophysj.104.041459. arXiv: 11244250625.

[59] D. Drasdo and M. Loeffler. "Individual-based models to growth and folding in one-layered tissues: intestinal crypts and early development". In: *Nonlinear Analysis: Theory, Methods & Applications* 47.1 (Aug. 2001), pp. 245–256. ISSN: 0362546X. DOI: 10.1016/S0362-546X(01)00173-0.

[60] F. A. Meineke, C. S. Potten, and M. Loeffler. "Cell migration and organization in the intestinal crypt using a lattice-free model". In: *Cell Proliferation* 34.4 (Aug. 2001), pp. 253–266. ISSN: 0960-7722. DOI: 10.1046/j.0960-7722.2001.00216.x. arXiv: 0034902642.

[61] R Rey and J. M. García-Aznar. "A phenomenological approach to modelling collective cell movement in 2D". In: *Biomechanics and Modeling in Mechanobiology* 12.6 (Nov. 2013), pp. 1089–1100. ISSN: 1617-7959. DOI: 10.1007/s10237-012-0465-9.

[62] F. J. Vermolen and A. Gefen. "A semi-stochastic cell-based formalism to model the dynamics of migration of cells in colonies". In: *Biomechanics and Modeling in Mechanobiology* 11.1-2 (Jan. 2012), pp. 183–195. ISSN: 1617-7959. DOI: 10.1007/s10237-011-0302-6.

[63] Gernot Schaller and Michael Meyer-Hermann. "Multicellular tumor spheroid in an off-lattice Voronoi-Delaunay cell model". In: *Physical Review E - Statistical, Nonlinear, and Soft Matter Physics* 71.5 (2005). ISSN: 15393755. DOI: 10.1103/PhysRevE.71.051910. arXiv: 0407029 [q-bio].

[64] Hisao Honda. "Geometrical Models for Cells in Tissues". In: *International Review of Cytology*. Vol. 81. C. 1983, pp. 191–248. ISBN: 012364481X. DOI: 10.1016/S0074-7696(08)62339-6.

[65] H. Honda, H. Yamanaka, and M. Dan-Sohkawa. "A computer simulation of geometrical configurations during cell division". In: *Journal of Theoretical Biology* 106.3 (1984), pp. 423–435. ISSN: 10958541. DOI: 10.1016/0022-5193(84)90039-0.

[66] Dapeng Bi et al. "Motility-driven glass and jamming transitions in biological tissues". In: *Physical Review X* 6.2 (2016), pp. 1–12. ISSN: 21603308. DOI: 10.1103/PhysRevX.6.021011. arXiv: 1509.06578.

[67] Daniel L. Barton et al. "Active Vertex Model for cell-resolution description of epithelial tissue mechanics". In: *PLOS Computational Biology* 13.6 (June 2017). Ed. by Stanislav Shvartsman, e1005569. ISSN: 1553-7358. DOI: 10.1371/journal.pcbi.1005569. arXiv: 1612.05960.

[68] Tim Odenthal et al. "Analysis of Initial Cell Spreading Using Mechanistic Contact Formulations for a Deformable Cell Model". In: *PLoS Computational Biology* 9.10 (Oct. 2013). Ed. by Andrew D. McCulloch, e1003267. ISSN: 1553-7358. DOI: 10.1371/journal.pcbi.1003267.

[69] Katarzyna A. Rejniak. "An immersed boundary framework for modelling the growth of individual cells: An application to the early tumour development". In: *Journal of Theoretical Biology* 247.1 (July 2007), pp. 186–204. ISSN: 00225193. DOI: 10.1016/j.jtbi.2007.02.019. arXiv: 34248638171.

[70] Z. Peng et al. "Lipid bilayer and cytoskeletal interactions in a red blood cell". In: *Proceedings of the National Academy of Sciences* 110.33 (Aug. 2013), pp. 13356–13361. ISSN: 0027-8424. DOI: 10.1073/pnas.1311827110. arXiv: arXiv:1408.1149.

[71] Igor V. Pivkin and George Em Karniadakis. "Accurate Coarse-Grained Modeling of Red Blood Cells". In: *Physical Review Letters* 101.11 (Sept. 2008), p. 118105. ISSN: 0031-9007. DOI: 10.1103/PhysRevLett.101.118105.

[72] Sebastian A. Sandersius and Timothy J. Newman. "Modeling cell rheology with the Subcellular Element Model". In: *Physical Biology* 5.1 (Apr. 2008), p. 015002. ISSN: 1478-3975. DOI: 10.1088/1478-3975/5/1/015002.

[73] S. A. Sandersius, C. J. Weijer, and T. J. Newman. "Emergent cell and tissue dynamics from subcellular modeling of active biomechanical processes". In: *Physical Biology* 8.4 (2011). ISSN: 14783967. DOI: 10.1088/1478-3975/8/4/045007. arXiv: 79961193688.

[74] Yousef Jamali, Mohammad Azimi, and Mohammad R. K. Mofrad. "A Sub-Cellular Viscoelastic Model for Cell Population Mechanics". In: *PLoS ONE* 5.8 (2010), e12097. ISSN: 1932-6203. DOI: 10.1371/journal.pone.0012097.

[75] Davide Ambrosi and Luigi Preziosi. "Cell adhesion mechanisms and stress relaxation in the mechanics of tumours". In: *Biomechanics and Modeling in Mechanobiology* 8.5 (Oct. 2009), pp. 397–413. ISSN: 1617-7959. DOI: 10.1007/s10237-008-0145-y.

[76] M. J. Gómez-Benito et al. "Influence of fracture gap size on the pattern of long bone healing: A computational study". In: *Journal of Theoretical Biology* 235.1 (2005), pp. 105–119. ISSN: 00225193. DOI: 10.1016/j.jtbi.2004.12.023.

[77] Sergio Gabarre et al. "Comparative Analysis of the Biomechanical Behaviour of Two Cementless Short Stems for Hip Replacement: Linea Anatomic and Minihip". In: *PLOS ONE* 11.7 (July 2016). Ed. by Jose Manuel Garcia Aznar, e0158411. ISSN: 1932-6203. DOI: 10.1371/journal.pone.0158411.

[78] C. Valero et al. "Nonlinear finite element simulations of injuries with free boundaries: Application to surgical wounds". In: *International Journal for Numerical Methods in Biomedical Engineering* 30.6 (June 2014), pp. 616–633. ISSN: 20407939. DOI: 10.1002/cnm.2621.

[79] D. Lacroix and P.J. Prendergast. "A mechano-regulation model for tissue differentiation during fracture healing: analysis of gap size and loading". In: *Journal of Biomechanics* 35.9 (Sept. 2002), pp. 1163–1171. ISSN: 00219290. DOI: 10.1016/S0021-9290(02)00086-6.

[80] Carlos Borau, Roger D. Kamm, and José Manuel García-Aznar. "A time-dependent phenomenological model for cell mechano-sensing". In: *Biomechanics and Modeling in Mechanobiology* 13.2 (Apr. 2014), pp. 451–462. ISSN: 1617-7959. DOI: 10.1007/s10237-013-0508-x.

[81] F. J. Vermolen and E. Javierre. "A finite-element model for healing of cutaneous wounds combining contraction, angiogenesis and closure". In: *Journal of Mathematical Biology* 65.5 (Nov. 2012), pp. 967–996. ISSN: 0303-6812. DOI: 10.1007/s00285-011-0487-4.

[82] P. Van Liedekerke et al. "Particle-based model to simulate the micromechanics of biological cells". In: *Physical Review E* 81.6 (June 2010), p. 061906. ISSN: 1539-3755. DOI: 10.1103/PhysRevE.81.061906.

[83] Florian Milde, Michael Bergdorf, and Petros Koumoutsakos. "A Hybrid Model for Three-Dimensional Simulations of Sprouting Angiogenesis". In: *Biophysical Journal* 95.7 (Oct. 2008), pp. 3146–3160. ISSN: 00063495. DOI: 10.1529/biophysj.107.124511.

[84] Payman Mosaffa, Antonio Rodríguez-Ferran, and José J. Muñoz. "Hybrid cell-centred/vertex model for multicellular systems with equilibrium-preserving remodelling". In: (2017), pp. 1–33. ISSN: 20407939. DOI: 10.1002/cnm.2928. arXiv: 1705.05441.

[85] Mark Alber et al. "Continuous Macroscopic Limit of a Discrete Stochastic Model for Interaction of Living Cells". In: *Physical Review Letters* 99.16 (Oct. 2007), p. 168102. ISSN: 0031-9007. DOI: 10.1103/PhysRevLett.99.168102. arXiv: 0703026 [physics].

[86] Hongyuan Jiang and Sean X. Sun. "Cellular Pressure and Volume Regulation and Implications for Cell Mechanics". In: *Biophysical Journal* 105.3 (Aug. 2013), pp. 609–619. ISSN: 00063495. DOI: 10.1016/j.bpj.2013.06.021.

[87] D B Staple et al. "Mechanics and remodelling of cell packings in epithelia". In: *The European Physical Journal E* 33.2 (Oct. 2010), pp. 117–127. ISSN: 1292-8941. DOI: 10.1140/epje/i2010-10677-0.

[88] Dapeng Bi et al. "A density-independent rigidity transition in biological tissues". In: *Nature Physics* 11.12 (Sept. 2015), pp. 1074–1079. ISSN: 1745-2473. DOI: 10.1038/nphys3471. arXiv: 1409.0593.

[89] Bo Li and Sean X. Sun. "Coherent Motions in Confluent Cell Monolayer Sheets". In: *Biophysical Journal* 107.7 (Oct. 2014), pp. 1532–1541. ISSN: 00063495. DOI: 10.1016/j.bpj.2014.08.006.

[90] Sascha Hilgenfeldt, Sinem Erisken, and Richard W Carthew. "Physical modeling of cell geometric order in an epithelial tissue". In: *Proceedings of the National Academy of Sciences* 105.3 (Jan. 2008), pp. 907–911. ISSN: 0027-8424. DOI: 10.1073/pnas.0711077105. arXiv: 38949170737.

[91] Kevin K. Chiou, Lars Hufnagel, and Boris I. Shraiman. "Mechanical Stress Inference for Two Dimensional Cell Arrays". In: *PLoS Computational Biology* 8.5 (May 2012). Ed. by Stanislav Shvartsman, e1002512. ISSN: 1553-7358. DOI: 10.1371/journal.pcbi.1002512. arXiv: arXiv:1112.5905v1.

[92] Dirk Drasdo, Stefan Hoehme, and Michael Block. "On the Role of Physics in the Growth and Pattern Formation of Multi-Cellular Systems: What can we Learn from Individual-Cell Based Models?" In: *Journal of Statistical Physics* 128.1-2 (June 2007), pp. 287–345. ISSN: 0022-4715. DOI: 10.1007/s10955-007-9289-x. arXiv: 34249873259.

[93] Ignacio Ramis-Conde et al. "Multi-scale modelling of cancer cell intravasation: the role of cadherins in metastasis". In: *Physical Biology* 6.1 (Mar. 2009), p. 016008. ISSN: 1478-3975. DOI: 10.1088/1478-3975/6/1/016008.

[94] Payman Mosaffa et al. "Cell-centred model for the simulation of curved cellular monolayers". In: *Computational Particle Mechanics* 2.4 (Dec. 2015), pp. 359–370. ISSN: 2196-4378. DOI: 10.1007/s40571-015-0043-x.

[95] Rafael A. Barrio et al. “Cell Patterns Emerge from Coupled Chemical and Physical Fields with Cell Proliferation Dynamics: The Arabidopsis thaliana Root as a Study System”. In: *PLoS Computational Biology* 9.5 (May 2013). Ed. by Anand R. Asthagiri, e1003026. ISSN: 1553-7358. DOI: 10.1371/journal.pcbi.1003026.

[96] Bruce S. Gardiner et al. “Discrete Element Framework for Modelling Extracellular Matrix, Deformable Cells and Subcellular Components”. In: *PLOS Computational Biology* 11.10 (Oct. 2015). Ed. by Jeffrey J. Saucerman, e1004544. ISSN: 1553-7358. DOI: 10.1371/journal.pcbi.1004544.

[97] G Brodland, D Chen, and J Veldhuis. “A cell-based constitutive model for embryonic epithelia and other planar aggregates of biological cells”. In: *International Journal of Plasticity* 22.6 (June 2006), pp. 965–995. ISSN: 07496419. DOI: 10.1016/j.ijplas.2005.05.002. arXiv: 31144461582.

[98] William T. Gibson et al. “Control of the Mitotic Cleavage Plane by Local Epithelial Topology”. In: *Cell* 144.3 (Feb. 2011), pp. 427–438. ISSN: 00928674. DOI: 10.1016/j.cell.2010.12.035.

[99] Edouard Hannezo, Jacques Prost, and J.-F. Joanny. “Theory of epithelial sheet morphology in three dimensions”. In: *Proceedings of the National Academy of Sciences* 111.1 (Jan. 2014), pp. 27–32. ISSN: 0027-8424. DOI: 10.1073/pnas.1312076111.

[100] J. Galle, L. Preziosi, and A. Tosin. “Contact inhibition of growth described using a multiphase model and an individual cell based model”. In: *Applied Mathematics Letters* 22.10 (Oct. 2009), pp. 1483–1490. ISSN: 08939659. DOI: 10.1016/j.aml.2008.06.051.

[101] Bart Smeets et al. “Quantifying the mechanical micro-environment during three-dimensional cell expansion on microbeads by means of individual cell-based modelling”. In: *Computer Methods in Biomechanics and Biomedical Engineering* 16.10 (Oct. 2013), pp. 1071–1084. ISSN: 1025-5842. DOI: 10.1080/10255842.2013.829461.

[102] H. Edelsbrunner, D. Kirkpatrick, and R. Seidel. “On the shape of a set of points in the plane”. In: *IEEE Transactions on Information Theory* 29.4 (July 1983), pp. 551–559. ISSN: 0018-9448. DOI: 10.1109/TIT.1983.1056714.

[103] Nitya Ramkumar and Buzz Baum. “Coupling changes in cell shape to chromosome segregation”. In: *Nature Reviews Molecular Cell Biology* 17.8 (June 2016), pp. 511–521. ISSN: 1471-0072. DOI: 10.1038/nrm.2016.75.

[104] Marco Milan, Sonsoles Campuzano, and Antonio Garcia-Bellido. “Cell cycling and patterned cell proliferation in the Drosophila wing during metamorphosis.” In: *Proceedings of the National Academy of Sciences* 93.21 (Oct. 1996), pp. 11687–11692. ISSN: 0027-8424. DOI: 10.1073/pnas.93.21.11687.

[105] Thomas Rüberg and José Manuel Garcí Aznar. “Numerical simulation of solid deformation driven by creeping flow using an immersed finite element method”. In: *Advanced Modeling and Simulation in Engineering Sciences* 3.1 (Dec. 2016), p. 9. ISSN: 2213-7467. DOI: 10.1186/s40323-016-0061-0.

[106] Grégory Beaune et al. “How cells flow in the spreading of cellular aggregates”. In: *Proceedings of the National Academy of Sciences* 111.22 (June 2014), pp. 8055–8060. ISSN: 0027-8424. DOI: 10.1073/pnas.1323788111.

[107] Xavier Trepat and Jeffrey J. JJ Fredberg. "Plithotaxis and emergent dynamics in collective cellular migration". In: *Trends in Cell Biology* 21.11 (2011), pp. 638–646. ISSN: 09628924. DOI: 10.1016/j.tcb.2011.06.006.Plithotaxis. arXiv: 80755139465.

[108] Monirosadat Sadati et al. "Collective migration and cell jamming". In: *Differentiation* 86.3 (2013), pp. 121–125. ISSN: 03014681. DOI: 10.1016/j.diff.2013.02.005. arXiv: NIHMS150003.

[109] Jin-Ah Park et al. "Unjamming and cell shape in the asthmatic airway epithelium". In: *Nature Materials* 14.10 (Aug. 2015), pp. 1040–1048. ISSN: 1476-1122. DOI: 10.1038/nmat4357.

[110] Jin-Ah Park et al. "Collective migration and cell jamming in asthma, cancer and development". In: *Journal of Cell Science* 129.18 (2016), pp. 3375–3383. ISSN: 0021-9533. DOI: 10.1242/jcs.187922.

[111] Simon Garcia et al. "Physics of active jamming during collective cellular motion in a monolayer". In: *Proceedings of the National Academy of Sciences* 112.50 (Dec. 2015), pp. 15314–15319. ISSN: 0027-8424. DOI: 10.1073/pnas.1510973112.

[112] Dhananjay T. Tambe et al. "Collective cell guidance by cooperative intercellular forces". In: *Nature Materials* 10.6 (2011), pp. 469–475. ISSN: 1476-1122. DOI: 10.1038/nmat3025.

[113] Néstor Sepúlveda et al. "Collective Cell Motion in an Epithelial Sheet Can Be Quantitatively Described by a Stochastic Interacting Particle Model". In: *PLoS Computational Biology* 9.3 (Mar. 2013). Ed. by Michael P. Brenner, e1002944. ISSN: 1553-7358. DOI: 10.1371/journal.pcbi.1002944.

[114] Bart Smeets et al. "Emergent structures and dynamics of cell colonies by contact inhibition of locomotion". In: *Proceedings of the National Academy of Sciences* 113.51 (Dec. 2016), pp. 14621–14626. ISSN: 0027-8424. DOI: 10.1073/pnas.1521151113.

[115] Chiara Malinverno et al. "Endocytic reawakening of motility in jammed epithelia". In: *Nature Materials* 16.5 (2017), pp. 587–596. ISSN: 1476-1122. DOI: 10.1038/nmat4848.

[116] Ismael González-Valverde and José Manuel García-Aznar. "A hybrid computational model to explore the topological characteristics of epithelial tissues". In: *International Journal for Numerical Methods in Biomedical Engineering* 33.11 (Nov. 2017), e2877. ISSN: 20407939. DOI: 10.1002/cnm.2877.

[117] Steve Pawlizak et al. "Testing the differential adhesion hypothesis across the epithelial-mesenchymal transition". In: *New Journal of Physics* 17.8 (2015). ISSN: 13672630. DOI: 10.1088/1367-2630/17/8/083049.

[118] Sri Ram Krishna Vedula et al. "Mechanics of epithelial closure over non-adherent environments". In: *Nature Communications* 6 (Jan. 2015), p. 6111. ISSN: 2041-1723. DOI: 10.1038/ncomms7111.

[119] Raimon Sunyer et al. "Collective cell durotaxis emerges from long-range intercellular force transmission". In: *Science* 353.6304 (Sept. 2016), pp. 1157–1161. ISSN: 0036-8075. DOI: 10.1126/science.aaf7119.

[120] Elizaveta A. Novikova et al. "Persistence-Driven Durotaxis: Generic, Directed Motility in Rigidity Gradients". In: *Physical Review Letters* 118.7 (Feb. 2017), p. 078103. ISSN: 0031-9007. DOI: 10.1103/PhysRevLett.118.078103. arXiv: 1512.06024.

[121] A. J. Loza et al. “Cell density and actomyosin contractility control the organization of migrating collectives within an epithelium”. In: *Molecular Biology of the Cell* 27.22 (2016), pp. 3459–3470. ISSN: 1059-1524. DOI: 10.1091/mbc.E16-05-0329.

[122] Adrian Moure and Hector Gomez. “Phase-field model of cellular migration: Three-dimensional simulations in fibrous networks”. In: *Computer Methods in Applied Mechanics and Engineering* 320 (2017), pp. 162–197. ISSN: 00457825. DOI: 10.1016/j.cma.2017.03.025.

[123] J. Escribano, M. T. Sánchez, and J. M. García-Aznar. “A discrete approach for modeling cell–matrix adhesions”. In: *Computational Particle Mechanics* 1.2 (June 2014), pp. 117–130. ISSN: 2196-4378. DOI: 10.1007/s40571-014-0006-7.

[124] Tommy Heck et al. “Modeling extracellular matrix viscoelasticity using smoothed particle hydrodynamics with improved boundary treatment”. In: *Computer Methods in Applied Mechanics and Engineering* 322 (2017), pp. 515–540. ISSN: 00457825. DOI: 10.1016/j.cma.2017.04.031.

[125] Julia C Arciero et al. “Continuum Model of Collective Cell Migration in Wound Healing and Colony Expansion”. In: *Biophysical Journal* 100.3 (Feb. 2011), pp. 535–543. ISSN: 00063495. DOI: 10.1016/j.bpj.2010.11.083.

[126] Andrea Ravasio et al. “Gap geometry dictates epithelial closure efficiency”. In: *Nature Communications* 6 (July 2015), p. 7683. ISSN: 2041-1723. DOI: 10.1038/ncomms8683.

[127] Pedro Moreo, José Manuel García-Aznar, and Manuel Doblaré. “Modeling mechanosensing and its effect on the migration and proliferation of adherent cells”. In: *Acta Biomaterialia* 4.3 (May 2008), pp. 613–621. ISSN: 17427061. DOI: 10.1016/j.actbio.2007.10.014.

[128] Xavier Trepat et al. “Physical forces during collective cell migration”. In: *Nature Physics* 5.6 (June 2009), pp. 426–430. ISSN: 1745-2473. DOI: 10.1038/nphys1269.

[129] Sean X. Sun, Sam Walcott, and Charles W. Wolgemuth. “Cytoskeletal cross-linking and bundling in motor-independent contraction”. In: *Current Biology* 20.15 (2010), R649–R654. ISSN: 09609822. DOI: 10.1016/j.cub.2010.07.004.

[130] Timothy A. Davis. “Algorithm 832”. In: *ACM Transactions on Mathematical Software* 30.2 (June 2004), pp. 196–199. ISSN: 00983500. DOI: 10.1145/992200.992206.

[131] Wes McKinney. “Data Structures for Statistical Computing in Python”. In: *Proceedings of the 9th Python in Science Conference*. Ed. by Stéfan van der Walt and Jarrod Millman. 2010, pp. 51–56.

[132] Chun Min Lo et al. “Cell movement is guided by the rigidity of the substrate”. In: *Biophysical Journal* 79.1 (2000), pp. 144–152. ISSN: 00063495. DOI: 10.1016/S0006-3495(00)76279-5. arXiv: NIHMS150003.

[133] Michelle L Wynn et al. “Follow-the-leader cell migration requires biased cell–cell contact and local microenvironmental signals”. en. In: *Physical Biology* 10.3 (June 2013), p. 035003. ISSN: 1478-3967. DOI: 10.1088/1478-3975/10/3/035003.

[134] Sangmyung Rhee, Chin Han Ho, and Frederick Grinnell. “Promigratory and procontractile growth factor environments differentially regulate cell morphogenesis”. In: *Experimental Cell Research* 316.2 (2010), pp. 232–244. ISSN: 00144827. DOI: 10.1016/j.yexcr.2009.09.021.

[135] O Moreno-Arotzena et al. "Fibroblast Migration in 3D is Controlled by Haptotaxis in a Non-muscle Myosin II-Dependent Manner". In: *Annals of Biomedical Engineering* 43.12 (Dec. 2015), pp. 3025–3039. ISSN: 0090-6964. DOI: 10.1007/s10439-015-1343-2.

[136] Carmela Palmiero et al. "Engineered dermal equivalent tissue in vitro by assembly of microtissue precursors." In: *Acta biomaterialia* 6.7 (July 2010), pp. 2548–53. ISSN: 1878-7568. DOI: 10.1016/j.actbio.2010.01.026.

[137] Yang Mei et al. "Modulating and modeling aggregation of cell-seeded microcarriers in stirred culture system for macrotissue engineering". In: *Journal of Biotechnology* 150.3 (Nov. 2010), pp. 438–446. ISSN: 01681656. DOI: 10.1016/j.jbiotec.2010.09.953.

[138] Yue Shao, Jianming Sang, and Jianping Fu. "On human pluripotent stem cell control: The rise of 3D bioengineering and mechanobiology". In: *Biomaterials* 52 (June 2015), pp. 26–43. ISSN: 01429612. DOI: 10.1016/j.biomaterials.2015.01.078.

[139] Kenneth M Yamada and Edna Cukierman. "Modeling Tissue Morphogenesis and Cancer in 3D". In: *Cell* 130.4 (Aug. 2007), pp. 601–610. ISSN: 00928674. DOI: 10.1016/j.cell.2007.08.006.

[140] Taro Toyoda et al. "Cell aggregation optimizes the differentiation of human ESCs and iPSCs into pancreatic bud-like progenitor cells". In: *Stem Cell Research* 14.2 (Mar. 2015), pp. 185–197. ISSN: 18735061. DOI: 10.1016/j.scr.2015.01.007.

[141] Francesco Pampaloni, Nariman Ansari, and Ernst H K Stelzer. "High-resolution deep imaging of live cellular spheroids with light-sheet-based fluorescence microscopy". In: *Cell and Tissue Research* 352.1 (Apr. 2013), pp. 161–177. ISSN: 0302-766X. DOI: 10.1007/s00441-013-1589-7.

[142] T J Newman. "Modeling multicellular systems using subcellular elements." In: *Mathematical biosciences and engineering : MBE* 2.3 (July 2005), pp. 613–24. ISSN: 1547-1063.

[143] Kevin J. Painter and Jonathan a. Sherratt. "Modelling the movement of interacting cell populations". In: *Journal of Theoretical Biology* 225.3 (Dec. 2003), pp. 327–339. ISSN: 00225193. DOI: 10.1016/S0022-5193(03)00258-3.

[144] Matthew J. Simpson, Kerry a. Landman, and Kaushik Bhaganagarapu. "Coalescence of interacting cell populations". In: *Journal of Theoretical Biology* 247.3 (Aug. 2007), pp. 525–543. ISSN: 00225193. DOI: 10.1016/j.jtbi.2007.02.020.

[145] A. Gerisch and M.A.J. Chaplain. "Mathematical modelling of cancer cell invasion of tissue: Local and non-local models and the effect of adhesion". In: *Journal of Theoretical Biology* 250.4 (Feb. 2008), pp. 684–704. ISSN: 00225193. DOI: 10.1016/j.jtbi.2007.10.026.

[146] C Borau, R D Kamm, and J M García-Aznar. "Mechano-sensing and cell migration: a 3D model approach". In: *Physical Biology* 8.6 (Dec. 2011), p. 066008. ISSN: 1478-3967. DOI: 10.1088/1478-3975/8/6/066008.

[147] Carlos Borau et al. "Probabilistic Voxel-Fe model for single cell motility in 3D". en. In: *In Silico Cell and Tissue Science* 1.1 (Oct. 2014), p. 2. ISSN: 2196-050X. DOI: 10.1186/2196-050X-1-2.

[148] Muhammad H Zaman et al. "Computational Model for Cell Migration in Three-Dimensional Matrices". In: *Biophysical Journal* 89.2 (Aug. 2005), pp. 1389–1397. ISSN: 00063495. DOI: 10.1529/biophysj.105.060723.

[149] Danying Shao, Wouter-Jan Rappel, and Herbert Levine. "Computational Model for Cell Morphodynamics". In: *Physical Review Letters* 105.10 (Sept. 2010), p. 108104. ISSN: 0031-9007. DOI: 10.1103/PhysRevLett.105.108104.

[150] N.A. N'Dri, W Shyy, and R Tran-Son-Tay. "Computational Modeling of Cell Adhesion and Movement Using a Continuum-Kinetics Approach". In: *Biophysical Journal* 85.4 (Oct. 2003), pp. 2273–2286. ISSN: 00063495. DOI: 10.1016/S0006-3495(03)74652-9.

[151] Ignacio Ramis-Conde, Mark A.J. Chaplain, and Alexander R.A. Anderson. "Mathematical modelling of cancer cell invasion of tissue". In: *Mathematical and Computer Modelling* 47.5-6 (Mar. 2008), pp. 533–545. ISSN: 08957177. DOI: 10.1016/j.mcm.2007.02.034.

[152] Ignacio Romero and Juan J Arribas. "Modeling and Simulations of the Dynamics of Growing Cell Clusters". In: *Advances in Cell Mechanics*. Berlin, Heidelberg: Springer Berlin Heidelberg, 2011, pp. 1–25. ISBN: 9780791843925. DOI: 10.1007/978-3-642-17590-9_1.

[153] Diego A. Vargas and Muhammad H. Zaman. "Computational Model for Migration of a Cell Cluster in Three-Dimensional Matrices". In: *Annals of Biomedical Engineering* 39.7 (July 2011), pp. 2068–2079. ISSN: 0090-6964. DOI: 10.1007/s10439-011-0290-9.

[154] Ignacio Ramis-Conde et al. "Modeling the Influence of the E-Cadherin-β-Catenin Pathway in Cancer Cell Invasion: A Multiscale Approach". In: *Biophysical Journal* 95.1 (July 2008), pp. 155–165. ISSN: 00063495. DOI: 10.1529/biophysj.107.114678.

[155] F. J. Vermolen, M. M. Mul, and A. Gefen. "Semi-stochastic cell-level computational modeling of the immune system response to bacterial infections and the effects of antibiotics". In: *Biomechanics and Modeling in Mechanobiology* 13.4 (Aug. 2014), pp. 713–734. ISSN: 1617-7959. DOI: 10.1007/s10237-013-0529-5.

[156] Nikodem J. Poplawski et al. "Front Instabilities and Invasiveness of Simulated 3D Avascular Tumors". In: *PLoS ONE* 5.5 (May 2010). Ed. by Gustavo Stolovitzky, e10641. ISSN: 1932-6203. DOI: 10.1371/journal.pone.0010641.

[157] Maciej H. Swat et al. "Emergent Stratification in Solid Tumors Selects for Reduced Cohesion of Tumor Cells: A Multi-Cell, Virtual-Tissue Model of Tumor Evolution Using CompuCell3D". In: *PLOS ONE* 10.6 (June 2015). Ed. by Michael Massiah, e0127972. ISSN: 1932-6203. DOI: 10.1371/journal.pone.0127972.

[158] Stephen Turner and Jonathan A Sherratt. "Intercellular adhesion and cancer invasion: a discrete simulation using the extended Potts model." In: *Journal of theoretical biology* 216.1 (May 2002), pp. 85–100. ISSN: 0022-5193. DOI: 10.1006/jtbi.2001.2522. arXiv: 0036304182.

[159] R. M. H. Merks and P. Koolwijk. "Modeling Morphogenesis in silico and in vitro : Towards Quantitative, Predictive, Cell-based Modeling". In: *Mathematical Modelling of Natural Phenomena* 4.4 (July 2009), pp. 149–171. ISSN: 0973-5348. DOI: 10.1051/mmnp/20094406.

[160] Nicholas J. Savill and Jonathan a. Sherratt. "Control of epidermal stem cell clusters by Notch-mediated lateral induction." In: *Developmental biology* 258.1 (June 2003), pp. 141–53. ISSN: 0012-1606. DOI: 10.1016/S0012-1606(03)00107-6.

[161] MunJu Kim, Damon Reed, and Katarzyna a. Rejniak. "The formation of tight tumor clusters affects the efficacy of cell cycle inhibitors: A hybrid model study". In: *Journal of Theoretical Biology* 352 (July 2014), pp. 31–50. ISSN: 00225193. DOI: 10.1016/j.jtbi.2014.02.027.

[162] Robert Dillon, Markus Owen, and Kevin Painter. "A single-cell-based model of multicellular growth using the immersed boundary method". In: *. . . : Moving interface problems and applications in fluid . . .* Vol. 0000. 2008, pp. 1–15. DOI: 10.1090/conm/466/09113.

[163] Jonathan F. Li and John Lowengrub. "The effects of cell compressibility, motility and contact inhibition on the growth of tumor cell clusters using the Cellular Potts Model". In: *Journal of Theoretical Biology* 343 (Feb. 2014), pp. 79–91. ISSN: 00225193. DOI: 10.1016/j.jtbi.2013.10.008.

[164] Nicola J. Armstrong, Kevin J. Painter, and Jonathan a. Sherratt. "A continuum approach to modelling cell–cell adhesion". In: *Journal of Theoretical Biology* 243.1 (Nov. 2006), pp. 98–113. ISSN: 00225193. DOI: 10.1016/j.jtbi.2006.05.030.

[165] W Mueller-Klieser. "Method for the determination of oxygen consumption rates and diffusion coefficients in multicellular spheroids". In: *Biophysical Journal* 46.3 (Sept. 1984), pp. 343–348. ISSN: 00063495. DOI: 10.1016/S0006-3495(84)84030-8.

[166] W Mueller-Klieser, J P Freyer, and R M Sutherland. "Influence of glucose and oxygen supply conditions on the oxygenation of multicellular spheroids." In: *British Journal of Cancer* 53.3 (Mar. 1986), pp. 345–53. ISSN: 0007-0920.

[167] S Dornan and M A Collins. "High efficiency electroporation of Lactococcus lactis subsp. lactis LM0230 with plasmid pGB301." In: *Letters in applied microbiology* 11.2 (Aug. 1990), pp. 62–4. ISSN: 0266-8254.

[168] F Brauer and C Castillo-Chávez. *Mathematical models in population biology and epidemiology*. Second. 2012. ISBN: 9781461416852.

[169] M2BE. *InSilico-Cell - More information at http://m2be.unizar.es/insilico_cell*. 2015.

[170] Tae-Yun Kang et al. "The realistic prediction of oxygen transport in a tissue-engineered scaffold by introducing time-varying effective diffusion coefficients". In: *Acta Biomaterialia* 7.9 (Sept. 2011), pp. 3345–3353. ISSN: 17427061. DOI: 10.1016/j.actbio.2011.05.015.

[171] Caroline Androjna et al. "Oxygen Diffusion through Natural Extracellular Matrices: Implications for Estimating "Critical Thickness" Values in Tendon Tissue Engineering". In: *Tissue Engineering Part A* 14.4 (Apr. 2008), pp. 559–569. ISSN: 1937-3341. DOI: 10.1089/tea.2006.0361.

[172] R. Sander. "Compilation of Henry's law constants (version 4.0) for water as solvent". In: *Atmospheric Chemistry and Physics* 15.8 (Apr. 2015), pp. 4399–4981. ISSN: 1680-7324. DOI: 10.5194/acp-15-4399-2015.

[173] Joe Dragavon et al. "A cellular isolation system for real-time single-cell oxygen consumption monitoring". In: *Journal of The Royal Society Interface* -1.-1 (Jan. 2008), pp. –1—1. ISSN: 1742-5689. DOI: 10.1098/rsif.2008.0106.

[174] Peter Carmeliet. "Angiogenesis in life, disease and medicine". In: *Nature* 438.7070 (Dec. 2005), pp. 932–936. ISSN: 0028-0836. DOI: 10.1038/nature04478.

[175] Aude Carreau et al. "Why is the partial oxygen pressure of human tissues a crucial parameter? Small molecules and hypoxia". In: *Journal of Cellular and Molecular Medicine* 15.6 (June 2011), pp. 1239–1253. ISSN: 15821838. DOI: 10.1111/j.1582-4934.2011.01258.x.